



# UFBA

UNIVERSIDADE FEDERAL DA BAHIA  
ESCOLA POLITÉCNICA  
PROGRAMA DE PÓS GRADUAÇÃO EM  
ENGENHARIA INDUSTRIAL - PEI

DOUTORADO EM ENGENHARIA INDUSTRIAL

LICIANNE PIMENTEL SANTA ROSA

MODELLING OF AMMONIA ABSORPTION PROCESS:  
FALLING FILM AND PACKED COLUMN



**SALVADOR**  
**2021**



LICIANNE PIMENTEL SANTA ROSA

**MODELLING OF AMMONIA ABSORPTION PROCESS:  
FALLING FILM AND PACKED COLUMN**

SALVADOR

2021

Ficha catalográfica elaborada pelo Sistema Universitário de Bibliotecas (SIBI/UFBA),  
com os dados fornecidos pelo(a) autor(a).

ROSA, LICIANNE PIMENTEL SANTA  
MODELLING OF AMMONIA ABSORPTION PROCESS: FALLING  
FILM AND PACKED COLUMN / LICIANNE PIMENTEL SANTA  
ROSA. -- SALVADOR, 2021.  
174 f.

Orientador: Karen Valverde Pontes.  
Coorientador: Glória Meyberg Nunes Costa.  
Tese (Doutorado - DOUTORADO EM ENGENHARIA  
INDUSTRIAL) -- Universidade Federal da Bahia, ESCOLA  
POLITÉCNICA, 2021.

1. falling film. 2. packed column. 3. absorption.  
4. ammonia and water. I. Valverde Pontes, Karen. II.  
Meyberg Nunes Costa, Glória. III. Título.

# “MODELLING OF AMMONIA ABSORPTION PROCESS: FALLING FILM AND PACKED COLUMN”

LICIANNE PIMENTEL SANTA ROSA

Tese submetida ao corpo docente do programa de pós-graduação em Engenharia Industrial da Universidade Federal da Bahia como parte dos requisitos necessários para a obtenção do grau de doutor em Engenharia Industrial.

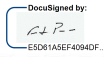
Examinada por:

Prof. Dra. Karen Valverde Pontes   
Doutora em Engenharia Química pela Universidade Estadual de Campinas, Brasil, 2008.

Prof. Dr. Cristiano Hora de Oliveira Fontes   
Doutor em Engenharia Química pela Universidade Estadual de Campinas, Brasil, 2001.

Prof. Dra. Rita Maria de Brito Alves   
Doutora em Engenharia Química pela Universidade de São Paulo, Brasil, 2003.

Prof. Dra. Maria Regina Wolf Maciel   
Doutora em Engenharia Química pela The Leeds University, Leeds, England, 1989.

Prof. Dr. Fernando Luiz Pellegrini Pessoa   
Doutor Engenharia Química pela Universidade Federal do Rio de Janeiro, Brasil, 1992.

Salvador, BA - BRASIL  
Abril/2021

To Edna Maria and João Santa Rosa, loves of my life.

**I DEDICATE.**

To Anna Victoria, my favorite little cousin.

**I OFFER.**

# ACKNOWLEDGMENTS

---

*“At times, our own light goes out and is rekindled by a spark from another person. Each of us has cause to think with deep gratitude of those who have lighted the flame within us”.*

ALBERT SCHWEITZER

To my parents, Edna and João, to my brothers: Thiago, Charles and Junior and all my family for the teachings and for the love offered. The strength of your love guided me through life and gave me the wings that I needed and always need to fly. Thank you for understanding my privation, moments of withdrawal and reclusion.

To Karen Pontes and Glória Meyberg, my advisors, who represent my references of seriousness, commitment and professionalism. They always treated me with an open heart, willingness, enthusiasm, patience and goodwill. No word is comprehensive enough to define their importance in my journey. “Inspiration” is the most appropriate. To Karen Pontes, for being my mentor in this trajectory, for encouraging me to do the sandwich doctorate and for making me believe that I was able to go beyond my own expectations. To Glória Meyberg, for every conversation and help throughout the development of this thesis. I am also grateful for the times that, pragmatically, she said: “*Pretinha, veja o quanto já aprendemos!*”. It calmed me down when I thought I wasn't going anywhere and showed me how important what I was trying to do.

To Professor Jens Repke for welcoming me to his research group (dtba) at TU-Berlin during the sandwich doctorate. To colleagues Erik and Alberto for making my journey possible, for all the scientific contributions and for helping me with the first steps in unknown lands. You were fundamental in making my dream come true! I would like to thank the entire dtba team for the welcome and the moments of relaxation. Danke schön, dtba!

To Laio, Epa, Maira, Poli, Gaby, Raquel, Tay, Rafa and Kami for existing in my life!

To Natan Cruz for all the help and to FAFEN, in particular to engineer Vieira for his precious contribution in making the data and operational information available with great patience and goodwill.

To Edilvane Andrade and Alberto Fraga for the motivation to achieve the sandwich doctorate.

To Tatiane Reis, on behalf of PEI employees, thank you for your promptness.

To CAPES for the financial support.

To all who were part of that dream, I dedicate my love and my immense gratitude!

To God, for life.

*„können Sie etwas sehen? ja, wunderbare Dinge“*

*" Can you see anything? Yes, wonderful things."*

JOHANN SEBASTIAN BACH

Abstract of the PhD Thesis presented to PEI/UFBA as part of the requirements needed to obtain the degree of Doctor (PhD).

## **MODELLING OF AMMONIA ABSORPTION PROCESS: FALLING FILM AND PACKED COLUMN**

Licianne Pimentel Santa Rosa

Supervisors: Prof<sup>a</sup>. Dr<sup>a</sup>. Karen Valverde Pontes

Prof<sup>a</sup>. Dr<sup>a</sup>. Glória Meyberg Nunes Costa

Absorbers belong to the group of industrial equipment used for separation/purification of process streams. Among the equipment to promote the absorption, falling film and packed column have an extensive application in industrial plants. So, this thesis aims to propose a phenomenological model for a falling film absorber and to carry out a comparative study between it and a packed column. The falling film model is described by differential mass and energy balances coupled with algebraic equations representing the mass and energy transfer as well as the phase-equilibrium. This modeling approach based on a full DAE (Differential and Algebraic Equations) set is more robust and flexible than the usual approach reported in the literature, wherein sequential algorithms are specifically tailored to solve the model. A packed absorption column is designed by empirical correlations and simulated in Aspen Plus. This thesis also investigates the rigorous thermodynamic description of two possible working fluids:  $\text{NH}_3\text{-H}_2\text{O}$  and the electrolyte system  $\text{NH}_3\text{-H}_2\text{O-CO}_2$ . The absorbers and thermodynamics models results are in accordance with the experimental data from literature. Regarding the comparative study of the absorbers, the technical analysis is based on phenomenological models to predict the efficiency of absorption, monitoring the temperature and concentration profiles. The economic analysis of the absorbers is based on the estimation of the investment and installation cost. The comparative study between the absorbers shows that the falling film type absorber has greater absorption capacity and it is 33% more compact than the column, although at the expense of doubling the investment. For higher concentration, the results suggest that the falling film absorber is preferable than the packed column.

**Keyword:** falling film, packed column, absorption, ammonia and water



# LIST OF FIGURES

---

## CHAPTER II- INDUSTRIAL EQUIPMENT CONTAINING FALLING FILM

Figure 1- Falling film schematic.....	8
Figure 2- (a) Falling film flow (b) tube flow.....	10
Figure 3- Schematic of a falling film evaporator.....	12
Figure 4- Falling film distillation column from Tavarez et. al., (2008).....	15
Figure 5- Falling film absorber (a) plates (Silver 2012), (b) tubes (GEA, 2017)....	17
Figure 6- Refrigeration cycle by ammonia and water absorption. adapted from: Kramer et al. (2016).....	20
Figure 7- Distillation column with plates, packed and falling film.....	22
Figure 8- Falling film schematic (a) Hewitt et al. (1996) e (b) Suntech (2020)....	23
Figure 9- Falling film formed in the tubes.....	23

## CHAPTER III: AN EQUATION-ORIENTED NOVEL APPROACH FOR MODELING THE FALLING FILM ABSORBER USING RIGOROUS THERMODYNAMIC AND TRANSPORT DESCRIPTION

Figure 1- (a) Plates falling film absorber and (b) differential control volume (CV) (adapted from Triché et al., 2016).....	28
Figure 2- Overview of the modeling and simulation framework.....	41
Figure 3- Validation of the VLE Equilibrium model: (a) liquid and (b) vapor phases at 6 atm (c) liquid (d) vapor phases at 10 atm.....	43
Figure 4- Temperature profile along the absorber length.....	47
Figure 5- Liquid (a) and vapor (b) phase concentration profiles along the absorber length, (c) liquid-vapor phase diagram for NH <sub>3</sub> /H <sub>2</sub> O at 6 bar.....	48
Figure 6- (a) Ammonia mass fraction gradients and (b) correlations with mass transfer coefficients ( $FV$ and $FL$ ) and (c) heat transfer coefficients for the vapor and liquid phases.....	49
Figure 7- (a) Analysis of the liquid inlet mass fraction of ammonia along the absorber, influence of coolant (b) and liquid (c) inlet temperature on absorption of ammonia.....	50

## **CHAPTER IV- TECHNICAL AND ECONOMICAL COMPARISON BETWEEN A FALLING FILM AND A PACKED COLUMN FOR ABSORPTION OF NH<sub>3</sub> BY A NH<sub>3</sub>/H<sub>2</sub>O SOLUTION**

Figure 1- (a) Plate falling film absorber (Cavallo, 2020) e (b) packed column absorber	65
Figure 2- Plate falling film absorber (adapted from Triche et al., 2016).....	67
Figure 3- Validation of the UNIQUAC thermodynamic model for the NH <sub>3</sub> -H <sub>2</sub> O VLE (a) ammonia molar fraction at the vapor phase and (b) total pressure.....	80
Figure 4- Variation of ammonia mass fraction at the outlet of the liquid (a) packed column diameter, (b) packed column length and (c) falling film length.....	83
Figure 5- (a) Concentration profile: amount of ammonia absorbed in the liquid phase and (b) liquid temperature profile versus height of the equipment for the falling film and the packed column.....	84
Figure 6- Liquid-vapor phase diagram for NH <sub>3</sub> -H <sub>2</sub> O (rosa et al., 2020).....	85
Figure 7- (a) Influence of ammonia inlet concentration and (b) liquid inlet temperature.	86
References.....	89

## **CHAPTER V- A COMPARATIVE STUDY OF THERMODYNAMIC MODELS TO DESCRIBE THE VLE OF THE TERNARY ELECTROLYTIC MIXTURE H<sub>2</sub>O, CO<sub>2</sub> AND NH<sub>3</sub>**

Figure 1- Ionic dissociation in the ternary system H <sub>2</sub> O-NH <sub>3</sub> -CO <sub>2</sub> .....	97
Figure 2- Interactions considered by the eNRTL model (Chen et al., 2001).....	108
Figure 3- Average ionic activity coefficient for a) NaCl and b) HCl.....	112
Figure 4- Average ionic activity coefficient for a) KNO <sub>3</sub> and b) NaNO <sub>3</sub> .....	113
Figure 5- Total pressure of the system H <sub>2</sub> O-NH <sub>3</sub> -CO <sub>2</sub> predicted by eN+NK and eN+IG and by eU+NK and eU+IG at 313 K a) at 6.33 molal NH <sub>3</sub> and b) AT 11.83 molal NH <sub>3</sub> and at 333 K c) at 6.05 molal NH <sub>3</sub> and c) at 11.95 molal NH <sub>3</sub> .....	116

# LIST OF TABLES

---

## CHAPTER III- AN EQUATION-ORIENTED NOVEL APPROACH FOR MODELING THE FALLING FILM ABSORBER USING RIGOROUS THERMODYNAMIC AND TRANSPORT DESCRIPTION

Table 1- Mass, component and energy balances at the CV.....	62
Table 2- Heat and mass transfer equations at the interface.....	64
Table 3- Correlations for TTP prediction in TEA.....	67
Table 4- Average relative deviation of transport and thermodynamic properties.....	75
Table 5- Validation of the falling film model against experimental data from Triché et al. (2016).....	77

## CHAPTER IV- TECHNICAL AND ECONOMICAL COMPARISON BETWEEN A FALLING FILM AND A PACKED COLUMN FOR ABSORPTION OF NH<sub>3</sub> BY A NH<sub>3</sub>/H<sub>2</sub>O SOLUTION

Table 1- Dimensions of the falling film (Triche et al., 2016).....	67
Table 2- Mathematical model of the falling film.....	69
Table 3- Operating conditions to validate the falling film model at a pressure of 6 bar...70	
Table 4- Correlations for heat and mass transfer coefficients.....	75
Table 5- Models for the VLE description of the ammonia and water mixture reported in the literature.....	76
Table 6- Parameters for cost estimation (adapted from Towler and Sinnott, 2008).....	78
Table 7- Validation of the falling film model with experimental data from Triché et al. (2016).....	81
Table 8- Operating conditions of the packed column at a pressure of 13 bar.....	81
Table 9- Packed column model validation against experimental data from Sieres and Fernández-Seara (2007).....	82
Table 10- Absorption packed column design.....	82
Table 11- Absorbers cost estimation.....	87

# LIST OF ABBREVIATIONS

---

<i>A</i>	Area (m <sup>2</sup> )
<i>z</i>	Length (m)
$\delta$	Thickness of the film (m)
<i>m</i>	Mass flowrates (kg.s <sup>-1</sup> )
$\dot{n}$	Mass flux kg.m <sup>-2</sup> s <sup>-1</sup>
<i>U</i>	Overall heat transfer coefficient though the wall (W-m <sup>-2</sup> K <sup>-1</sup> )
<i>q</i>	Sensible heat flux (W-m <sup>-2</sup> )
<i>H</i>	Enthalpy (J-kg <sup>-1</sup> )
$\tilde{h}$	Partial Mass Enthalpy (J-kg <sup>-1</sup> )
<i>Q</i>	Heat flux(W-m <sup>-2</sup> )
<i>P</i>	Pressure (bar)
<i>R</i>	Ideal gas constant ( )
<i>T</i>	Temperature (K)
<i>d</i>	Diameter (m)
<i>x</i>	Liquid phase composition
<i>y</i>	Vapour phase composition
$\alpha$	Heat transfer coefficient (W-m <sup>-2</sup> K <sup>-1</sup> )
<i>Res</i>	Conductive resistance (W-m <sup>-2</sup> K <sup>-1</sup> )
<i>F</i>	Mass transfer coefficient (kg-m <sup>-2</sup> s <sup>-1</sup> )
<i>Z</i>	Mass fraction of ammonia in the absorbed/desorbed flux
$\psi$	Correction factor
<i>C<sub>p</sub></i>	Specific heat (J-kg <sup>-1</sup> K <sup>-1</sup> )
<i>M</i>	Molecular Weigth (g-mol <sup>-1</sup> )
<i>Sc</i>	Schmidt number
<i>Pr</i>	Prandtl number
<i>D</i>	Diffusivity (m-s <sup>-2</sup> )
$\mu$	Viscosity (Pa-s <sup>-1</sup> )
$\lambda$	Thermal conductive (W-m <sup>-1</sup> K <sup>-1</sup> )
$\rho$	Density (kg-m <sup>-3</sup> )
<i>Re</i>	Reynolds Number

$H'$	Henry's constant (bar)
$v$	Partial molar volume
$f$	Fugacity (bar)
$\gamma$	Activity Coefficient
$a_{22}$	Parameter of the Prausnitz <i>et al.</i> (1978) equation of state
$b$	Parameter of the Prausnitz <i>et al.</i> (1978) equation of state
$\varphi$	Fugacity Coefficient
$ap$	Parameter for the empirical correlation from Pretek and Klomfar (1995)
$mp$	Parameter for the empirical correlation from Pretek and Klomfar (1995)
$np$	Parameter for the empirical correlation from Pretek and Klomfar (1995)

*Superscript*

*	Asymmetric convention
$S$	Saturation State
$P_0$	Reference Pressure
$\infty$	Infinite Dilution

*Subscript*

$hv$	Hydraulic diameter of the vapor in the control volume
0	Reference State
$L$	Liquid Phase
$V$	Vapor Phase
$w$	Coolant
$i$	Component index
$int$	Interface
$h$	Heat
$k$	Correlation composition parameter index

# CONTENTS

---

## CHAPTER I- INTRODUCTION

I.1. Motivation / Justification.....	1
I.2. Objectives.....	2
I.3. Methodological aspects.....	3
I.4. Thesis Structure.....	4
I.5. References.....	5

## CHAPTER II- INDUSTRIAL EQUIPMENT CONTAINING FALLING FILM

II.1. Introduction.....	8
II.2. The falling film technology.....	8
II.3. Equipment containing falling film.....	11
II.4. Falling film absorber / desorbent applications.....	14
II.5. Conclusions.....	22
II.6. References.....	22

## CHAPTER III- AN EQUATION-ORIENTED NOVEL APPROACH FOR MODELING THE FALLING FILM ABSORBER USING RIGOROUS THERMODYNAMIC AND TRANSPORT DESCRIPTION

III.1. Initial Considerations.....	26
III.2. Introduction.....	27
III.3. Mathematical modeling.....	30
III.4. Results and Discussions.....	45
III.5. Conclusion.....	54
III.6. References.....	56

**CHAPTER IV- TECHNICAL AND ECONOMICAL COMPARISON BETWEEN  
A FALLING FILM AND A PACKED COLUMN FOR ABSORPTION OF NH<sub>3</sub> BY  
A NH<sub>3</sub>/H<sub>2</sub>O SOLUTION**

IV.1. Initial Considerations.....	65
IV.2. Introduction.....	65
IV.3. Modelling of Absorbers.....	69
IV.4. Cost estimation of the absorbers.....	79
IV.5. Results.....	82
IV.6. Conclusion.....	90
IV.7. References.....	92

**CHAPTER V- A COMPARATIVE STUDY OF THERMODYNAMIC MODELS  
TO DESCRIBE THE VLE OF THE TERNARY ELECTROLYTIC MIXTURE  
H<sub>2</sub>O, CO<sub>2</sub> AND NH<sub>3</sub>**

V.1. Initial Considerations.....	98
V.2. Introduction.....	98
V.3. Thermodynamic model for the VLE of electrolyte systems.....	105
V.4. Results and Discussion.....	115
V.5. Conclusion.....	121
V.6. References.....	122

**CHAPTER VI- CONCLUSIONS AND SUGGESTIONS FOR FUTURE WORKS**

VI.1. Conclusion.....	126
VI.2. Suggestions for future work.....	127

**APPENDIX A- FALLING FILM MODEL FOR ABSORPTION / DESORPTION  
PROCESS INTRODUCTION**

1. Introduction .....	i
2. Mass, component and energy balances.....	iii

3. Summary of Mass, component and energy balances at CV.....	viii
4. Interface Equations.....	ix
5. Discretization of the energy and mass balances equations.....	xv
6. References .....	xvii

**APPENDIX B- PHYSICAL AND THERMAL PROPERTIES FOR NH<sub>3</sub> AND H<sub>2</sub>O MIXTURE**

1. Introduction .....	xviii
2. Specific Heat.....	xviii
3. Enthalpies of the mixture ammonia and water.....	xxi
4. Partial Specific Enthalpies for the liquid phase.....	xxi
5. Viscosity.....	xxv
6. Thermal Conductivity.....	xxvi
7. Density.....	xxviii
8. Diffusivity.....	xxx
9. References.....	xxxix



# CHAPTER I- INTRODUCTION

---

*“When a human awakens to a great dream and  
throws the full force of his soul over it, all the  
universe conspires in your favor.”*

JOHANN WOLFGANG VON GOETHE

## **I.1. Motivation / Justification**

Equipment for separation/purification processes, whether based on physical or chemical principles, are extremely important in engineering projects and processes. They represent a significant fraction of the capital invested in chemical plants and refineries. Among industrial equipment designed to promote separation, absorbers are widely used, as packed columns, plate columns or falling film. Falling film absorbers is a key equipment in the absorption refrigeration cycle where the refrigerant absorbed by an absorbent solution is desorbed upstream in a highly endothermic process, yielding the refrigeration effect. Packed column has also been employed as absorber in absorption refrigeration cycles. The falling film, though, offers the advantage of being a compact equipment, therefore can be integrated with other unit operations into a single equipment to enhance absorption/desorption.

The falling film absorber consists of a tube or plate where the liquid flows downward by gravity under specific conditions, forming a thin liquid film on its walls. It is possible to get a large contact surface due the thin layer of falling liquid, which allows to increase the rates of heat and mass transfer between liquid and vapor phases. The mathematical modeling of the falling film absorber has enormous industrial importance because it allows process monitoring, development of strategies to improve the absorption process and increase the absorption rates based on the optimization and control of operating conditions. The model can also guide studies towards lower energetic consumption and improved efficiency. Moreover, if the model is formulated and solved by an equation-oriented (EO) approach, unlike the usual approach in literature (Sieres and Fernández-

Seara, 2007, Triché *et al.*, 2016, 2017; Aminyavari *et al.*, 2017), more flexibility is afforded. In EO approach the process model is treated as a set of equations to be solved simultaneously. Flexible models can be applied for absorbers with different geometries and working fluids and can be easily integrated with commercial simulators as well as used in optimization problems. The modeling of the falling film absorber must consider simultaneous description of heat- and mass-transfer besides the phase equilibrium at the interface and the complex fluid regime.

The first step when developing a rigorous model for falling film or packed column is the precise description of the vapor-liquid equilibrium (VLE) of any working fluid because it greatly influences the mass- and heat transfer coefficients as well as the thermodynamic and transport properties (TTP), e.g. enthalpy, heat capacity, viscosity, thermal conductivity etc. The VLE allows determining the equilibrium temperature, pressure and concentrations, therefore VLE plays a key role in the design and operation of the separation processes. Therefore, models able to describe equilibrium conditions are extremely important for the design and operation of the process. To propose more accurate phenomenological models for the falling film absorber, then, thermodynamic models must be carefully chosen for describing the VLE of the working mixture, as the pair  $\text{NH}_3/\text{H}_2\text{O}$ , which is commonly used in refrigeration cycles due to its stability over a wide range of operating temperatures and pressures. There is a plenty of empirical correlations in the literature (Pretek and Klomfar, 1995 and Conde, 2006) for calculating the phase equilibrium of some mixtures, such as the ammonia-water. The use of these correlations, though, limits the model to a given specific system. For greater flexibility of the model, this work proposes using rigorous thermodynamic models, based on equations of state to describe the VLE at the interface, in order to the equation-oriented approach for modeling the falling film can be extended to any working fluid.

## **I.2. Objectives**

### **i. General Objective**

The objectives of this work are to propose a rigorous and flexible phenomenological model for a falling film absorber and to carry out a comparative study of its efficiency with a packed column.

## ii. Specific Objectives

- Evaluate the thermodynamic models to represent different working fluids, as  $NH_3$  e  $H_2O$  and  $NH_3, CO_2$  e  $H_2O$ ;
- Develop a phenomenological mathematical model to represent the falling film absorber;
- Implement CAPE-OPEN interfaces for calculating thermodynamic and transport properties in the falling film model;
- Validate the model of the falling film absorber with experimental data from the literature for the working fluid  $NH_3$  e  $H_2O$ ;
- Carry out a comparative study in terms of absorption capacity and equipment installation cost between the falling film absorber and the packed column applied to ammonia absorption.

### I.3. Methodological aspects

One of the objectives of this work is to model and simulate a falling film absorber whose process solution is the mixture of ammonia and water and to carry out a comparative study of its efficiency with a packed column. For the implementation of the falling film model developed in this work, the MOSAICmodeling (<http://mosaic-modeling.de/>) is used. This software was developed by TU-Berlin and allows code generation in various computing environments. The proposed model can be generated in several programming languages, as well as incorporated into commercial simulators. This fact was decisive in the choice of this platform because established commercial simulators, such as Aspen Plus, do not offer the model for the falling film contactors.

The falling film model approach is proposed as a system of differential and algebraic equations to be solved simultaneously, without the need to program tailor-made algorithms. This approach provides flexibility to the model, as it can be easily integrated with flowchart simulations and large-scale simultaneous optimization problems. Another differential, compared to the models usually proposed in the literature (Sieres and Fernández-Seara, 2007, Triché *et al.*, 2016, 2017; Aminyavari *et al.*, 2017), is the rigorous

calculation of the vapor-liquid equilibrium at the interface. The phase equilibrium is described by a general representation, which can be extended to other working fluids, relying on a rigorous thermodynamic modeling. Another important aspect regarding the methodology adopted in this work is related to the calculation of thermodynamic and transport properties (TTP) in the model of the falling film absorber. They are calculated by the Thermodynamics for Engineering Applications (TEA) software and integrated to the model via CAPE-OPEN interfaces.

A packed absorption column to promote the absorption of ammonia is designed by empirical correlations from Norton Chemical Company (Norton, 1977). Given the design parameters, type of packing, height and diameter of the column, the commercial simulator Aspen Plus was used to simulate the packed column for the absorption of ammonia by a solution of ammonia and water.

An important concern when extending the falling film model to others mixtures is in the modeling of VLE, modeling of thermodynamics and transport phenomena properties and the heat and mass transfer coefficients, since they play a key role in the accuracy of the process model. As a first step to demonstrate the flexibility of the equation-oriented approach for modeling the falling film absorber, the VLE of the electrolytic mixture  $\text{NH}_3\text{-CO}_2\text{-H}_2\text{O}$  has been investigated due to its potential application in carbon capture processes. The addition of  $\text{CO}_2$  triggers species dissociation in the liquid phase. Since the species do not dissociate completely in aqueous solution, the molecular compounds are in chemical equilibrium with the electrolytes. Therefore, thermodynamic models for electrolyte and non-electrolyte systems (or mixtures) have been compared and validated with experimental data from literature.

### **I.4. Thesis Structure**

This thesis is composed of six chapters, including this introductory chapter, and two appendices.

Chapter II (Industrial Equipment Containing Falling Film) aims to provide a summary of the industrial equipment that uses falling film technology, with an emphasis on absorbers. In addition, some industrial processes are exemplified: refrigeration absorption cycle and integrated column with a section of falling film.

Chapter III (A Rigorous Approach for Modeling and Simulation of an Ammonia Water Falling Film Absorber) presents an equation-oriented novel approach for modeling the falling film absorber using rigorous thermodynamic and transport description. The content of this chapter was published in the Chemical Engineering Research and Design (ROSA, L. P. S, PONTES, K. V., COSTA, G. M. N., PENTEADO, A. T., ESCHE, E. REPKE, J. -U. An equation-oriented novel approach for modeling the falling film absorber using rigorous thermodynamic and transport description. Chemical Engineering Research and Design, 159: 179–194, 2020). This chapter aims to describe the proposed rigorous and flexible model for falling film absorbers. Initially, a review of the literature on models for falling films is presented. Subsequently, the falling film is modeled in an equation-oriented approach and the proposed model is validated with experimental data from the literature. The results discuss the influence of the operating variables on the performance of the absorption process.

Chapter IV (Technical and Economical Comparison Between a Falling Film and a Packed Column for Absorption of  $\text{NH}_3$  by a  $\text{NH}_3/\text{H}_2\text{O}$  Solution) aims to carry out a comparative study between the falling film absorber and the packed column. A packed column is designed from empirical correlations and modeled in Aspen Plus. The falling film is based on the phenomenological model proposed in the Chapter III. The performance of the absorbers was evaluated based on the concentration and temperature profiles at the liquid phase. An evaluation of the efficiency in terms of ammonia concentration in the liquid phase, design, operational parameters and equipment cost estimates between the absorbers is also presented.

Chapter V (A Comparative Study of Thermodynamic Models to Describe the VLE of the Ternary Electrolytic Mixture  $\text{H}_2\text{O}-\text{CO}_2-\text{NH}_3$ ) presents the analysis of the thermodynamic model to represent the mixture  $\text{H}_2\text{O}-\text{CO}_2-\text{NH}_3$ . The content of the chapter was published in the Chemical Product and Process Modeling (ROSA, L. P. S., CRUZ, N., PONTES, K. V., COSTA, G. M. N. Comparative Study of Thermodynamic Models to Describe the VLE of The Ternary Electrolytic Mixture  $\text{H}_2\text{O}-\text{CO}_2-\text{NH}_3$ . Chemical Product and Process Modeling, 2021). The bibliographic review of the models used to describe the electrolyte system  $\text{H}_2\text{O}-\text{CO}_2-\text{NH}_3$  is presented. The UNIQUAC equations for electrolytes and NRTL for electrolytes are used to describe the liquid phase, and the Nakamura equation and the ideal gas equation are used to describe the vapor phase. In addition, a comparative study is carried out on the influence of the selected models to

represent the non-idealities of the liquid and vapor phase and on the description of the equilibrium data of the system  $\text{H}_2\text{O}-\text{CO}_2-\text{NH}_3$ . Another contribution of this chapter is related to the possibility of considering the vapor phase as an ideal gas at the operating conditions studied, without losing precision.

Finally, Chapter VI summarizes the conclusions obtained in this thesis and offers suggestions for future work.

This thesis further has two appendices. Appendix A aims to show the mass and energy balance equations for the falling film which is used for absorption and desorption processes and Appendix B aims to show the models used to calculate transport and thermodynamics properties (enthalpies and specific heat, diffusivity etc.) for the system ammonia-water.

## I.5. References

AMINYAVARI, M., APRILE, M., TOPPI, T., GARONE, S., MOTTA, M., A detailed study on simultaneous heat and mass transfer in an in-tube vertical falling film absorber. *International Journal of Refrigeration* 80 (2017) 37–51.

CONDE, M., Thermophysical properties of ammonia-water mixtures for the industrial design of absorption refrigeration equipment, M. CONDE Engineering, (2006).

FERNANDEZ-SEARA J., SIERES J., RODRIGUEZ C, Vazquez M Ammonia–water absorption in vertical tubular absorbers. *Int. Therm Sci* (2005) 44, 277–288.

Norton Chemical Company, Design Information for Packed Towers, Bulletin DC-II, Akron, OH: Norton Chemical Company, 1977.

PRETEK, J. and KLOMFAR, J. Simple functions for fast calculations of selected thermodynamic properties of the ammonia-water system: *Int. J. Refrigeration* 18 (1995), 228–234.

SIERES, J FERNANDEZ-SEARA J., Modeling of simultaneous heat and mass transfer processes in ammonia–water absorption systems from general correlations. *Heat Mass Transfer* 44, (2007), 113–123.

TRICHÉ D., BONNOTA, S., PERIER-MUZETA, M., BOUDÉHENNA F. DEMASLESA H., CANEY, N. Modeling and experimental study of an ammonia-water falling film Absorber SHC 2015, *International Conference on Solar Heating and Cooling for Buildings and Industry Energy Procedia* 91, (2016), 857 – 867.

TRICHÉ D., BONNOTA, S., PERIER-MUZETA, M., BOUDÉHENNA F. DEMASLESA H., CANEY, N. PERIER-MUZET, M. Experimental and numerical study of a falling film absorber in an ammonia-water absorption chiller. *International Journal of Heat and Mass Transfer* 111, (2017), 374–385.

# CHAPTER II- INDUSTRIAL EQUIPMENT CONTAINING FALLING FILM

---

*“Just remember, once you're over the hill you  
begin to pick up speed.”*

ARTHUR SCHOPENHAUER

## **II.1. Introduction**

There are several equipment for process separation and the selection of the most suitable for a given process depends on the objectives to be achieved (output stream specifications) and on economic factors as well. They involve unitary operations based on amount of momentum (decantation, grinding, etc.), mass transfer (extraction, adsorption, etc.) and heat transfer (heat exchangers, etc.) (Fonsceca Jr, 2013). Some separation equipment, on the other hand, can join the heat- and mass transfer, as evaporation, crystallization, absorbers with endothermic / exothermic absorption, distillation and falling film, for example. The falling film has been widely applied in industrial processes such as evaporation, absorption or even inside an absorption column.

Considering that this thesis focuses on the falling film type absorber, this chapter provides a synthesis of the literature on industrial equipment that uses the falling film technology, with an emphasis on absorbers. Firstly, phenomenological aspects related to falling film are discussed to provide a background on the principle of operation of this technology. Then, some industrial processes that use falling film absorbers, such as refrigeration absorption cycle and urea production, will be detailed. In addition, general aspects related to the modeling of falling film absorbers will be discussed.



## II.2. The falling film technology

The falling film is found in a variety of industrial processes that involve simultaneous heat- and mass transfer, such as absorption, desorption, evaporation, distillation etc. Generally, the operating principle of the falling film consists of a tube or plate where the liquid flows downward by gravity under controlled conditions, forming a thin liquid film on its walls, as Figure 1 depicts. The main advantage of this device is the large contact surface of the thin layer of falling liquid, which allows high rates of heat- and mass transfer between liquid and vapor phases, requiring a small flow of liquid (Teleken, 2013). Depending on the application, the liquid might evaporate or the vapor might be absorbed or desorbed.

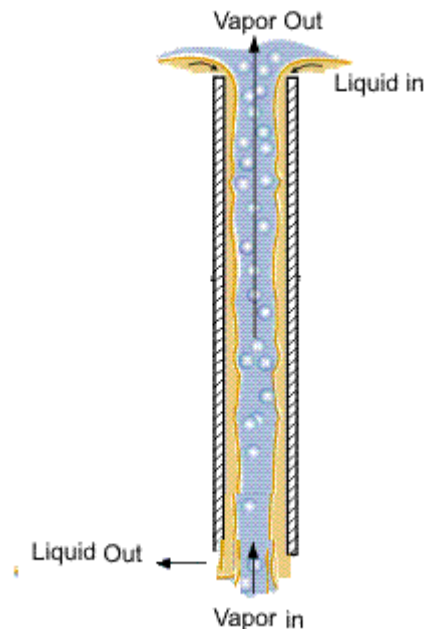


Figure 1- Falling Film representation (Adaptation from Hewitt, 2020 )

Due to the formation of falling film, these devices have some specific characteristics (Teleken, 2013):

- Large contact surface of the thin layer of falling liquid;
- Low residence time;
- High rates of heat and mass transfer;
- Low thermal resistance.

The surface velocity of the falling liquid phase must be high enough to ensure that the liquid film completely wet the column/plate wall, avoiding the formation of dry spots and their eventual rupture. This rupture causes a discontinuity in the film and preferential flow can occur (Ribatski and Jacobi, 2005). The rupture of the film is an undesirable phenomenon, as it can reduce efficiency and lead to overheating or corrosion of the equipment wall. On the other hand, the surface velocity of the film should not be too high to prevent it from falling off the wall because, at very high velocity, the film does not remain stable and its adherence to the wall is compromised (Gonçalves, 2015). The surface velocity of the film is changed according to each type of fluid and geometry used. More viscous fluids tend to form more stable films while less viscous ones develop higher velocities and thinner films, then more susceptible to breakage.

Given the importance of surface velocity, related hydrodynamic aspects need to be discussed. The classification of fluid a flow in falling film is not as trivial as in internal flows in pipes. Figure 2a shows the velocity profile for the flow inside a falling film and the Figure 2b shows the velocity profile for the flow inside a pipe. The classification of fluid flow is given based on the Reynolds number of the film, defined by:

$$Re_{film} = \frac{2\Gamma}{\mu_L} \quad (\text{II.1})$$

where  $\Gamma$  is the mass flow rate per tube perimeter unit and  $\mu_L$  is the viscosity of the liquid. According to Grossman (1984), flows involving falling film can be classified, depending on the Reynolds number of the film, in three regimes: laminar flow ( $Re_{film} \leq 20$ ), flow with waves on the surface, partially laminar and partly turbulent ( $20 < Re_{film} \leq 4000$ ) and completely turbulent ( $Re_{film} > 4000$ ).

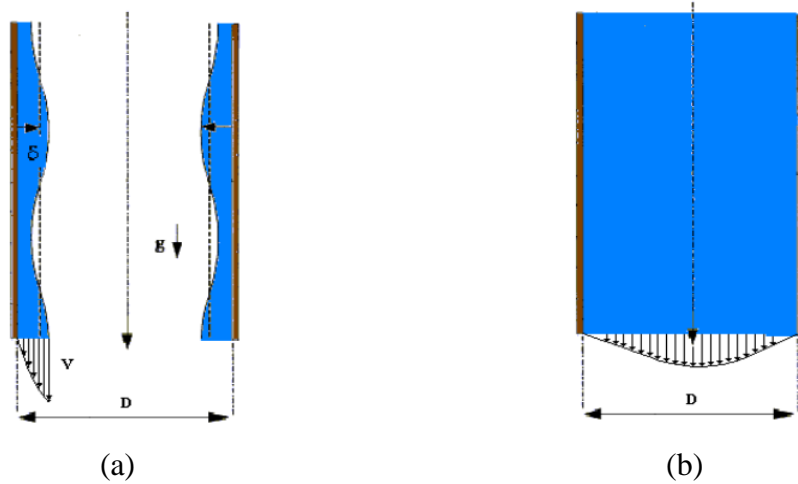


Figure 2- Velocity Profile: (a) Falling film flow (b) Tube flow

Another hydrodynamic aspect that must be taken into account in fluid flows inside the falling film is the definition of the thickness of the falling liquid, since it has a great influence on the heat and mass transfer characteristics. Regarding the heat and mass transfer, thickness is associated with its resistance: the greater the thickness, the greater the resistance and, consequently, the lower the heat and mass exchange. Koskie et al. (1989), however, pointed out that, due to the disturbances caused by waves at the film interface, the knowledge of the thickness is not a trivial task. Nusselt (1916), then, introduced the theoretical analysis of the falling film and, through balances of viscous and gravitational forces, proposed the following expressions for calculating the thickness of the film:

$$\delta_{film} = Re_{film}^{\frac{1}{3}} \left( \frac{3\mu_L^2}{g\rho_L^2} \right)^{1/3} \quad Re \leq 1600 \quad (II.2)$$

$$\delta_{film} = Re_{film}^{\frac{1}{3}} \left( 0.137^2 \frac{\mu_L^2}{g\rho_L^2} \right)^{1/3} \quad Re > 1600 \quad (II.3)$$

where  $Re_{film}$  is the Reynolds number from the film,  $\mu_L$  is the viscosity of the liquid,  $g$  é gravity and  $\rho_L$  is the specific gravity of the liquid. Viscosity of liquids generally decrease with temperature, allowing higher flow rates and lower residence times. The liquid layer must be quite thin to allow a high thermal transfer coefficient but, on the other hand, must not be encrusted in the tubes because of the thin layer.

According to Goel (2005), the key features of an efficient design of a falling film are high heat and mass transfer coefficients, large surface contact area, low-pressure drop in the liquid, vapor and coolant phases. A higher pressure drop in the vapor phase will raise the equipment temperature, and consequently the coolant temperature. The flow of the vapor is inherently linked to the pressure drop, when the velocity of fluid increases, the collision between molecules increases resulting into greater loss of kinetic energy, in turn, greater pressure drop.

### **II.3. Equipment containing falling film**

This section aims to briefly present some industrial equipment that uses the falling film technology. There is a wide application of falling film in evaporators, absorbers and distillation columns, which will be detailed next.

#### *i. Evaporators*

Evaporation is a unit operation that aims to concentrate a solution by eliminating the solvent by boiling. As can be seen in Figure 3, evaporators have a thermal surface, which transfers heat to the solution and a compartment that collects the concentrated solution (Araújo, 2012). Evaporators might be classified into three categories regarding the vapor separation mechanism: natural circulation; forced circulation and falling film. This section emphasizes the falling film evaporators, which will be detailed below.

Falling film evaporators are composed by a shell and tubes or plates, in which the product circulates through the tubes and the steam through the shell, heating the outer walls of the tubes or plates. The liquid falls evenly through the tubes due to gravity, forming a thin layer that is heated by contact with the inner wall of the tubes. Figura 3 shows the schematic of a falling film evaporator.

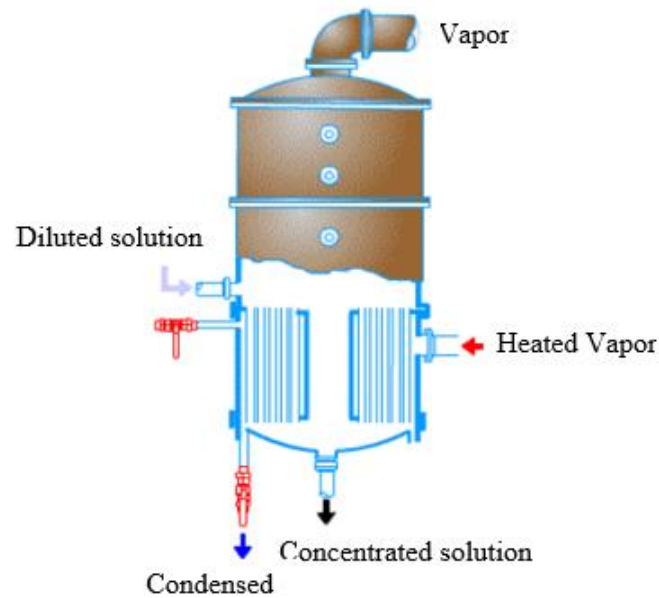


Figure 3- Schematic of a falling film evaporator.

Falling film evaporators have been widely studied in the literature, specially, according to McCabe et. al. (1991), to concentrate materials that are highly sensitive to heat and need minimum time of heat exposure. Marquardt et al (2010) published the second edition of the book *Process Thermal Desalination Process*, dedicating one chapter to the modeling, control and dynamics of horizontal falling film evaporators. The authors synthesized the state of the art of dynamic modeling and control of horizontal falling film evaporators. In addition, results inherent to controllability limitations or applications of advanced control schemes are reported in the book. Silva et al. (2011) compared flash with falling film type evaporators for concentrating sugar cane juice solution based on process modeling in EMSO software (Environment for Modeling Simulation and Optimization). They observed that both evaporators present satisfactory results in terms of juice concentration, however, the falling film absorber offers more heat transfer rates. Karlsson et al. (2013) studied heat transfer coefficients over a wide range of Prandtl numbers (from 10 to 2800) in a pilot falling film evaporator to concentrate black liquor. This dimensionless number is the ratio between momentum and thermal diffusivity and, in heat transfer problems, monitors the relative thickness and thermal boundary layers. Results showed that viscosity was clearly the most important parameter for the heat transfer coefficient while the mass flow had little influence. The experimental results were compared with heat transfer correlations from the literature, but none of the studied correlations was able to reproduce the heat transfer coefficient for the entire Prandtl

number range studied. Dumma et al. (2015) modeled a triple effect falling film evaporator observing an increase of 199.19% in the evaporated mass compared to single stage evaporator. The authors further observed that a decrease in supply pressure implies a decrease in the mass flow of the evaporated liquid. Liu et al (2017) studied the influence of the distributor on the performance of the falling film evaporator. The distributor determines the uniformity of the fluid distribution in the falling film evaporator. The authors used a plate-type dispenser positioned just below the liquid inlet and observed that the liquid is better distributed in the evaporator when the fluid velocity is increased.

*ii. Distillations columns*

Distillation is a unit operation to separate the components based on the difference in volatility of the components of a liquid mixture. It depends on the distribution of the components between the vapor phase and the liquid phase. The falling film distillation is a non-conventional distillation method that has been applied in several works in the literature as well as in industrial processes as in petrochemical, refrigeration and food processing (Wang et al., 2010).

Falling film distillation is a process with a low residence time where it is possible to obtain high rates of mass and heat transfer (Gonçalves, 2015). In addition, the equipment has a simple structure when compared to conventional distillation. As can be seen in Figure 4, it basically consists of concentric vertical tubes through which the liquid flows downward forming a film on the walls of the tube. At the inner tube the film is formed and evaporation and condensation occur. The energy-carrying fluid (steam) circulates in the tube in the middle to promote the evaporation of the film. The external tube thermally insulates the column. The steam is condensed and collected at the top of the column, while the liquid exits at the bottom of the column.

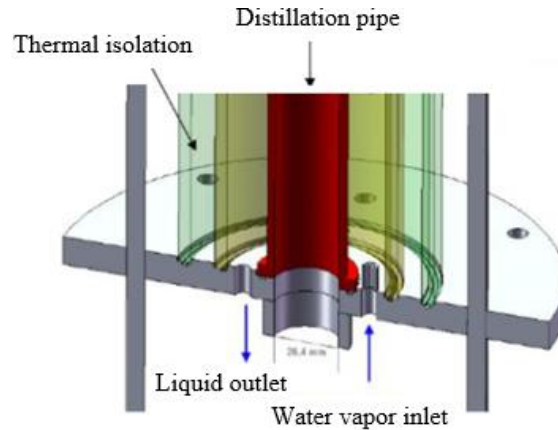


Figure 4- Falling film distillation column (Tavarez et. al., 2008)

Lopes (2014) carried out the simulation of a falling film distillation column to distillate petroleum. Teleken (2013) performed a computational fluid dynamic (CFD) study to evaluate the efficiency of the feed distribution system on the falling film distillation process for ethanol and water separation. The author investigated the process with two distinct temperature profiles, isothermal and non-isothermal, on the evaporation surface. Batistella and Maciel (1996) compared the distillation of thermally sensitive components carried out in centrifugal distillation column and in a falling film column. The author concluded that the falling film distillation column can operate at a comparatively lower temperature than the centrifugal distillation column but with longer residence time. The longer residence time of the falling film can lead to the thermal decomposition of the components. Thus, the choice of the appropriate distiller must be made considering the temperature limit and the acceptable exposure time. Gonçalves (2015) simulated the flow of falling films on the inner wall of a cylindrical distillation column using two groups of fluids: viscous fluids (soy oil and Spindura oil) and the less viscous fluids (water) with the goal to evaluate the phenomenon of heat transfer with phase change. They considered the isothermal condition and the heating of the wall for partial liquid vaporization. The author could study the fluid dynamic behavior and heat transfer phenomenon at this equipment. He concluded that heat flow through the wall was more intense in regions where the thickness of the liquid film is greater, that is, in the first half of the column, mainly at the point close to the feed. Therefore, the highest degree of evaporation occurred in the first half of the column, where both the heat flow and the thickness were greater.

### ii. Absorbers

Absorption is an operation in which one or more components of the feed gas mixture dissolves in the liquid. It is the inverse of desorption (stripping), when the volatile compounds in the liquid are transferred to the gas phase (Green, 2007). Absorption and desorption or stripping have important applications in the purification of products, in refrigeration cycles, as well as in environmental protection processes. Desorption or stripping is commonly used to remove volatile organic compounds (VOC's), such as benzene in wastewater. The fundamental objective of the absorption / desorption column is to create an intimate contact between the liquid and gaseous phases to allow the diffusion of chemical species between the constituent phases.

Several absorber configurations have been studied due to the need to increase the rates of heat and mass transfer, and the requirement for more compact and efficient equipment. The most common absorbers are falling film, packed bed and bubble absorbers (Gallo, 2016). Revello (1998) highlights that falling film absorbers have been widely used in mass transfer studies due to their simplicity in experimental construction and in the determination of the gas-liquid contact area. Many studies have been carried out on gas absorption in liquid films with different flow regimes, geometries and boundary conditions (Grossman, 1983). Figure 5 shows two types of falling film absorbers: plate and tube. The fundamentals of the modelling of the two absorbers is the same, the difference relies in the contact surface area, since they have different geometries.



Figure 5- Falling film absorber: (a) plates (Triche et. al., 2017), (b) tubes (Gea, 2017).

Among the various applications of absorbers, this work is concentrated on falling film absorber for ammonia and water refrigeration cycles. Many prototypes of falling film absorbers applied to refrigeration cycles have been published in the literature. Nishimura



et al. (2011) presented a prototype absorber which enables to observe a falling film of aqueous lithium bromide on the tubes. The prototype allows to measure the temperature distributions of the falling film, cooling water and tubes. The ratios of wettability of tubes surface were estimated, and heat transfer values on the absorber were evaluated. They calculated the flux of heat transfer and validated against experimental data. Fonseca Jr. (2013) proposed a prototype of a vertical falling film absorber that was designed and built to be applied in the absorption refrigeration cycle. The prototype allows to determine heat and mass transfer correlations in the steam absorption process by water-lithium bromide solutions. Triché et al. (2016) developed an experimental apparatus and mathematical model of a plate falling film plate absorber. The authors used ammonia and water as the working fluid and considered simultaneous heat and mass transfer in the model. The numerical results were validated with experimental data. Aminaravy et al. (2017) also used ammonia and water as the working fluid, however the absorber was a vertical falling film with tubes. The authors used the experimental results obtained by their prototype to validate the model proposed for them.

#### **II.4. Falling Film Absorption / Desorption Applications**

This section aims to survey some applications of absorption and desorption involving falling film. Firstly, the use of absorbers in the refrigeration cycle will be discussed. It is the most common application and one of the oldest refrigeration methods. According to More et al. (2018), different pairs of fluids (refrigerant and absorbent), are used in falling film absorption: ammonia-water; water-lithium bromide; ionic liquids where  $\text{H}_2\text{O}/[\text{emim}][\text{BF}_4]$ ,  $\text{H}_3/[\text{N}_{11}\text{H}(\text{EtOH})][\text{MeCOO}]$  are the most common. Secondly, the use of falling film integrated with plates and packing in a separating column is discussed. This equipment is found in the urea production process at the Bahia Nitrogen Fertilizer Factory (Fafen).

##### *a. Absorption Refrigeration Cycle*

Chiller is a machine that removes heat from a liquid in a refrigeration system. They are used for controlled cooling of products, mechanisms and factory machinery in a wide range of industries. They are often used in the plastic industries, injection and blow molding, metal working cutting oils, welding equipment, die-casting and machine tooling, chemical processing, pharmaceutical formulation, food and beverage processing,

paper and cement processing, vacuum systems, X-ray diffraction, power supplies and power generation stations, analytical equipment, semiconductors, compressed air and gas cooling. They are also used to cool high-heat specialized items such as Magnetic resonance imaging (MRI) machines and lasers, and in hospitals, hotels and campuses. To achieve low temperatures in industrial systems, different refrigeration cycles are used. The most used are heat pump systems, absorption refrigeration systems and vapor compression cycle (Flori e Vîlceanu, 2012). Absorption systems offer some advantages, such as high reliability, quiet operation, long service life, low maintenance cost and the possibility to use renewable energies (Vasilescu et al., 2011).

The performance of an absorption refrigeration system is extremely dependent on the chemical and thermodynamic properties of the working fluid. A fundamental requirement for an absorbent / refrigerant combination is that, in the liquid phase, they need to be miscible in the operating temperature range of the cycle (Moraes, 2012). Ashrae (1981) highlights further characteristics of the absorbent / refrigerant pair:

- **Affinity:** the absorbent must have great chemical affinity with the refrigerant. A good absorbent / coolant pair is defined by the amount of heat generated during absorption. In other words, the amount of energy (or heat) released on absorption is a crude measure of chemical affinity.
- **Volatility ratio:** the refrigerant must be more volatile than the absorbent, so that the separation between them is facilitated.
- **Viscosity:** Fluids must have low viscosity to promote the processes of heat and mass transfer, as well as to minimize problems related to the pumping of fluids.
- **Absence of solid phase:** the refrigerant-absorbent pair must not form a solid phase under the operating conditions of the absorption system, as this may cause equipment shut down.
- **Chemical stability:** fluids must be stable, as any instability can result in the formation of harmful substances such as: gases, solids or corrosive species.
- **Corrosion:** it is important that the working fluids do not attack the materials that make up the absorption system. Generally, corrosion inhibitors are used to preserve materials and equipment.

- Safety: it is also important that the working fluids are neither toxic nor flammable, being harmless to the environment.

According to Flores et al. (2014), the lithium bromide and water pair presents a risk of crystallization in compositions above 68%, thus compromising the operation of the refrigeration cycle. On the other hand, the ammonia and water mixture is more stable under wide operating conditions (Srikhirin et al., 2001). In addition, it can be used at low temperatures, since the freezing point of ammonia is 196.15 K. Figure 6 depicts a single-stage absorption refrigeration cycle with ammonia and water as absorbent-refrigerant pair. The refrigerant produces a cooling effect in the evaporator and releases heat into the atmosphere through the condenser. This cycle can be divided into two parts: high pressure and low pressure. The cycle starts when the stream with high ammonia concentration at low pressure passes through the evaporator (stream 1) where ammonia vaporizes in a highly endothermic process, providing the cooling effect and yielding a vapor stream with 99% in mass of ammonia (2). At the absorber, the liquid mixture, which comes out of the expansion valve (stream 7) with low ammonia concentration (weak solution) absorbs, exothermically, the ammonia from the gas stream 2, yielding a solution rich in ammonia (stream 3). The rich solution is pumped to higher pressure to a heat exchanger to be preheated before entering the generator, where a hot source provides heat and part of the liquid evaporates being released by the solution. The remaining solution (stream 6), poor in ammonia, returns to the absorber after being pre-cooled in the heat exchange and passing through the expansion valve (stream 7). This is a pressure reducing valve to maintain the pressure difference between the generator and the absorber. The vapor phase, rich in ammonia, reaches the condenser (stream 5) and rejects heat to the environment until saturation in the liquid phase is achieved (stream 8). Stream 8 passes through the expansion valve and enters the evaporator, closing the cycle.

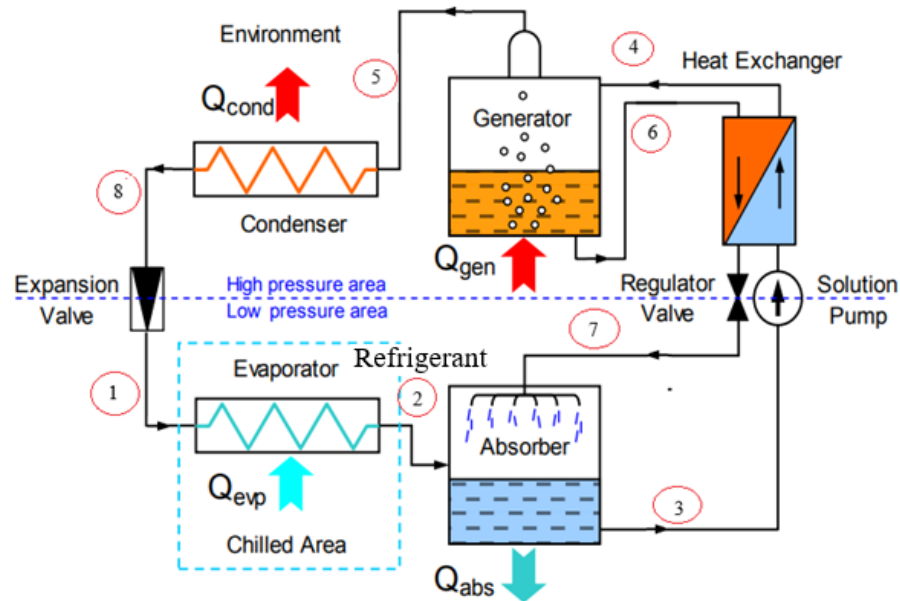


Figure 6- Refrigeration cycle by ammonia and water absorption. Adapted from: Kramer et al. (2016)

Among the equipment that make up the absorption refrigeration cycle, the absorber is the operation that determines the overall performance of the system since the amount of refrigerant (ammonia) absorbed reflects in the heat exchange in the evaporator to yield the chiller effect. (Lázaro-Colán, 2012; Mittermaier and Ziegler, 2015). The falling film is the most common type of absorbers used in absorption refrigeration cycle (Goel and Goswamy, 2005a, 2005b; Triché *et al.*, 2016; Aminaravy et al., 2017 and Rosa et al., 2020), however the use of packed column is also reported (Selim and Elsayed 1999a, 1999b). Therefore, the falling film absorber used in a refrigeration cycle with ammonia and water is the main focus of this thesis.

#### *b) Separating column of the urea production process*

The falling film might also be integrated with other unit operations for more specific applications, such as the purifying column depicted in Figure 7. This column operated in the urea production process of Fafen (Nitrogen Fertilizer Factory) located at the petrochemical pole in Camaçari to purify the electrolyte solution containing Urea-NH<sub>3</sub>-CO<sub>2</sub>-H<sub>2</sub>O. This purification is carried out by dragging unreacted ammonia, carbon dioxide and water from the solution, consequently concentrating the solution in urea. This column is divided into three sections: plates (top), falling film (center) and packing (bottom). There are two diffusers, one above the first plate and the other above the falling film section, which are essential for a uniform and non-preferential liquid flow inside the

column. The second diffuser feeds liquid to a support where the tubes of the falling film are inserted (Figure II.8). According to FAFEN operation manual (FAFEN, 2007), this column operates at low pressure, about 3.43 bar and temperature slightly above 100 ° C.

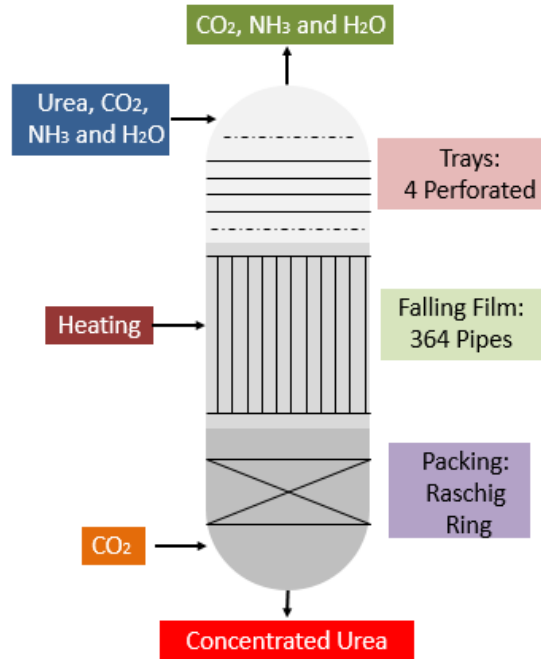


Figure 7- Distillation column with plates, packed and falling film.

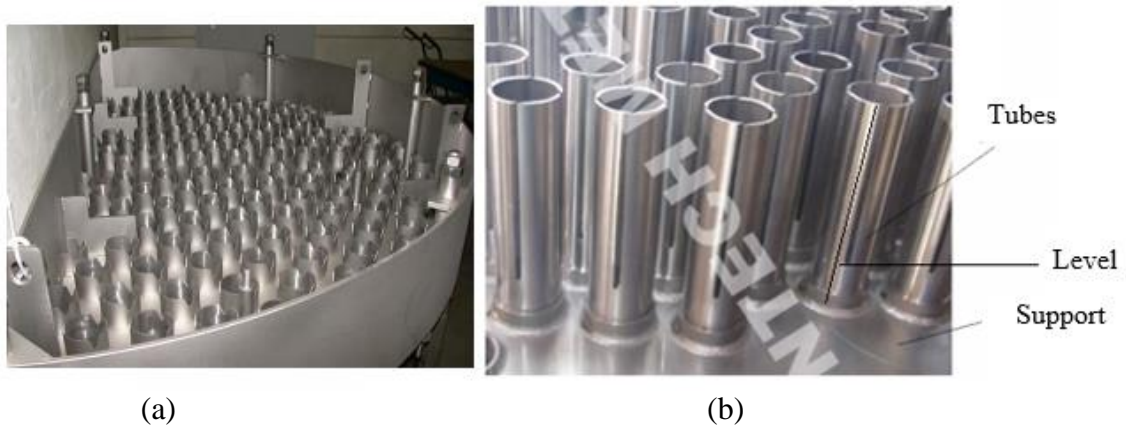


Figure 8- Falling film Schematic (a) Hewitt et al. (1996) e (b) Suntech (2020).

When the level on the support increases, the liquid reaches the top of the tubes (Figure 9) and flows down the walls of the tubes. The central part of the tubes is free of liquid and is filled with the gas stream, containing CO<sub>2</sub>, H<sub>2</sub>O and NH<sub>3</sub>, the latter two being removed from the liquid stream by desorption. CO<sub>2</sub> is injected at the bottom of the column to favor the entrainment of gases that are desorbed from the falling film. The tubes are

inside a hull devoid of baffles where saturated steam is condensed to provide heat to the desorption. The stream does not contact the fluid inside the tubes.

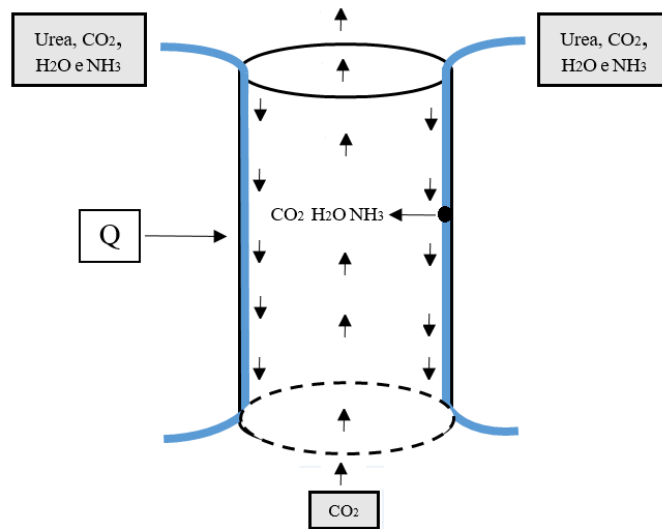


Figure 9- Falling film formed in the tubes.

## II.5. Conclusions

This chapter presented a synthesis of the literature on industrial equipment that uses falling film technology, with emphasis on absorbers. Falling film type absorbers have been widely used by the industry due to the high rates of heat and mass transfer and can be found in different geometries, such as: vertical tubes, plates, horizontal tubes etc. A very important and widespread application of falling film absorbers is in the absorption refrigeration cycle. A model representing the falling film would be able to predict the behavior of the system, therefore would be a valuable tool for design, operation and optimization. Therefore, the next chapter is dedicated to develop a flexible and rigorous model to describe a falling film absorber.

## II.6. References

AMINYAVARI, M., APRILE, M., TOPPI, T., GARONE, S., MOTTA, M., A detailed study on simultaneous heat and mass transfer in an in-tube vertical falling film absorber, *International Journal of Refrigeration* 80 (2017) 37–51.

ASHRAE. Equipment. In: *ASHRAE Handbooks*. Atlanta, 1981, p. 3.2-3.12.

BATISTELLA, C. B.; WOLF MACIEL, M. R. Modeling, simulation and analysis of molecular distillators: centrifugal and *falling film*. Computer Chemical Engineering., 20, 1996, 19-24.

BOHRA, L. K., Analysis of Binary Fluid Heat and Mass Transfer in Ammonia-Water Absorption. PhD Dissertation Presented to The Academic Faculty, Georgia Institute of Technology, (2007).

DUNNA, V. and KISHORE, .P.S. Thermal Analysis on Triple Effect Falling Film Evaporator International Journal for Scientific Research & Development| Vol. 3, Issue 06, 2015 | ISSN (online): 2321-0613.

FLORES, V. H. F., ROMÁN, J. C., ALPIREZ, G. M. Performance Analysis of Different Working Fluids for an Absorption Refrigeration Cycle, American Journal of Environmental Engineering4(4A), (2014), 1- 10.

FLORI, M., VÎLCEANU, L., Performance Characteristics of Vapor Compression Refrigeration Systems. Annals of Faculty Engineering Hunedoara- International Journal of Engineering 2, (2012), 145-148.

FONSCECA Jr. J. A., Metodologia experimental para estudo da transferência de calor e massa no processo de absorção do vapor d'água por filmes verticais descendentes de água-brometo de lítio. Dissertação de Mestrado Em Ciências Mecânicas, Universidade de Brasília, 2013.

GEA 2007, Distillation Technology, Retrieved from <https://www.gea.com/en/products/distillation-fermentation/distillation/reboiler-for-distillation-plants.jsp>.

GEANKOPLIS, C. J. Transport Processes and Unit Operations. 3 ed. Englewood Cliffs: Prentice Hall, 1993.

GOEL, N, GOSWAMI DY. A compact Falling Film Absorber. Journal of Heat Transfer September, (2005b) vol 127/ 957.

GOEL, N, GOSWAMI DY. A compact Falling Film Absorber. Journal of Heat Transfer 127, (2005b), 957-965.

GONÇALVES, C., S. Simulação de películas líquidas descendentes em geometria axissimétrica com e sem evaporação. Dissertação de mestrado do Programa Pós Graduação em Engenharia Química da Universidade Federal de Santa Catarina, 2015

GROSSMAN, G. Simultaneous heat and mass transfer in film absorption under laminar flow. International Journal of Heat and mass transfer 26, (1983), 357-71.

HEWITT, G. F., SHIRES, G. L., AND BOTT, T. R. Process Heat Transfer. Begell House, New York and CRC Press, Boca Raton, FL, 1994.

HEWITT, G. F. EVAPORATORS A-to-Z Guide To Thermodynamics, Heat & Mass Transfer, And Fluids Engineering (2020).

KANG, Y.T., AKISAWA, A., KASHIWAGI, T. Analytical investigation of two different absorption modes: falling film and bubble types. *Int. J. Refrigeration* (2000) 23, 430–443.

KARLSSON, E., GOURDON, A, OLAUSSON B. L., VAMLING, L. Heat transfer for falling film evaporation of black liquor up to very high Prandtl numbers. *International Journal of Heat and Mass Transfer* 65 (2013) 907–918.

Koskie, J. E., Mudawar, I., & Tiederman, W. G. Parallel-wire probes for measurement of thick liquid films. *International Journal of Multiphase Flow*, (1989), 15(4), 521–530.

KRAMER, G., SIMENFALVI, Z., SZEPESI, G. L. Modeling of Ammonia-Water Based Absorption Refrigeration Systems – The Refrigeration Circuit. *ANNALS of Faculty Engineering Hunedoara – International Journal of Engineering Tome XIV*. (2016).

LÁZARO-COLÁN, V. A., Experimental study of an absorption column of water vapor and ammonia in water, PhD thesis (2012) Sao Paulo, Federal University (USP), Sao Paulo, Brazil

LEITE, B., Modeling of the absorber and the generator of ammonia/water heat absorption refrigeration cycle base on the falling film technology on inclined plates., Master thesis (2015) Sao Paulo, Federal University (USP), Sao Paulo, Brazil.

MARQUARDT, W. MHAMDI, W. GEFFERS, F. FLEHMI. Optimization of MSF F. Desalination Plants, *THERMAL DESALINATION PROCESSES – Vol. I – On-line*, 2010

McCABE, W. L., JULIAN, C. J. Operaciones básicas de Ingeniería Química. Barcelona: Editora Reverté, 1991.

MITTERMAIER, M, ZIEGLER, F. Theoretical evaluation of absorption and desorption processes under typical conditions for chillers and heat transformers. *International Journal of Refrigeration* 59, (2015), 91-101.

MORENO, D., FERRO, V. R., DE RIVA, J., SANTIAGO, R., MOYA, C., LARRIBA, M., & PALOMAR, J. Absorption refrigeration cycles based on ionic liquids: Refrigerant/absorbent selection by thermodynamic and process analysis. *Applied Energy*, (2018), 213, 179–194.

NISHIMURA, N.; NOMURA, T.; IYOTA, H.; U., NORIO. Development of a High Performance and Compact Absorber for Absorption Refrigerator. *Transactions of the Japan Society of Refrigerating and Air Conditioning Engineers*, Volume 17, Issue 3, pp. 223-235 (2011).

PRATA, J. E., Modeling of a falling film absorber for a refrigeration cycle by absorption of ammonia and water. Master thesis (2012) Sao Paulo, Federal University (USP), Sao Paulo, Brazil.



SILVA P.R.S., SECCHI, A.R., BISCAIA JR, E.C. Modelagem e Simulação Dinâmica de Evaporadores Contínuos. 10<sup>o</sup> Conferencia Brasileira de dinâmica, controle e aplicações, (2011).

SRIKHIRIN, P., APHORNRATANA, S., CHUNGPABULPATANA, S. A review of absorption refrigeration Technologies. *Renewable and Sustainable Energy Reviews* 5, (2001) 343–372.

TAVARES, E. G.; MILANEZ, F.H.; BOLZAN, A.; MARANGONI, C.; TELEKEN, J. G.; WERLE, L. O.; QUADRI, M. B.; MACHADO, R. A. F. Projeto Destubcal: Desenvolvimento de tecnologia por tubos de calor, aplicável ao melhoramento de petróleo extra-pesado, em ambiente de produção offshore. Relatório técnico parcial 4 – Florianópolis: Universidade Federal de Santa Catarina, 2008.

TELEKEN, J. G. Modelagem Matemática e Análise Fluidodinâmica do Processo de Destilação por Filme Líquido Descendente. Tese (Doutorado em Engenharia Química) – Florianópolis: Universidade Federal de Santa Catarina, Curso de Engenharia Química, Departamento de Engenharia Química e Engenharia de Alimentos; 2013.

TRICHÉ, D., Numerical and experimental study of coupled mass and heat transfers in the absorber of an ammonia-water absorption machine. PhD Thesis (2016) Université Grenoble Alpes, France.

VASILESCU, C., FERREIRA, C.A. I. Solar driven multi-effect sub-zero ammonia based sorption cycles. *Proc. International Sorption Heat Pump Conference 11*, (2011), 885-892.

WANG, Q.; MA, X.; LAN, Z.; CHEN, J.; BAI, T. Heat Transfer Characteristics of Falling Film Process on Coated Division Tubes: Effect of the Surface Configurations. *Industrial Engineering Chemistry Research*, 49, 2010, 6622-6629.

# CHAPTER III- AN EQUATION-ORIENTED NOVEL APPROACH FOR MODELING THE FALLING FILM ABSORBER USING RIGOROUS THERMODYNAMIC AND TRANSPORT DESCRIPTION

---

*“There are no eternal facts, as there are no absolute truths.”*

FRIEDRICH NIETZSCHE

## **III.1. Initial Considerations**

Falling liquid films are largely employed in heat and mass transfer processes in a variety of industrial systems, including absorption processes using  $\text{NH}_3$  and  $\text{H}_2\text{O}$  as working fluid. This study develops a new approach based on differential algebraic model for the absorption of  $\text{NH}_3$  from a gaseous stream by a solution of  $\text{NH}_3$  and  $\text{H}_2\text{O}$  in a falling film absorber at steady-state. Unlike the usual approach in literature, wherein sequential algorithms are specifically tailored to solve the model, the full set of differential algebraic equations (DAE) has been formulated and solved in an equation-oriented fashion. A rigorous modeling of the vapor-liquid equilibrium at the interface is proposed and compared with the usually employed empirical correlations. Thermal and transport properties (TTP) are computed by CAPE-OPEN interfaces, providing robustness and flexibility to the model. The TTP and the falling film model are validated with experimental data from literature. The results indicate that the falling liquid films imposes the dominant mass transfer resistance compared to the gas phase, whereas the coolant-side imposes the dominant heat transfer resistance. The simultaneous solution of the DAE system is very efficient, robust and flexible, as it can be applied for absorbers with different geometries and working fluids.

### III.2. Introduction

There is a significant requirement for refrigeration at deep-freezing temperatures in a variety of industrial segments such as chemical, pharmaceutical, and food processing. In order to achieve low temperatures in industrial systems, one of the most commonly used refrigeration cycle is the absorption refrigeration system (Flori and Vîlceanu, 2012). The absorber is the most critical unit operation for the overall performance (Lázaro-Colán, 2012; Mittermaier and Ziegler, 2015). In the absorber, the refrigerant at the vapor phase is absorbed by an absorbent solution and desorbed in an upstream equipment in a highly endothermic process, producing the refrigerant at deep-freezing temperatures. A wide variety of refrigerant-absorbent combinations, both organic and inorganic, have been suggested for vapor absorption cooling systems. The two most common working fluids in absorption refrigeration cycles are LiBr/H<sub>2</sub>O and NH<sub>3</sub>/H<sub>2</sub>O due to their excellent thermal properties that make them capable to be used in cooling systems at commercial scale (Ariyadi and Coronas, 2016). The design of the absorber also plays an important role on the performance and efficiency of the system. The most common are falling liquid films and packed columns. Among them, falling film absorbers have received much attention by researchers due to their applications in many modern devices.

Many numerical and analytic studies have been performed about falling film absorbers with ammonia and water as working fluids. Killon and Garimella (2000) presented a review of the mathematical models that couple heat and mass transfer phenomena in falling film absorption. The authors show a detailed review of the governing equations, solution methods, boundary conditions, simulations and validation as well. Kang *et al.* (2000) model a vertical plate falling film absorber, wherein the aqueous ammonia solution flows counter-currently to the vapor (ammonia) and the coolant (ethylene glycol), validating the results against experimental data. Goel and Goswamy (2005b) investigated the combined heat and mass transfer process in a horizontal tube falling film absorber. Bohra (2007) conducted a detailed investigation of ammonia-water absorption heat and mass transfer in a horizontal tube falling film absorber, reporting experiments and modelling results. Triché *et al.* (2016) modeled an ammonia-water falling film absorber, which is a corrugated plate heat exchanger, considering coupled heat and mass transfer. The model predictions are validated with experimental data. Aminaravy *et al.* (2017) presented a model for a concurrent vertical

tube falling film absorber to predict the simultaneous heat and mass transfer phenomena in the absorber. The authors validate their model against experimental data obtained from an AHT (Absorption Heat Transformers) absorber.

The usual numerical approach in literature to model the falling film process is to consider finite control volume for the balances, yielding a set of algebraic equations, which are solved sequentially and iteratively by tailored sequential algorithms (Goel and Goswami, 2005a, 2005b; Sieres and Fernández-Seara, 2007; Triché *et al.*, 2016, 2017; Aminyavari *et al.*, 2017). There is no attempt to obtain a differential model which has to be discretized by, e.g., finite differences, as the current equation-oriented approach. Many authors who have modeled a  $\text{NH}_3/\text{H}_2\text{O}$  falling film absorber have used similar sequential approaches (Goel and Goswami, 2005a, 2005b; Sieres and Fernández-Seara, 2007; Triché *et al.*, 2016, 2017; Aminyavari *et al.*, 2017). Goel and Goswami (2005a), for example, proposed an algorithm that, for a given initial guess of the coolant temperature, computes the equations describing the liquid and vapor differential segments sequentially from the top to the bottom. This procedure is repeated for different guesses of the coolant temperature, given by the average of the inlet and outlet coolant temperatures, until all unknown variables converge to a given tolerance. According to Sieres and Fernández-Seara (2007), this numerical approach may fail to converge due to the asymptotic discontinuity of the molar fluxes at the interface. Therefore, the corresponding concentration profiles during the heat and mass transfer processes have to be properly predefined. To skip the asymptotic discontinuity of the molar fluxes, Aminyavari *et al.* (2017) suggest to compute the molar fluxes by the basic equations presented by Bird *et al.* (2006) and Treybal (1968) and used e.g. by Kim *et al.* (2003). Despite of that, these authors still employed the sequential approach proposed by Goel and Goswami (2005a).

This study aims to develop a model described by differential mass and energy balances coupled with algebraic equations representing the mass and energy transfer as well as the phase-equilibrium at the interface. The resulting set of equations consists of complex and high non-linear differential algebraic equations (DAE). For the first time, an equation-oriented approach is proposed to solve the falling-film absorber simultaneously. One contribution of this study, therefore, is to formulate a unique set of DAE, which is discretized by the finite differences, and solved simultaneously by standard residual minimization algorithms without the need to program specific

procedures such as tearing-sequences. This approach is more systematic and requires a good initialization of the equation system's iteration variables along the absorber height but allows for a more efficient solution because it overcomes state-of-the-art numerical problems. The equation oriented-approach further provides flexibility to the model as it can be easily integrated into flowsheet simulations and large-scale simultaneous optimization problems. The proposed model is validated with experimental data from Triché *et al.* (2016) for a vertical falling film with corrugated plates, wherein the vapor and the refrigerant flow co-currently (from the top to the bottom), whereas the coolant fluid flows counter-currently (from the bottom to the top).

The phase equilibrium is usually described by simplified empirical correlations proposed by Pretek and Klomfar (1995) for the ammonia-water system to predict the compositions at the interface at a given temperature and pressure for a narrow composition range (Conde, 2006; Triché *et al.*, 2016, 2017). However, a more general representation, which can be extended to other working fluids, might be obtained if a rigorous thermodynamic model is employed. For the ammonia-water system, for example, the equilibrium model proposed by Prausnitz *et al.* (1978) accurately describes the vapor-liquid equilibrium over the entire composition range. The flexible model formulation proposed herein allows for the inclusion of either the empirical correlations or the rigorous equilibrium model at the interface. The underlying thermodynamic model might be changed accordingly to describe different components and the non-idealities of the vapor and liquid phases. This gives flexibility to the numerical approach and therefore is another contribution to the usual approach found in literature.

When modeling falling films absorbers, the prediction of Thermodynamic and Transport Phenomena Properties (TTP), such as specific heat, specific enthalpy, partial mass enthalpy, binary diffusivity, viscosity, thermal conductivity, and density, also plays a key role in the accuracy of the model. Despite that, the authors do not clearly state which TTP are used in the falling film model (Goel and Goswami, 2005a, 2005b; Sieres and Fernández-Seara (2007,) Triché *et al.*, 2016, 2017; Aminyavari *et al.*, 2017) and do not attempt to previously validate the TTP against experimental data. Although the system NH<sub>3</sub>/H<sub>2</sub>O is well known in literature, the calculation of its TTP is still rather scattered. The current model accesses libraries in TEA (Thermodynamics for Engineering Applications) via CAPE-OPEN Interface Standard (CoLan, 2018) to compute the TTP,

which are validated against experimental data from literature to ensure precision of the falling film model. Therefore, another contribution of this study is to discuss and validate the TTP.

The chapter is organized as follows. First, in section 2 the model of the falling film absorber is presented based on the main assumptions, material and energy balances and the equilibrium at the interface. Section 3 illustrates the validation of the model against experimental data from literature and also shows the simulation of temperature and concentrations profiles along the length of the absorber, allowing to analyze how the inlet conditions influence the absorption performance. The results section further discusses the dominant resistances to mass and energy transfer.

### **III.3. Mathematical modeling**

The  $\text{NH}_3/\text{H}_2\text{O}$  falling film absorber might be designed with vertical pipes, vertical plates (Figure 1a), horizontal pipes etc. Regardless of the geometry, the absorption principle is the same: vapor of ammonia (refrigerant) is absorbed by the  $\text{NH}_3/\text{H}_2\text{O}$  solution (absorbent). Since the absorption is an exothermic process, water or another refrigerant is used as coolant to avoid an undesired temperature increase in the liquid phase in order to keep the liquid solution far from the boiling point and to sustain the absorption process as well.

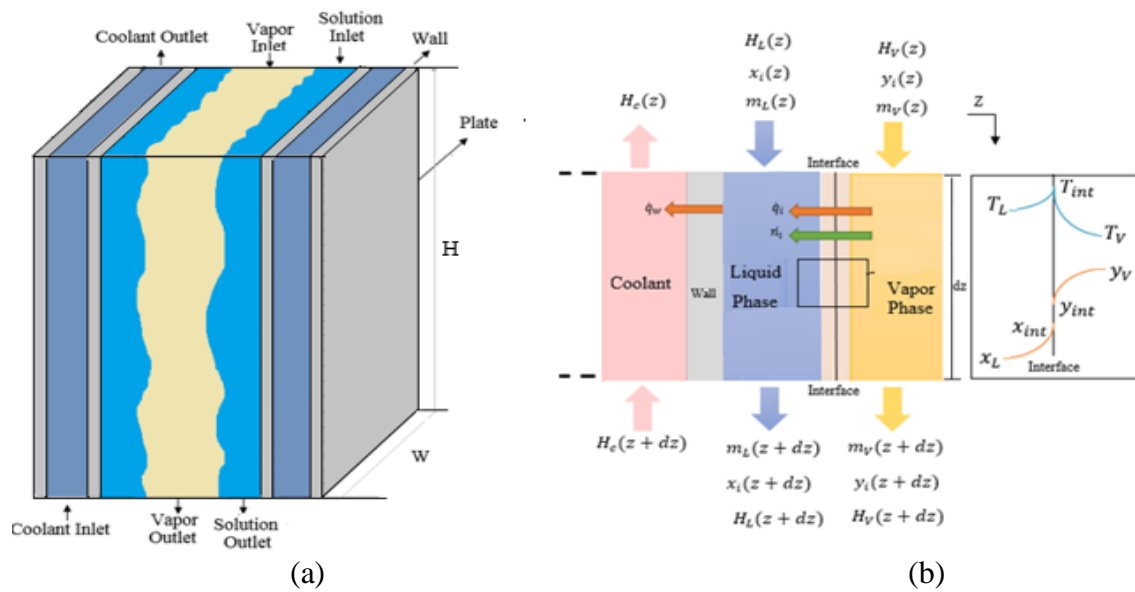


Figure 1- (a) Plates falling film absorber and (b) Differential control volume (CV) (Adapted from Triché et al., 2016).

Some assumptions may be considered when modeling falling film absorbers, as also suggested by Aminaravy *et al.* (2017) and Triché *et al.* (2016, 2017):

- The flows of heat, liquid and gas are assumed to be equally distributed through the plates of the falling film absorber;
- The flow is one-dimensional and in steady-state;
- The flow is well-established at the inlet;
- The heat losses to the environment are neglected (insulated or adiabatic equipment);
- No chemical reaction is taking place;
- Gas/vapor and liquid are in equilibrium at the interface;
- The heat and mass transfer surfaces are equal and the heat and mass transfer resistances are confined to a thin region close to the interface;
- The only driving force for the mass transfer is the concentration difference between the liquid solution and the gas/vapor, i.e., mass transfer due to pressure and temperature difference is neglected;
- The pressure drop is neglected;

A differential control volume (CV) is illustrated in Figure 1b. The positive sign convention for heat and mass fluxes is adopted, meaning that the heat and mass fluxes

flow from the vapor phase to the liquid phase and heat, from the liquid phase to the coolant. The vapor and liquid streams are fed at the top, whereas the coolant flows counter-currently. When the liquid and vapor phases come into contact, the absorption/desorption occurs.

The mass and energy balances are written for an infinitesimal volume with length  $dz$ . The infinitesimal area of the interface where mass and heat transfer between liquid and vapor occurs is given by:

$$dA_i = L \cdot dz \quad (1)$$

where  $L$  is the length of the heat and mass exchange area and  $dz$  is the height of the infinitesimal element. If the falling-film is constituted of pipes, for example,  $L = \pi(d - 2\delta)$  where  $d$  is the inner diameter of the pipe,  $\delta$  (m) is the thickness of the film. If the falling-film is constituted of plates,  $L = W$ , where  $W$  is width of the plates. The falling film absorber modeled here is a corrugated plate heat exchanger presented by Triché *et al.* (2016). It can be represented by Figure 1b, where gas and liquid flow between every two plates. More details about the geometry and measurement devices can be found in Triché *et al.* (2016). The falling film absorber is modeled by mass, component, and energy balances of the liquid, vapor and coolant phases, as well as heat and mass transfer equations at the interface and thermodynamic equilibrium at the interface. The next sections describe each part of the model proposed here.

#### *a. Material and energy balances at the bulk phases and at the coolant*

The mass, component, and energy balances for each phase, vapor, liquid, as well as the coolant in the CV (Figure 1b) are summarized in Table 1. In Table 1,  $L$  is the total length of the heat and mass exchange area,  $NC$  is the number of components,  $z$  is the length (m),  $m_L$  and  $m_V$  are the liquid and vapor mass flowrates ( $\text{kg}\cdot\text{s}^{-1}$ ),  $\dot{n}_{i,int}$  is the mass flux of component  $i$  ( $\text{kg}\cdot\text{m}^{-2}\cdot\text{s}^{-1}$ ), which is calculated by the mass transfer equations at the interface,  $y_i$  and  $x_i$  are mass fractions of component  $i$  at the gas and liquid phases, respectively;  $T_L$  is the bulk liquid temperature (K);  $T_c$  is the coolant temperature (K);  $L_c$  is the length of the heat exchange area for the coolant;  $m_c$  is the coolant mass flowrate ( $\text{kg}\cdot\text{s}^{-1}$ );  $H_c$  ( $\text{J}\cdot\text{kg}^{-1}$ ) is the coolant enthalpy;  $Q_c$  ( $\text{W}\cdot\text{m}^{-2}$ ) is the coolant heat flux;  $U$  is the overall heat transfer coefficient for the wall ( $\text{W}\cdot\text{m}^{-2}\cdot\text{K}^{-1}$ );  $\dot{q}_V$  and  $\dot{q}_L$  are the sensible heat



fluxes ( $\text{W}\cdot\text{m}^{-2}$ ) for the vapor and liquid phases calculated at the interface. The enthalpy of the liquid mixture,  $H_L$  ( $\text{J}\cdot\text{kg}^{-1}$ ), is computed by the correlation proposed by Pretek and Klomfar (1995), as already applied by others (Conde, 2006; Triché *et al.*, 2016, 2017), according to:

$$H_L = h_0 \sum_i a_i \left( \frac{T}{T_0} - 1 \right)^{m_i} x_{NH_3}^{n_i} \quad (2)$$

where  $T$  is the temperature,  $x_{NH_3}$  is the ammonia mass fraction in liquid phase,  $h_0 = 100 \cdot 10^3$  ( $\text{J}\cdot\text{kg}^{-1}$ ) is the reference enthalpy,  $T_0 = 273.16$  (K) is the reference temperature and the parameters  $a_i$ ,  $m_i$  and  $n_i$  are given in Pretek and Klomfar (1995). The gas phase is assumed to behave as an ideal mixture, so that the enthalpy ( $H_V$ ,  $\text{J}\cdot\text{kg}^{-1}$ ) might be computed as:

$$H_V = \sum_i y_i h_{V,i} \quad (3)$$

where  $y_i$  is composition of component  $i \in \{NH_3, H_2O\}$  in vapor phase and  $h_{V,i}$  is the specific enthalpy of the pure components  $i \in \{NH_3, H_2O\}$ , given by:

$$h_{V,i} = \int_{T_0}^T C_{PV,i} dT \quad (4)$$

where  $T$  (K) is temperature,  $T_0$  is the reference temperature and  $C_{PV,i}$  is the specific heat capacity of component  $i$  computed using correlations from literature, which are summarized in Appendix A.

Table 1- Mass, component and energy balances at the CV.

<b>Vapor phase</b>		
Mass balance	$\frac{dm_V}{dz} = -L \sum_{i=1}^{NC} \dot{n}_{i,int}$	
Component mass balance	$\frac{d(m_V y_i)}{dz} = \frac{d(m_{V,i})}{dz} = -\dot{n}_{i,int} L \quad i = 1, \dots, NC$	
Energy balance	$\frac{dH_V}{dz} = \frac{(-\dot{q}_V + H_V \sum_{i=1}^{NC} \dot{n}_{i,int}) L}{m_V}$	
<b>Liquid phase</b>		
Mass balance	$\frac{dm_L}{dz} = L \sum_{i=1}^{NC} \dot{n}_{i,int}$	
Component mass balance	$\frac{d(m_L x_i)}{dz} = \frac{d(m_{L,i})}{dz} = \dot{n}_{i,int} L \quad i = 1, \dots, NC$	
Energy balance	$\frac{dH_L}{dz} = \frac{(\dot{q}_L - H_L \sum_{i=1}^{NC} \dot{n}_{i,int}) L - L_c U (T_L - T_c)}{m_L}$	
<b>Coolant</b>		
Energy balance	$\frac{dH_c}{dz} = -\frac{L_c Q_c}{m_c} = -\frac{L_c U (T_L - T_c)}{m_c}$	
<b>Boundary conditions</b>		
$m_L(z=0) = m_{L0}$	$m_V(z=0) = m_{V0}$	$H_c(z=L) = H_{cL}$
$x_i(z=0) = x_{i0}$	$y_i(z=0) = y_{i0}$	
$H_L(z=0) = H_{L0}$	$H_V(z=0) = H_{V0}$	

*b. Mass and heat transfer equations at the interface*

The simultaneous heat and mass transfers and the dominant transfer resistance, i.e., which phase offers the highest resistance to mass and energy transfers, are key aspects in the mathematical modeling of falling film absorbers. The knowledge of the dominant transfer resistance allows ascertaining the limiting steps to the absorption process. Many studies on absorption modeling consider heat and mass transfers separately, reasoning that there is negligible heat interaction so that the process might be considered isothermal (Vyazovov, 1940; Cosenza, 1990; Deng, 1999; Miller, 2001). Chen *et al.* (2010), on the other hand, state that the mass exchange increases/decreases the liquid temperature at the interface accordingly, consequently influencing the equilibrium states and the mass transfer. The heat and mass transfer, therefore, should be considered simultaneous (Grossman, 1983; Kim, 1998; Habib and Wood, 2001; Ho *et al.*, 2004; Goel and

Goswamy, 2005a, 2005b; Sieres *et al.*, 2007; Triché *et al.*, 2016, 2017; Aminyavari *et al.*, 2017). There is disagreement in literature regarding the dominant mass transfer resistance. Potnis *et al.* (1997), Gommed *et al.* (2001) and Aminyavari *et al.* (2017) conclude that the vapor phase offers the dominant transfer resistance. On the other hand, Kang *et al.* (1998, 2000), Goel and Goswami (2005a, 2005b), Sieres *et al.* (2005), Fernández-Seara and Sieres *et al.* (2007), Lin *et al.* (2011) and Triché *et al.* (2017) conclude that the liquid phase offers the dominant transfer resistance for the mass transfer. Given the uncertainty of the relative magnitude of the mass resistance in the liquid and gas phases, both contributions (gas and liquid) are considered in this study. This investigation is fundamental to understand which phase (liquid or vapor) controls the mass and heat transfer phenomenon on the absorption process.

Taking into account that there is no mass accumulation and no reaction at the interface, continuity of the total mass and heat flux at the interface might be assumed for any components being transferred, then:

$$\dot{n}_{i,L} = \dot{n}_{i,V} = \dot{n}_{i,int} \quad i = 1, \dots, NC \quad (5)$$

$$\dot{q}_L = \dot{q}_V = \dot{q}_{int} \quad (6)$$

where  $\dot{n}$  ( $\text{kg}\cdot\text{m}^{-2}\cdot\text{s}^{-1}$ ) and  $\dot{q}$  ( $\text{W}\cdot\text{m}^{-2}$ ) are the mass and heat fluxes respectively,  $i$  indicates the component,  $NC$  is the number of components, the subscripts  $L$  and  $V$  represent the vapor and liquid phase respectively, and  $int$  indicates the interface.

The heat and mass transfer equations at the vapor-liquid interface are then summarized in Table 2, where  $K_L$  ( $\text{m}\cdot\text{s}^{-1}$ ) and  $K_V$  ( $\text{m}\cdot\text{s}^{-1}$ ) are the mass transfer coefficients of the liquid and the vapor phase respectively;  $\rho_V$  and  $\rho_L$  are the densities of vapor and liquid phases respectively ( $\text{kg}\cdot\text{m}^{-3}$ );  $\dot{n}_{i,int}$  ( $\text{kg}\cdot\text{m}^{-2}\cdot\text{s}^{-1}$ ) is the mass flux of components  $i$ ;  $\dot{\alpha}$  ( $\text{W}\cdot\text{m}^{-2}\cdot\text{K}^{-1}$ ) is the heat transfer coefficient;  $x_i$  and  $y_i$  are the mass fractions of component  $i$  at the liquid and vapor bulk respectively and  $x_{i,int}$  and  $y_{i,int}$  are the liquid and vapor mass fractions of component  $i$  at the interface. The partial mass enthalpies for the component  $i$  in liquid phase,  $\tilde{h}_{L,i}$  ( $\text{J}\cdot\text{kg}^{-1}$ ), are computed according to (Ziegler and Trepp, 1984):

$$\tilde{h}_{L,i} = H_L + x_i \frac{\partial H_L}{\partial x} \quad (7)$$

where  $x_i$  is mass fraction of component  $i \in \{NH_3, H_2O\}$  in liquid phase and  $H_L$  is the mass enthalpy of liquid mixture. The partial mass enthalpies for the component  $i$  in vapor phase,  $\tilde{h}_{V,i}$ , are considered equal to the specific enthalpies of the pure components,  $h_{V,i}$ , because at low pressures the non-ideal behavior of the vapor phase is negligible.  $Z$  is the mass fraction of ammonia in the absorbed/desorbed flux, expressed as (Treybal, 1968):

$$Z = \frac{\dot{n}_{NH_3}}{\sum_i^{NC} \dot{n}_{i,int}} \quad (8)$$

The value of  $Z$  indicates the variation of exchanged mass fluxes along the absorber. For an absorption involving  $NH_3/H_2O$  mixture in the vapor and in liquid phases, for example, if  $Z$  is greater than 1, water is desorbed from liquid into vapor ( $\dot{n}_{H_2O} < 0$ ) and, if  $Z$  is less than 1, water is absorbed from vapor into liquid ( $\dot{n}_{H_2O} > 0$ ). In summary, positive values of the mass flux indicates absorption from vapor into liquid and negative values of mass flux indicate desorption from liquid into vapor.

The mass fluxes of ammonia and water,  $\dot{n}_{i,int}$  ( $kg \cdot m^{-2} \cdot s^{-1}$ ), are calculated according to Treybal (1968), as also carried out by Goel and Goswami (2005a, 2005b), Lin *et al.* (2011), Sieres and Fernández-Seara (2007). The equations are presented in Table 2, given the composition at the interface and at the liquid and vapor bulk concentrations. Regarding the heat fluxes at the interface, they consist of two parts: the convective heat transfers due to the temperature gradient between both phases and the sensible heat transfer due to the mass transfer across the interface (Bird *et al.*, 2006).

Table 2- Heat and mass transfer equations at the interface.

Mass flux at the vapor interface	$\sum_{i=1}^{NC} \dot{n}_{i,int} = K_V \rho_V \ln \frac{(Z - y_{NH_3,int})}{(Z - y_{NH_3})}$
Mass flux at the liquid interface	$\sum_{i=1}^{NC} \dot{n}_{i,int} = K_L \rho_L \ln \frac{(Z - x_{NH_3})}{(Z - x_{NH_3,int})}$
Heat transfer equation at the interface	$\dot{\alpha}_V (T_V - T_{int}) + \sum_{i=1}^{NC} \dot{n}_{i,int} \tilde{h}_{v,i} = \dot{\alpha}_L (T_{int} - T_L) + \sum_{i=1}^{NC} \dot{n}_{i,int} \tilde{h}_{L,i}$

The algorithm proposed by Sieres and Fernández-Seara (2007) uses  $Z$  and the compositions at the interface as tear-variables, thus suitable initial guesses are required for these variables. However, the authors point out that their algorithm may fail if the combination of these guess values makes the logarithmic terms not defined. Aminyavary *et al.* (2017) try to overcome this numerical problem using another correlation to compute the fluxes at the interface, without defining  $Z$ . The simultaneous approach proposed herein does not require any equation tearing, as detailed in Section 2.5, then it can efficiently solve the falling film model using the equations in Table 2, although they depend on  $Z$ .

### c. Mass and heat transfer coefficients

The heat transfer coefficient for the liquid phase,  $\dot{\alpha}_L$  ( $\text{W}\cdot\text{m}^{-2}\text{K}^{-1}$ ) can be calculated using the Chilton-Colburn (1934) analogy:

$$\dot{\alpha}_L = \psi_{hL} \alpha_L \quad (9)$$

$$\alpha_L = K_L \left( C_{PL} M_L \left[ \frac{Sc_L}{Pr_L} \right]^{2/3} \right) \quad (10)$$

where  $M_L$  ( $\text{kgmol}^{-1}$ ) is molecular weight,  $K_L$  ( $\text{m}\cdot\text{s}^{-1}$ ) is the mass transfer coefficient for the liquid phase,  $C_{PL}$  ( $\text{J}\cdot\text{kg}^{-1}\text{K}^{-1}$ ) is the specific heat capacity of the liquid mixture and is calculated assuming the ideal mixture law, as recommended by Conde (2006), Prata (2012) and Leite (2015). The specific heat capacity of the pure components  $C_{PL,i}$  is

computed according to Perry (1999).  $Pr_L$  is the Prandtl number ( $Pr_L = \frac{\mu_L C_{P,L}}{\lambda_L}$ ) and  $Sc_L$  is the Schmidt number ( $Sc_L = \frac{\mu_L}{D_L \rho_L}$ ), where  $D_L$  is the binary diffusivity for the liquid phase, computed according to (Wilke and Chang, 1955),  $\mu_L$  is the viscosity (Pa·s<sup>-1</sup>),  $\lambda_L$  (W·m<sup>-1</sup>·K<sup>-1</sup>) is the thermal conductivity and  $\rho_L$  (kg·m<sup>-3</sup>) is the density. The correction factor,  $\psi_{hL}$ , takes into account the finite mass transfer effect and is calculated according to (Triché *et al.*, 2016):

$$\psi_{hL} = \frac{\left( \frac{\sum_{i=1}^{NC} \dot{n}_{i,int} C_{P,L,i}}{\alpha_L} \right)}{1 - e^{\left( -\frac{\sum_{i=1}^{NC} \dot{n}_{i,int} C_{P,L,i}}{\alpha_L} \right)}} \quad (11)$$

The heat transfer coefficient for the vapor phase,  $\alpha_V$  (W·m<sup>-2</sup>·K<sup>-1</sup>), can be calculated from the correlation given by Kakaç *et al.* (1987):

$$\alpha_V = \psi_{hV} \alpha_V \quad (12)$$

$$\alpha_V = 7.541 \left( \frac{\lambda_V}{d_{hv}} \right) \quad (13)$$

where  $\lambda_V$  (W·m<sup>-1</sup>·K<sup>-1</sup>) is the thermal conduction in the vapor phase,  $d_{hv}$  (m) is hydraulic diameter of the vapor in the control volume. This correlation is valid if  $Re < 2200$  and fully developed conditions. The correction factor ( $\psi_{hV}$ ) is calculated by (Triché *et al.*, 2016):

$$\psi_{hV} = \frac{\left( \frac{\sum_{i=1}^{NC} \dot{n}_i C_{P,V,i}}{\alpha_V} \right)}{1 - e^{\left( -\frac{\sum_{i=1}^{NC} \dot{n}_i C_{P,V,i}}{\alpha_V} \right)}} \quad (14)$$

The mass transfer coefficient for the vapor phase  $K_V$  (m·s<sup>-1</sup>) can also be calculated by applying the Chilton-Colburn (1934) analogy:

$$K_V = \frac{\alpha_V}{C_{P,V} M_V \left[ \frac{Sc_V}{Pr_V} \right]^{2/3}} \quad (15)$$

where  $M_V$  (kgmol<sup>-1</sup>) is molecular weight,  $\alpha_V$  (m·s<sup>-1</sup>) is heat transfer coefficient for the vapor phase (Equation 13),  $C_{P,V}$  (J·kg<sup>-1</sup>·K<sup>-1</sup>) is the ideal gas specific heat capacity of the

mixture. The specific heat for the pure components  $C_{pV,i}$  is taken from Van Ness *et al.* (2007).  $Pr_V$  is the Prandtl number  $\left(Pr_V = \frac{\mu_V C_{pV}}{\lambda_V}\right)$ ,  $Sc_V$  is the Schmidt number  $\left(Sc_V = \frac{\mu_V}{D_V \rho_V}\right)$ , where  $D_V$  is binary diffusivity for the vapor phase (Wilke and Chang, 1955),  $\mu_V$  is viscosity (Pa·s<sup>-1</sup>),  $\lambda_V$  is thermal conductivity and  $\rho_V$  (kg·m<sup>-3</sup>) is density.

The mass transfer coefficient,  $K_L$  (m·s<sup>-1</sup>) between the liquid phase and the interface is obtained from the correlation developed by Yih (1987). This equation is only valid in a falling film with a Reynolds number between 49 and 300 and in fully developed conditions (Triché, 2016). It may be calculated by:

$$K_L = 0.01099 Re_{film}^{0.3955} Sc_L^{0.5} \left(\frac{D_L \rho_L}{M_L}\right) \left[\frac{g \rho_L^2}{\mu_L^2}\right]^{\frac{1}{3}} \quad (16)$$

where  $Re_{film}$  is the Reynolds number for the liquid film,  $Sc_L$  Schmidt number for the liquid phase,  $M_L$  is the molecular weight (kg·mol<sup>-1</sup>),  $D_L$  is binary diffusivity,  $\mu_L$  is viscosity (Pa·s<sup>-1</sup>),  $\rho_L$  is density (kg·m<sup>-3</sup>).

The Thermodynamics and Transport Phenomena Properties (TTP), namely viscosity (Pa·s<sup>-1</sup>), thermal conductivity (W·m<sup>-1</sup>K<sup>-1</sup>), and density (kg·m<sup>-3</sup>) for the pure components in liquid and vapor phases as well as for the liquid mixture, are calculated by the software TEA (Thermodynamics for Engineering Applications, Van Baten, 2016) via CAPE-OPEN interfaces. CAPE-OPEN is a set of software interfaces standardized for plug and play inter-operability between a given process modelling environment and a third-party process modelling component (CoLan, 2018). The property packages TEA offers a number of different methods to compute the TTP. The embedded methods listed in Table 3 are chosen due to their suitability to the system and to the operating conditions studied. This choice might be easily changed according to the system and its operating conditions. The use of CAPE-OPEN interfaces might be used in any process model so that the user can, on the one hand, concentrate on the development of the model itself and, on the other hand, have access to a variety of methods to compute the TTP for different components and operating conditions. This approach, then, provides great flexibility to the model.

The specific heats of pure components and mixture as well as the binary diffusivity coefficients for liquid and vapor phases are computed using correlations from literature, which are summarized in Appendix A.

Table 3- Correlations for TTP prediction in TEA.

Property	Pure Components			Mixture	
	Liquid	Vapor		Liquid	Vapor
<b>Density</b>	COSTALD/Hankinson and Thompson	EOS-Soave Kwong	Redlich	COSTALD/Hankinson and Thompson	EOS-Soave Redlich Kwong
<b>Viscosity</b>	Letsou-Stiel Method: Temperature Correlation	Yoon and method	Thodos	Logarithmic mixing (mass based)	Brokaw
<b>Thermal Conductivity</b>	Pachaiyappan Method	DIPPR procedure 9B-1		Ideal	Ideal

The overall heat transfer coefficient for the wall is given by:

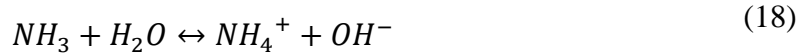
$$U = \frac{1}{\frac{1}{\alpha_{L,w}} + R_w + \frac{1}{\alpha_c}} \quad (17)$$

where  $R_w$  ( $\text{W}\cdot\text{m}^2\text{K}^{-1}$ ) is the conductive resistance of the plate made of inox,  $\alpha_{L,w}$  ( $\text{W}\cdot\text{m}^2\text{K}^{-1}$ ) is the heat transfer coefficient between the liquid film and the plate given by  $\alpha_{L,w} = 1.88 \frac{\lambda_L}{\delta_{film}}$  (Wilke, 1962), for  $Re < 2469 Pr^{-0.646}$  and fully developed conditions, where  $\lambda_L$  ( $\text{W}\cdot\text{m}^{-1}\text{K}^{-1}$ ) is the thermal conductivity,  $\delta_{film}$  (m) is the falling film thickness.  $\alpha_c$  ( $\text{W}\cdot\text{m}^2\text{K}^{-1}$ ) is the heat transfer coefficient between the coolant and the plate, calculated by  $\alpha_c = 4.363 \frac{\lambda_c}{D_h}$  (Goel and Goswami, 2005a), for fully developed laminar flow conditions, where  $\lambda_c$  ( $\text{W}\cdot\text{m}^{-1}\text{K}^{-1}$ ) is thermal conductivity and  $D_h$  is hydraulic diameter.

*d. Equilibrium at the interface*

Liquid and vapor compositions at the interface,  $x_{i,int}$  and  $y_{i,int}$ , are calculated from phase equilibrium at the interface. According to Seader and Henley (1998), it is necessary to know whether the components dissociate during the absorption process. Since ammonia is a weak electrolyte, it ionizes appreciably in a large excess of water, according to:





If the liquid phase is a diluted solution, the phase equilibrium for weak electrolytes might be modeled as Edwards *et al.* (1975 and 1978). When the ammonia molar fraction in the liquid phase is above  $10^{-3}$ , though, the ionization is negligible (Prausnitz *et al.*, 1978). Since the ammonia molar fraction in the studied falling film greatly exceeds  $10^{-3}$  at all points, it is reasonable to assume that there is no dissociation in the liquid phase. There are two approaches to calculate the compositions at the interface for ammonia and water mixture that have been previously proposed in literature: a rigorous thermodynamic model by Prausnitz *et al.* (1978), which accurately describes the ammonia-water system over the entire composition range; or a simplified empirical correlation for pressures below 20 bar, according to Pretek and Klomfar (1995). A brief comparison is presented in the following.

*i. Rigorous Thermodynamic Model*

Some assumptions might be made for the vapor-liquid equilibrium (VLE) of ammonia and water: vapor phase is an ideal gas at the operating temperature and pressure conditions of the studied falling film ( $P = 6$  bar and  $290 \leq T \leq 365$  K), as also assumed by other authors (Triché *et al.*, 2016); there is no dissociation, so ammonia is not an electrolyte. The vapor-liquid equilibrium for the system ammonia and water are then written as:

$$y'_{NH_3} P = x'_{NH_3} \gamma_{NH_3}^* H' \exp\left(\frac{\bar{v}_{NH_3}^\infty P}{RT}\right) \quad (19)$$

$$y'_{H_2O} P = x'_{H_2O} \gamma_{H_2O} f_{H_2O,L}^{P_0} \exp\left(\frac{\bar{v}_{H_2O} P}{RT}\right) \quad (20)$$

where  $y'$  and  $x'$  are molar fraction in vapor and liquid phase, respectively,  $\bar{v}_i^\infty$  is the partial molar volume at the infinite dilution of component  $i$  in the solvent (water), available at Krichevsky and Kasamovsky (1935),  $R$  is the universal gas constant,  $T$  is temperature,  $P$  is pressure,  $H'$  is Henry's constant for molecular ammonia in water, whose values are determined from experimental data in the dilute region (Edwards *et al.*, 1975, 1978),  $\gamma_{H_2O}$  is the activity coefficient of water which is calculated by Prausnitz *et al.*

(1978),  $\gamma_{NH_3}^*$  is the activity coefficient of ammonia in a symmetric convection, which is calculated by a hyperbolic tangent function (Prausnitz *et al.*, 1978):

$$\ln(\gamma_{NH_3}^*) = b \cdot \tanh\left(\frac{a_{22}x'_{NH_3}}{b(1-x'_{NH_3})}\right) \quad (21)$$

where  $x'_{NH_3}$  is the ammonia molar fraction in liquid phase, the parameter  $a_{22}$  is obtained from Prausnitz *et al.* (1978) and the parameter  $b$  is determined by:

$$b = \ln\left(\frac{f_{NH_3,L}^{P_0}}{H'}\right) \quad (22)$$

where  $f_{NH_3,L}^{P_0}$  is the fugacity of pure liquid ammonia at the system temperature, corrected to zero pressure:

$$f_{NH_3,L}^{P_0} = \varphi_{NH_3}^S P_{NH_3}^S \exp\left(-\frac{v_{NH_3} P_{NH_3}^S}{RT}\right) \quad (23)$$

where  $P_{NH_3}^S$  is the vapor pressure of pure ammonia (Macriss *et al.*, 1964),  $v_{NH_3}$  is the molar volume of pure liquid ammonia (Din, 1956) and  $\varphi_{NH_3}^S$  is the fugacity coefficient at saturation, determined by the Soave-Redlich-Kwong equation of state. This approach uses rigorous thermodynamic models to describe the VLE, which might be changed accordingly to describe different components and the non-idealities of the vapor and liquid phases.

## ii. Empirical Correlations

Alternatively, it can be assumed that the temperature at the interface is the saturation temperature, so that empirical correlations for bubble and dew point temperatures can be used to compute the compositions at the interface, as carried out by Conde (2006) and Triché *et al.* (2016, 2017). The empirical correlations developed by Pretek and Klomfar (1995) for the bubble and dew point temperatures are respectively given by:

$$T(P, x_{NH_3}) = T_0 \sum_{k=1}^{14} a p_k (1 - x_{NH_3})^{m p_k} \left[ \ln \frac{P_0}{P} \right]^{n p_k} \quad (24)$$

$$T(P, y_{NH_3}) = T_0 \sum_{j=1}^{17} ap_j (1 - y_{NH_3})^{\frac{mp_j}{4}} \left[ \ln \frac{P_0}{P} \right]^{np_j} \quad (25)$$

where  $T$  is temperature,  $P$  is pressure, the subscript 0 indicates the reference state,  $T_0 = 100$  K and  $P_0 = 2$  MPa,  $x$  and  $y$  are the mass fraction in liquid and vapor phase, respectively, the parameters  $ap$ ,  $mp$  and  $np$  are given by Pretek and Klomfar (1995) for  $k$  and  $j$  parameters. These correlations are the resulting functions, which best reproduce the selected experimental data ( $193.15 \text{ K} \leq T \leq 453.15 \text{ K}$  and  $0.02 \text{ bar} \leq P \leq 20 \text{ bar}$ ) used by the authors (Pretek and Klomfar, 1995). Therefore, for a given pressure and temperature at the interface, it is possible to solve the system of algebraic equations (24 and 25) to calculate the interface compositions,  $x$  and  $y$ .

*e. Solution procedure*

The falling film absorber model is represented by a system of differential algebraic equations (DAE), composed by  $5 + 2 \cdot NC$  differential equations (Table 1), 3 algebraic equations, which describe the mass fluxes and the temperature at the interface (Table 2) and  $NC + 2$  equations to compute the compositions at the interface (Equations 19-20 or 24-25 plus the summation of the mass fractions at each phase). The vector  $\mathbf{X}$  represents the algebraic and state variables of the DAE system:

$$\mathbf{X} = [m_L, m_V, x, y, H_L, H_V, H_C, n, T_{int}, x_{int}, y_{int}] \quad (26)$$

Since the coolant flows counter-currently to the gas and liquid process streams, boundary conditions are specified for both  $z = 0$  and  $z = L$  and the system cannot be solved as an initial value problem, but as a contour value problem. The DAE system is, therefore, discretized by the finite differences method (forward for the liquid and vapor side and backward for the coolant side), resulting in a set of  $(10 + 3 \cdot NC) \cdot nd$  algebraic non-linear equations, where  $nd$  is the number of discretization points considering a uniform grid. One of the challenges of the equation-oriented approach used herein is that the values of all state variables along the absorber length must be properly initialized. This has been done by specification of variables along the absorber, such as enthalpies, mass flow rate etc. The initial guess for the iteration variables was given by simulated data from literature.

The discretized DAE system, i.e. algebraic non-linear system, is implemented in MOSAICmodeling (<http://mosaic-modeling.de/>), which is a free, web-based modeling environment capable of automatically generating code for process simulation and optimization in different programming languages (Merchan *et al.*, 2015 and Tolksdorf *et al.*, 2019). The model is then solved in Matlab using the native function *fsolve*, which is based on the residual minimization method. The TTP are computed via CAPE-OPEN interfaces using the libraries in TEA. The functions, which calculate heat and mass transfer coefficients, are defined as “Empty Body Functions” in MOSAICmodeling. These act as place-holder function calls and definitions in the system of equations. Once MOSAICmodeling generates the code for the solution in Matlab, interfaces with a CAPE-OPEN-compliant property package such as TEA are manually programmed, allowing for the external calculation of TTP, as shown in Rosa *et al.* (2018). To enable the CAPE-OPEN function calls in Matlab, the plug-in Matlab Thermo Import from AmsterCHEM is used (van Baten, 2016). Figure 2 depicts the entire modeling and simulation framework. The more interested reader should read MOSAIC (2018) and AMSTERCHEM (2018) for more details.

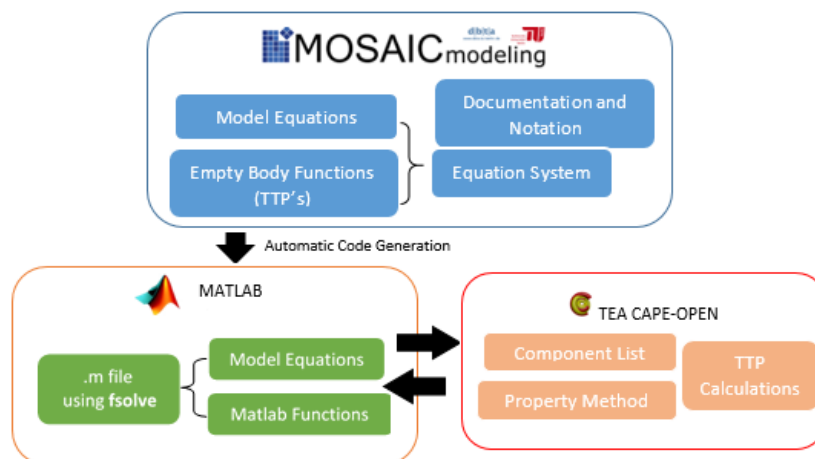


Figure 2- Overview of the modeling and simulation framework.

The proposed model, therefore provides an equation-oriented formulation of the falling film absorber, which can be integrated with other simulation or optimization environments and take advantage of state-of-the-art solution techniques for large-scale NLPs. Furthermore, unlike the other approaches usually carried out in literature, changes on some underlying equation or on the working fluid can be made in a straightforward manner.

### III.4. Results and Discussions

This section firstly compares the modeling approach regarding the equilibrium at the interface according to the discussion in Section 2.4. Secondly, it presents the validation of the TTP properties and of the falling film model against experimental data from literature. The validated model is then simulated and an analysis of the main mass and heat transfer resistances and the effect of inlet conditions on the process performance is performed.

#### *a. Evaluation of the phase equilibrium models*

The empirical and rigorous approaches to describe the equilibrium at the interface are validated against the experimental data from Clifford *et al.* (1932), who reported VLE data for the system  $\text{NH}_3/\text{H}_2\text{O}$  at temperatures up to 423.15 K and at pressures up to 20 bar. This range includes the operating conditions,  $P = 6$  bar and  $298 < T < 318$  K, which are used to validate our modeling approach. Figure 3 compares the rigorous equilibrium as suggested by Prausnitz *et al.* (1978) and the simplified empirical correlations by Pretek and Klomfar (1995) with the experimental data from Clifford *et al.* (1932) at 6.08 bar and 10.13 bar. Both approaches can precisely describe the VLE of the mixture with deviations of the same order of magnitude for temperatures between 303.15 K and 323.15 K, which correspond the falling film operating conditions. The average relative deviations for the liquid and vapor mass fraction at 6.08 bar are 1.53% and 0.70%, respectively, if the empirical correlations are used, and 3.15% for the liquid phase and 0.46%, respectively, if the rigorous model is employed. The deviations at 10.13 bar are very similar. The empirical correlations present a slightly better fit than the rigorous VLE formulation at higher temperatures, especially for the liquid phase. This overfit might be expected since the parameters of the empirical correlations are adjusted with the same experimental data from Clifford *et al.* (1932). On the one hand, these empirical correlations usually employed in literature to model the falling film absorber are only valid for the mixture  $\text{NH}_3/\text{H}_2\text{O}$  in a pressure range from 0.02 to 20 bar. On the other hand, the rigorous model formulation is based on the thermodynamic formalism which gives flexibility to the falling film model since the VLE equations might be suited to other

component mixtures in a straightforward manner. Therefore, the remaining simulations are carried out using the rigorous VLE formulation from Prausnitz *et al.* (1978).

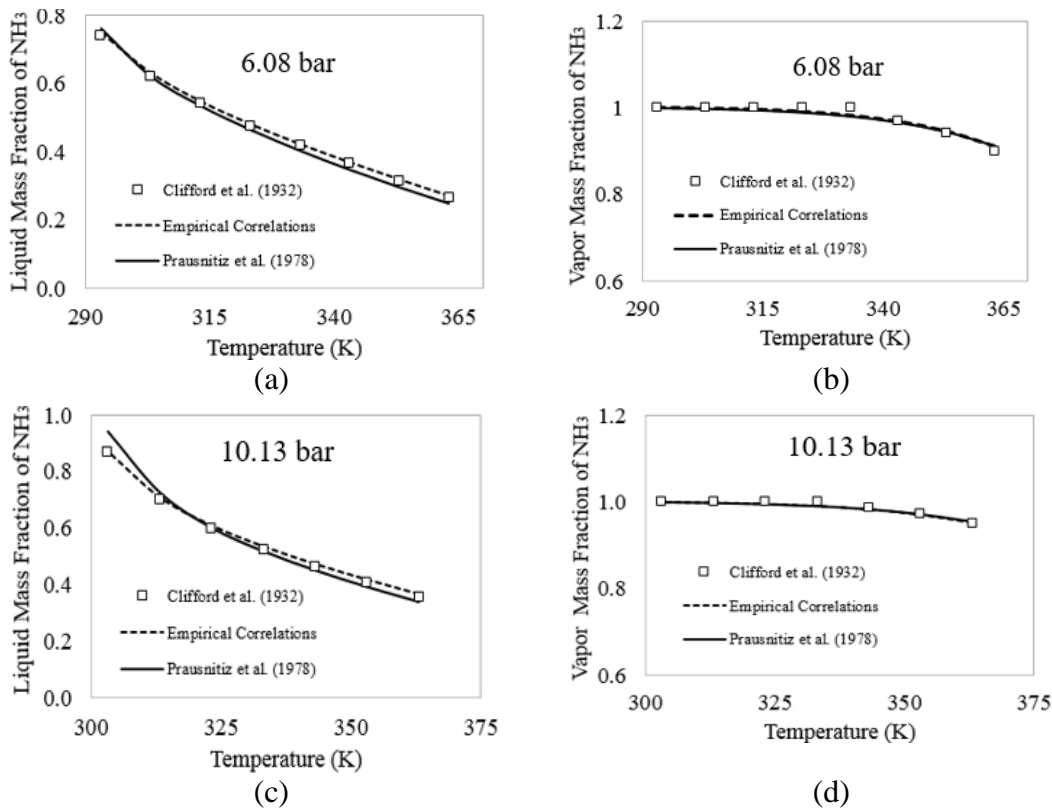


Figure 3- Validation of the VLE equilibrium model: (a) liquid and (b) vapor phases at 6.08 bar c) liquid d) vapor phases at 10.13 bar

*b. Validation of the Thermodynamics and Transport Phenomena Properties*

Although the mixture NH<sub>3</sub>/H<sub>2</sub>O is well-known to many industrial applications, the correlations to calculate their TTPs are not clearly stated neither validated by those who model the falling film absorber (Goel and Goswami, 2005a, 2005b; Sieres and Fernández-Seara (2007,) Triché *et al.*, 2016, 2017; Aminyavari *et al.*, 2017). Aware that the deviations of the TTPs correlations might propagate to the falling film output variables, we firstly validate the TTPs against experimental data from literature in order to ensure precision of the falling film model. Viscosity, density, and thermal conductivity for the pure components and for the mixture are calculated in the temperature range from 273.15 to 373.5 K and pressure 1 to 33 bar. Table 4 summarizes the average relative deviations between experimental and simulated data. As the ammonia mass fraction at the vapor phase is above 0.99, the deviations of the mixture properties at the vapor phase are similar to the pure component deviations, therefore they are not show in Table 4 for the sake of

simplicity. The small deviations indicate that the model has a very good agreement with the experimental data from literature. The correlations for specific heat capacities are validated against experimental data from literature, which cover the temperature range from 290 to 390 K for the pure component (Perry, 1999; NIST, 1998) and from 280 to 360 K for the liquid mixture (Fujita *et al.*, 2008). Table 4 summarizes the average relative deviations, indicating that the model can satisfactorily predict the specific heat. As mentioned above, the deviations for the mixture at the vapor phase are not shown since it is almost pure ammonia.

The enthalpy of the mixture is validated against experimental data from IGT (1964), which are taken between 345 K and 514 K. The average deviations are 3.49% for the liquid phase when  $0.02 \leq x_{NH_3} \leq 0.99$  and 3.99% at the vapor phase when  $0.93 \leq y_{NH_3} \leq 0.99$ , indicating the quality of fit of the correlation used. As the partial mass enthalpies at the liquid phase for each component are obtained from the mixture's enthalpy (Equation 7), which is already validated, there is no need to further compare the partial mass enthalpies with experimental data. The specific enthalpies for the pure component at the vapor phase are derived from the specific heat, which is satisfactorily validated as Table 4 shows.

Table 4- Average Relative Deviation of Transport and Thermodynamic Properties.

Property	NH <sub>3</sub>		H <sub>2</sub> O		NH <sub>3</sub> /H <sub>2</sub> O
	Liquid	Vapor	Liquid	Vapor	Liquid
<b>Density (kg/m<sup>3</sup>)</b> 294.5 K < T < 343.0 K 4.29 bar < P < 33.14 bar	0.70% <sup>[1]</sup>	1.87% <sup>[2]</sup>	0.08% <sup>[3]</sup>	0.68% <sup>[2]</sup>	0.74% <sup>[11]</sup> @ $x_{NH_3} = 0.176$
<b>Viscosity (Pa·s)</b> 290.0 K < T < 340.0 K 1 bar < P < 10 bar	2.55% <sup>[4]</sup>	1.41% <sup>[5]</sup>	3.06% <sup>[6]</sup>	1.37% <sup>[7]</sup>	5.51% <sup>[7]</sup> @ $x_{NH_3} = 0.150$
<b>Thermal conductivity (W/m·K)</b> 273.15 K < T < 373.5 K 1 bar < P < 10 bar	5.74% <sup>[8]</sup>	3.38% <sup>[9]</sup>	1.74% <sup>[10]</sup>	0.68% <sup>[7]</sup>	2.43% <sup>[9]</sup> @ $0 \leq x_{NH_3} \leq 0.27$
<b>Specific Heat Capacity (kJ/Kg·K)</b> 290.0 K < T < 390.0 K 1 bar < P < 15.35 bar	1.32% <sup>[2]</sup>	0.11% <sup>[12]</sup>	2.41% <sup>[12]</sup>	0.08% <sup>[2]</sup>	1.70% <sup>[13]</sup> @ $0.15 \leq x_{NH_3} \leq 0.84$

<sup>[1]</sup>Cragoe *et al.* (1921), <sup>[2]</sup>Perry (1999), <sup>[3]</sup>Aznar *et al.* (1984), <sup>[4]</sup>Laeseck *et al.* . (1999), <sup>[5]</sup>Trautz (1931), <sup>[6]</sup>Agaev *et al.* (1968), <sup>[7]</sup>Timrot (1950), <sup>[8]</sup>Varlashkin *et al.* (1953), <sup>[9]</sup>Golubev (1964), <sup>[10]</sup>Less *et al.* (1898), <sup>[11]</sup>Liu *et al.* (2012), <sup>[12]</sup>NIST (1998), <sup>[13]</sup>Fujita *et al.* (2008).

*c. Model validation: Falling Film Absorber*

The model proposed here is validated against experimental data from Triché *et al.* (2016) at four operating conditions, which present only slight changes. The outlet variables used for validation are: liquid temperature  $T_L$  (K), coolant temperature  $T_C$  (K), ammonia mass fraction  $x_{NH_3}$  and heat absorbed by the coolant  $Q_C$  (kW). In order to ensure convergence, the minimum number of discretization points is  $nd = 5$ , which was compared with  $nd = 10$  to check the model precision. Table 5 compares the model prediction with the experimental data for cases in which the model is discretized with  $nd = 5$  and  $nd = 10$ . The model is able to predict the experimental data with very small deviations, capturing even the slight changes in the operating conditions. When  $nd = 10$ , the model is described by  $(10 + 3 \cdot NC) \cdot nd = 160$  non-linear algebraic equations and the execution time is 81s in a computer with Intel (R), Core (TM) i3-3217U, RAM memory 4.00GB, operational system 64 bits. When the number of discretization points is reduced to  $nd = 5$ , there are  $(10 + 3 \cdot NC) \cdot nd = 80$  non-linear algebraic equations and the execution time decreases to 11s. A finer discretization does not necessarily mean higher precision, as might be observed in Table 5, because it results in a larger-size non-linear algebraic system, which is more difficult to converge and requires a better initialization of more iteration variables. A grid with 5 discretization points is then considered for the simulations since it ensures convergence with a great accuracy. Both approaches to compute the equilibrium at the interface, rigorous and empirical, are further compared, corroborating the good fit of the rigorous equilibrium, which gives flexibility and robustness to the model. Unlike Sieres and Fernández-Seara (2007), who report numerical problems due to the asymptotic discontinuity in the flux's calculation (Table 5), the non-linear algebraic system is solved here successfully, further suggesting the robustness of the proposed approach.



Table 5- Validation of the falling film model against experimental data from Triché *et al.* (2016).

Test	nd	$T_L$ (K)			$T_c$ (K)			$x_{NH_3}$		
		Exp	Deviation (%)		Exp	Deviation (%)		Exp	Deviation(%)	
			Empirical	Rigorous		Empirical	Rigorous		Empirical	Rigorous
1	5	303.7	0.04	0.08	305.8	0.52	0.51	0.591	0.72	2.30
	10		0.28	0.37		0.31	0.01		0.68	0.63
2	5	303.5	0.31	0.57	305.5	0.21	0.04	0.588	1.48	3.47
	10		1.21	1.08		1.25	1.12		0.20	0.34
3	5	304.0	0.23	0.06	305.8	0.18	0.03	0.588	2.58	3.16
	10		1.06	0.89		1.17	1.27		0.87	1.12
4	5	303.2	0.96	0.23	305.1	0.58	0.18	0.591	0.72	3.22
	10		0.87	0.85		0.86	1.24		1.84	1.18

*d. Analysis of the mass and heat transfer phenomena*

This section investigates the behavior of the falling film absorber after it has been successfully validated. Firstly, the falling film absorber behavior is evaluated for the nominal case with the following inlet conditions, taken from the experimental condition reported by Triché *et al.* (2016):  $m_v = 5.25 \cdot 10^{-3}$  kg/s,  $m_L = 1.67 \cdot 10^{-2}$  kg/s,  $T_v = 296.9$  K,  $T_L = 312.0$  K,  $x_{NH_3} = 0.46$ ,  $y_{NH_3} = 0.995$ ,  $P = 6.03$  bar,  $T_c = 300.20$  K and  $m_c = 0.326$  kg/s. Then, the dominant mass and heat transfer resistances are investigated in order to understand which phase (liquid or vapor) controls the mass and heat transfer phenomenon on the absorption process.

Figure 4 illustrates temperature profiles for the liquid and vapor phases as well as the coolant and the interface along the absorber length for the nominal case. The ammonia absorption by ammonia-water solution is an exothermic process, then heat is rejected from the liquid phase to the coolant, which maintains the absorption temperatures, keeps the liquid solution far from boiling and helps to shift the equilibrium favorably in the direction of the absorption. As a result, the temperature of the liquid phase decreases from top to bottom while the coolant temperature increases from bottom to top, since it flows counter-currently. The temperature at the interface and at the liquid bulk are nearly the same indicating that the liquid-side transfer resistance is negligible. Here, unlike observed by Triché *et al.* (2016) and Goel and Goswami (2005a), the interface temperature is not always slightly higher than the liquid temperature, what occurs due to the heat generated by the absorption at the interface. This is explained by the different approach used to compute the equilibrium at the interface because, if the empirical correlations are used to calculate the compositions at the interface, the same results from Triché *et al.* (2016) are

observed. Here, a rigorous thermodynamic model is employed instead of empirical correlations. As discussed in Section 3.1, there is a slight difference between the empirical and rigorous correlations describing the VLE at the interface. Regarding the vapor temperature, it increases at the first section of the absorber until it reaches the interface temperature near  $z=0.39$  m due to the heat generated by the absorption process. After that point, since the temperature at the vapor phase is slightly higher than the interface temperature, according to the energy balance at the interface (Table 2), the heat flux is reversed and then the vapor phase slowly cools down.

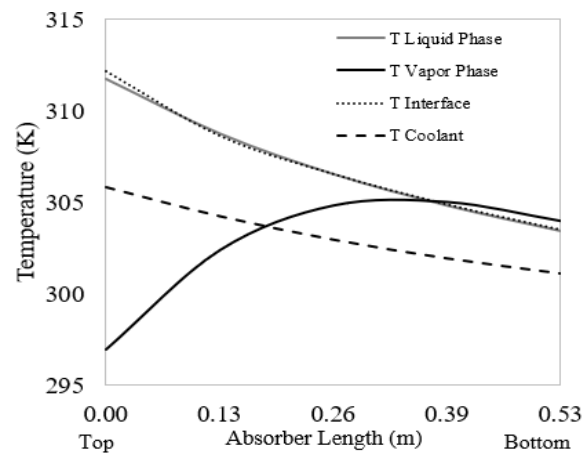


**Figure 4-** Temperature profile along the absorber length.

Figure 5a and 5b depicts the concentration profiles along the absorber. As expected, ammonia is continuously absorbed into the liquid phase as its mass fraction increases along the absorber length due to the higher ammonia content in the vapor phase. In the vapor phase, the ammonia mass fraction firstly decreases not only due to the ammonia absorption into the liquid phase but also due to the water desorption from the liquid phase into the vapor phase ( $Z > 1$ ). When  $Z < 1$ , though, water is absorbed into the liquid phase so that the ammonia mass fraction in vapor phase stops changing. The same behavior has been observed by Sieres *et al.* (2005), Pérez-Blanco (1995), and Triché *et al.* (2016, 2017). Figure 5 further indicates that  $y \geq y_{int}$ ,  $x_{int} \geq x$  and  $y_{int} > x_{int}$  ensuring that ammonia is continuously absorbed, as also observed by Sieres *et al.* (2007). The interface mass fractions ( $x_{int}$  and  $y_{int}$ ) increase along the absorber as the interface temperature decreases, as shown in Figures 4, 5a and 5b. This behavior might be understood with the help of the liquid-vapor phase diagram illustrated in Figure 5c. At a given temperature at the interface, the equilibrium composition is indicated. For a lower

interface temperature, the phase diagram indicates that the mass fraction of both liquid and vapor phases will increase.

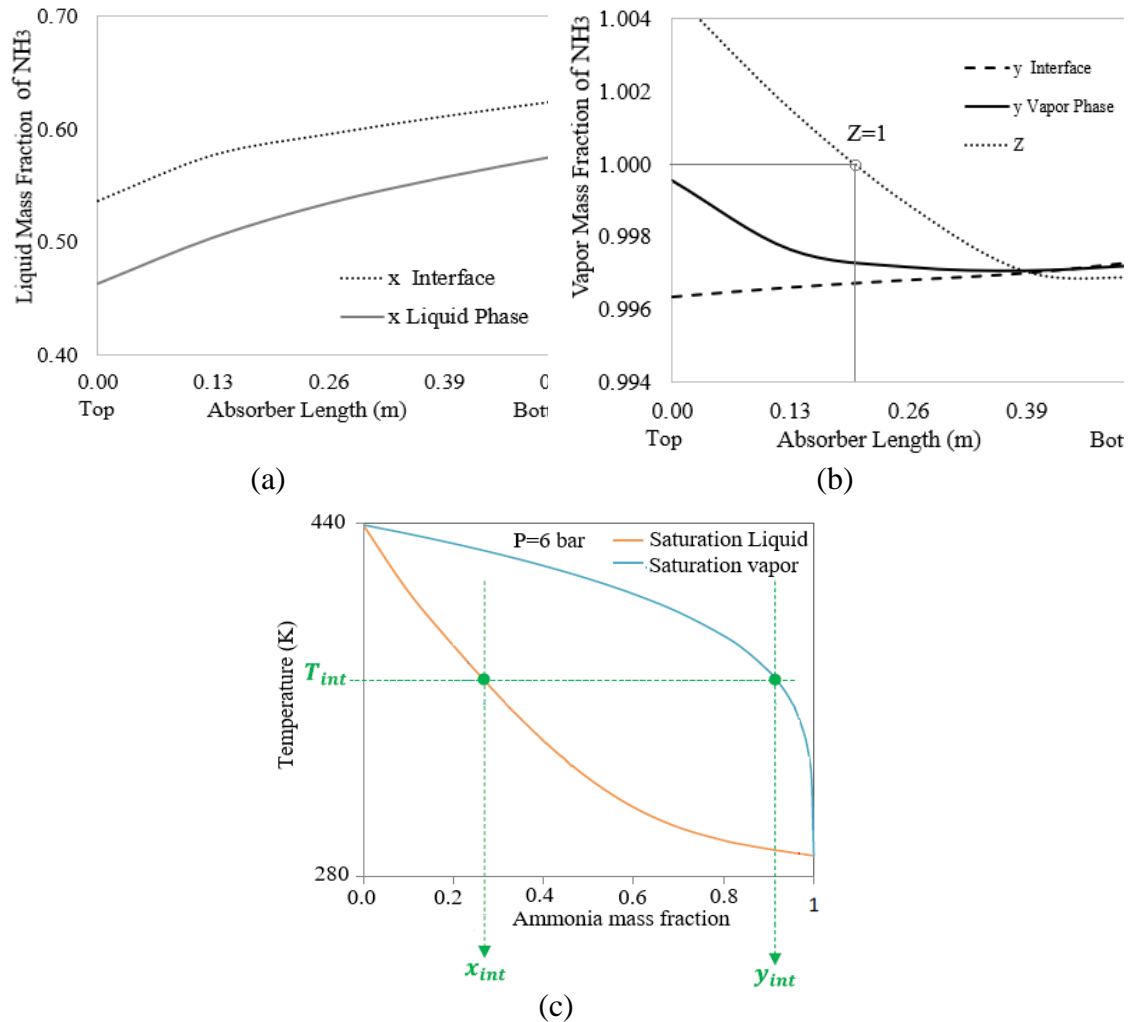


**Figure 5-** Liquid (a) and vapor (b) phase concentration profiles along the absorber length, (c) liquid-vapor phase diagram for NH<sub>3</sub>/H<sub>2</sub>O at 6 bar.

The dominant resistance in heat and mass transfer is not a consensus in literature; therefore, this phenomenon is investigated here. The simplified driving force for mass transfer is the difference between the concentration at the gas phase and at the interface,  $y_{NH_3} - y_{int,NH_3}$ , and between the concentration at the interface and at the liquid phase,  $x_{int,NH_3} - x_{NH_3}$ , which are illustrated in Figure 6 for the nominal case. Since the gradient at the liquid phase is much higher than at the vapor phase, the overall mass transfer resistance is mostly due to the liquid phase. Analyzing the mass transfer parameters for the vapor,  $F_V = K_V \cdot \rho_V$ , and liquid phase,  $F_L = K_L \cdot \rho_L$  in Figure 6b, we arrive to the same

conclusion: the liquid side controls the mass transfer since  $F_L > F_V$  along the falling film. These findings corroborate the conclusion from Kim (2003), Perez-Blanco (1988) and Goel and Goswami (2005a, 2005b). Triché et al. (2017) and Goel and Goswami (2005a) affirm that the heat transfer resistance at the vapor phase ( $1/\alpha_V$ ) is large whereas at the liquid phase ( $1/\alpha_L$ ) is negligible. Figure 6c shows the heat transfer coefficients in liquid and vapor phases, indicating that the resistance at the vapor phase is two orders of magnitude greater than the resistance at the liquid solution.

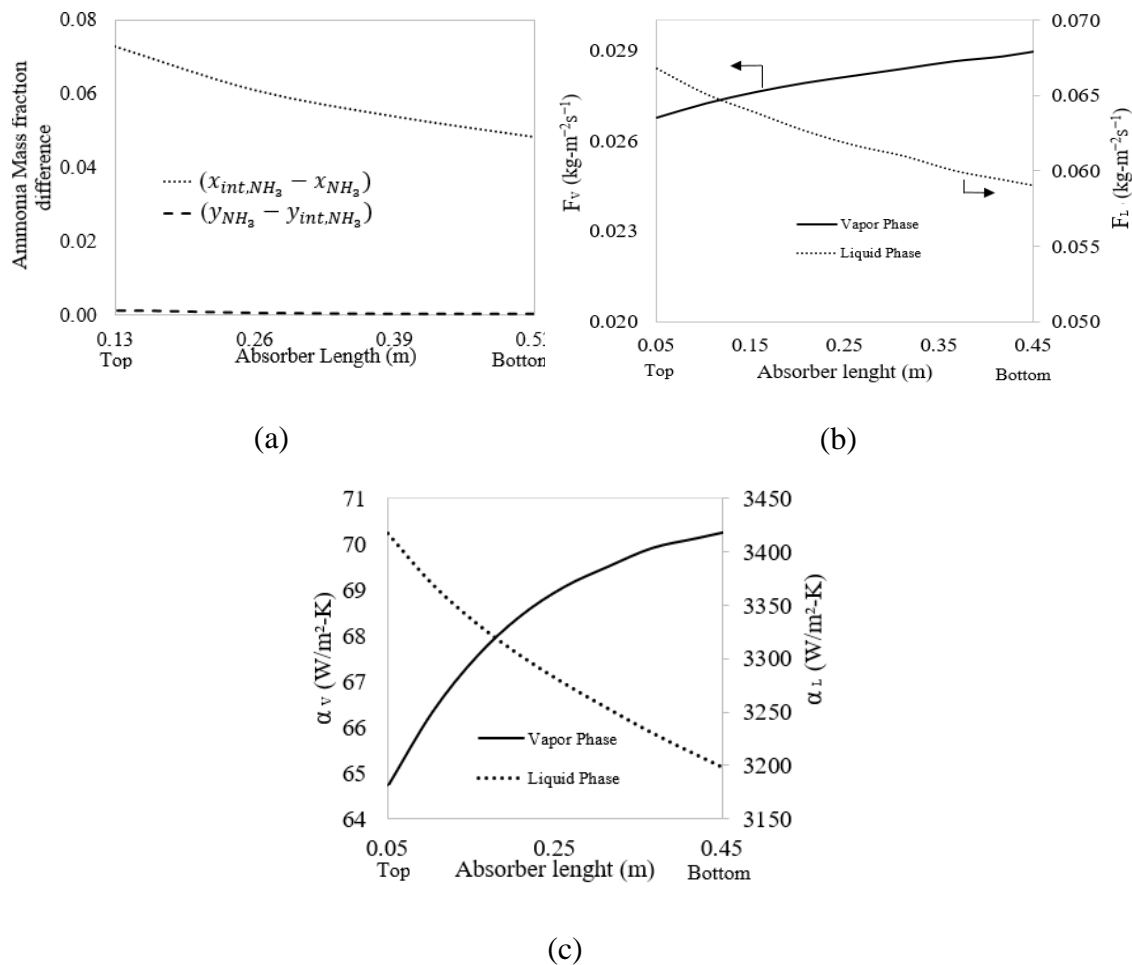


Figure 6- (a) Ammonia mass fraction gradients and (b) Correlations with mass transfer coefficients ( $F_V$  and  $F_L$ ) and (c) heat transfer coefficients for the vapor and liquid phases and.

e. Analysis of the inlet conditions in the absorption performance

The falling film absorber has the goal to absorb the refrigerant (ammonia) from the vapor phase, concentrating the solution. This section, then, investigates the effect of some inlet variables on the ammonia mass fraction at the liquid phase,  $x_{NH_3}$ . This investigation might be useful to better understand the variables that greater influence the ammonia

content at the outlet stream. Based on the conclusion that the dominant mass transfer resistance occurs at the liquid side, the following inlet variables are investigated: liquid and coolant inlet temperature,  $T_{L,in}$  and  $T_{c,in}$ , inlet mass fraction of ammonia at the liquid phase  $x_{NH_3,in}$  and coolant inlet mass flowrate  $m_{c,in}$ . Figure 7a shows the ammonia mass fraction at liquid phase along the absorber length for different  $x_{NH_3,in}$  as well as the ammonia mass fraction gradient between the liquid interface and the liquid phase. The lower the inlet mass fraction of ammonia, the higher is the gradient, since the concentration at the vapor phase has not changed. This favors the ammonia absorption into the liquid phase, yielding an increase in the ammonia mass fraction at the liquid phase.

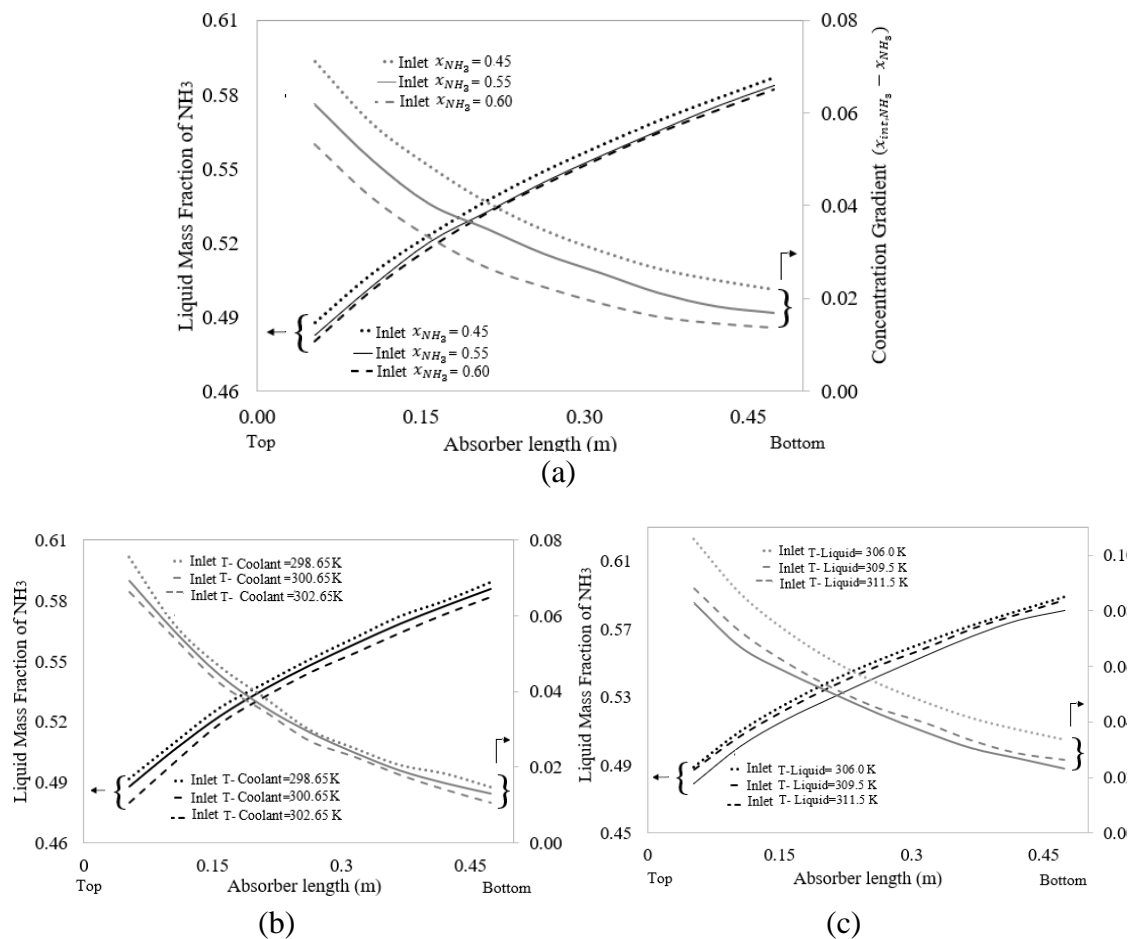


Figure 7- (a) Analysis of the liquid inlet mass fraction of ammonia along the absorber, Influence of coolant (b) and liquid (c) inlet temperature on absorption of ammonia

The influence of coolant and liquid inlet temperatures on the absorption of ammonia are illustrated in Figure 7b and Figure 7c, respectively. The concentration gradients are

greater at the top because of the more pronounced difference in ammonia concentration between the liquid and vapor phases. At the top occurs the lowest concentrations of ammonia in the liquid phase, while the vapor stream feeds the top with  $y_{NH_3} = 0.995$ . As the absorption occurs along the falling film, the liquid phase gets richer in ammonia so that the concentration gradient decreases. The coolant inlet temperature ranges from 298.5 to 300.5 K, according to Goel and Groswami (2005a), as it covers typical thermal conditions of the cooling units for this process. The lower the inlet coolant temperature, the lower will be the liquid temperature along the absorber's length since the heat generated by the absorption is transferred to the coolant. As a result, the higher will be the ammonia content at the interface, according to the phase diagram in Figure 5c, resulting in a higher concentration gradient between the interface and the bulk phases, as illustrated by Figure 7a and b. The same behavior is observed for decreasing liquid inlet temperatures. Analyzing the coolant inlet mass flow rate, it has the same effect as the decrease in the inlet coolant temperature since a higher flow rate increases the heat flux from the liquid to the coolant. For the sake of simplicity, the profiles are not shown here. The sensitive analyses indicate that lower inlet coolant temperature or lower liquid inlet temperature allows a higher ammonia absorption, as desired. These results, therefore, might be useful to monitor or to maximize the ammonia content at the outlet stream by the formulation of an optimization problem where the objective function could be a function of operating parameters as  $x_{NH_3,out} = f(T_{L,in}, T_{c,in}, x_{NH_3,in}, m_{L,in}, m_{c,in}, m_{V,in})$ . It is important to be aware of the constraints imposed by the other equipment in the absorption refrigeration system.

### III.5. Conclusion

This study presents a model of a plate falling film absorber, which is solved using an equation-oriented approach. The model consists of mass and energy balances, heat and mass transfer equations as well as thermodynamic equilibrium and transport property calculations. The finite differences method is applied and the resulting set of algebraic non-linear equations is solved simultaneously by a residual minimization method. The model has been successfully validated with data from literature, showing a maximum relative deviation of 3.47%. For the considered operating conditions, results indicate that the overall resistance for mass transfer along the falling film absorber is controlled by the

liquid phase whereas the coolant side heat transfer resistance dominates the overall heat transfer resistance.

Additionally, this study proposes computing the phase equilibrium for the binary  $\text{NH}_3\text{-H}_2\text{O}$  system using the thermodynamic formalism. This approach is compared with the usual practice in literature, which uses empirical correlations. The results show that both approaches are able to describe the compositions at the interface under a broad range of operating conditions. The empirical correlations, though, are restricted for the operating conditions where the parameters were validated and for the ammonia and water mixture. The rigorous vapor-liquid equilibrium at the interface, on the other hand, gives flexibility to the model since the thermodynamic model might be changed in a straightforward manner to better represent the mixture and the operating conditions accordingly. The computation of the TTP using CAPE-open interfaces is another relevant feature of the proposed approach since it gives further flexibility to the model since the correlations that describe the TTP might be easily changed to better fit the system investigated. Additionally, we not only detail the modeling of the TTP but also validate their correlations prior to incorporating them into the falling film model.

The results corroborate that the proposed modeling approach can efficiently solve the falling film model on the basis of a unique set of differential algebraic equations. The equation-oriented approach does not need a tailored sequential algorithm neither fails with the numerical problems reported in literature. Therefore, the simultaneous approach proposed here is more robust and more flexible since it can be extended to other mixtures and integrated to a process flowsheet or optimization problems. This study motivates future applications of this numerical approach in absorbers with different geometries, as vertical and horizontal pipes, packed columns, and with other working fluids as well. Furthermore, the implementation of this model in an equation-oriented fashion enables its further utilization for simultaneous large-scale flowsheet optimizations, allowing the optimal design and operation of absorption refrigeration machines.

### III.6. References

AGAIEV, N. A., USIBOVA, A. D., DOKL. A., NAUK A.Z., Viscosity of ordinary and heavy water at high pressures in the temperature range from 0 to 150 °C. Soviet Physics Doklady 13, (1968), 334-337.

AMINYAVARI, M., APRILE, M., TOPPI, T., GARONE, S., MOTTA, M., A detailed study on simultaneous heat and mass transfer in an in-tube vertical falling film absorber. International Journal of Refrigeration 80 (2017) 37–51.

AMSTERCHEM                      CAPE-OPEN                      Thermo                      Imp  
<https://www.amsterchem.com/matlabthermo.html>, Accessed 26.03.2018.

AZNAR, M. A., GIMENO R. J., PEREZ, G. D., CARRASCO G., AFINIDAD, J. L., Density and excess volume of alkyl pyridine-water systems. Chem. Eng. Data 41, (1984), 355.

BIRD, B., STEWART, W., LIGHTFOOT, E. Transport Phenomena, Revised second ed. JohnWiley & Sons, Inc., (2006).

BOHRA, L. K., Analysis of Binary Fluid Heat and Mass Transfer in Ammonia-Water Absorption. PhD Dissertation Presented to The Academic Faculty, Georgia Institute of Technology, (2007).

CHEN, J., H., BO, S., MA, X., CHEN, Z. L., Numerical simulation on the falling film absorption process in a counter-flow absorber. Chemical Engineering Journal 156 (2010) 607–612.

CHILTON, T.H., COLBURN, A.P., Mass transfer (absorption) coefficients prediction from data on heat transfer and fluid friction. Ind. Eng. Chem. (1934) 26 1183–1187.

CLIFFORD, I. L., HUNTER, E., The system ammonia-water at temperatures up to 150°C and at pressures up to twenty atmospheres, J Phys Chem (1932) 37 i01-118.

CoLan documentation. (2011, May). Retrieved from <http://www.colan.org/>.

CONDE, M., Thermophysical properties of ammonia-water mixtures for the industrial design of absorption refrigeration equipment, M. CONDE Engineering, (2006).

COSENZA, F., VLIET, G.C., Absorption in falling water/LiBr films on horizontal tubes, ASHRAE Transactions 96, (1990), 693–701.

CRAGOE, C. S., HARPER, D. R. Specific Volume of Liquid Ammonia Sci. Pap. Bur. Stand. (U. S.) 17 (1921), 287-315.



DENG, S. M., MA W. B., Experimental studies on the characteristics of an absorber using LiBr/H<sub>2</sub>O solution as working fluid, *International Journal of Refrigeration* (1999) 22:293–301.

DIN, F., *Thermodynamic Functions of Gases*, Vol. 1, Butterworths, London (1956).

EDWARDS, T. J.; NEWMAN, J.; PRAUSNITZ, J. M. Thermodynamics of aqueous solutions containing volatile weak electrolytes, *AIChE J.* 21, (1975), 248-259.

EDWARDS, T. J., MAURER G., NEWMAN, J., PRAUSNITZ, J. M., Vapor-Liquid Equilibria in Multicomponent Aqueous Solutions of Volatile Weak Electrolytes, *AIChE J.*, v. 24 (1978), 966-976.

FERNANDEZ-SEARA J., SIERES J., RODRIGUEZ C, Vazquez M Ammonia–water absorption in vertical tubular absorbers. *Int. Therm Sci* (2005) 44, 277–288.

FUJITA, I., SUZUKI, T., UEMATSU, M. *J. Chem. Thermodyn.* 40, (2008), 260-264.

GOEL, N, GOSWAMI DY. Analysis of a counter-current vapor flow absorber. *International Journal of Heat and Mass Transfer* 48, (2005a), 1283-1292.

GOEL, N, GOSWAMI DY. A compact Falling Film Absorber. *Journal of Heat Transfer* 127, (2005b), 957-965.

GOLUBEV, I. F.; SOKOLOVA, V. P. TEPLOENERGETIKA, Thermal conductivity of ammonia at various temperatures and pressures, *Journal of heat transfer* 11, (1964), 64-67.

GOMMED, K., GROSSMAN, G., Koenig, M.S., Numerical study of absorption in a laminar falling film of ammonia-water. *ASHRAE Trans.* 107, (2001), 453–462.

GROSSMAN, G. Simultaneous heat and mass transfer in film absorption under laminar flow. *International Journal of Heat and mass transfer* 26, (1983), 357-71.

ARIYADI, H. M. and CORONAS, A. Absorption Capacity of Ammonia into Ionic Liquids for Absorption Refrigeration Applications. *Journal of Physics: Conference Series* 745, (2016), 032105.

HABIB, H. M. and WOOD, B. D. Simultaneous Heat and Mass Transfer in Film Absorption with the Presence of Non-Absorbable Gases. *Journal of Heat Transfer* 123, (2001), 984-989.

HERBINE, GS, PEREZ-BLANCO H Model of an ammonia–water bubble absorber. ASHRAE ASHRAE Tech Data Bull 11, (1995), 102–110.

HIRSCHFELDER, J., CURTISS, C. F., BIRD, R. B. Molecular Theory of Gases and Liquids. Wiley, New York (1954) ISBN 0471400653.

HO, J.C., ISLAM, M. R., WIJEYSUNDERA, N.E.. Simplified models for coupled heat and mass transfer in falling-film absorbers. International Journal of Heat and Mass Transfer 47, (2004), 395–406.

KILLION, J. D. AND GARIMELLA, S. A critical review of models of coupled heat and mass transfer in falling-film absorption. International Journal of Refrigeration, 24(8), (2001), 755–797.

KRICHEVSKY, I. R. and KASARNOVSKY, J. S. Thermodynamical Calculations of Solubilities of Nitrogen and Hydrogen in Water at High Pressures. J. Am. Chem. Soc. 57, (1935), 2168-2171.

KAKAÇ, S., AUNG, W., SHAH, R.K. Handbook of Single-phase Convective Heat Transfer. (1987) Wiley NewYork.

KANG, Y.T., AKISAWA, A., KASHIWAGI, T. Analytical investigation of two different absorption modes: falling film and bubble types. Int. J. Refrigeration 23, (2000), 430–443.

KANG, Y.T., KASHIWAGI, T., CHRISTENSEN, R.N. Ammonia-water bubble absorber with a plate heat exchanger. ASHRAE Trans. Pt 1B, (1998), 1565–1575.

KIM, B., Heat and mass transfer in a falling film absorber of ammonia-water absorption systems, Heat Transfer Eng. 19 (3), (1998), 53–63.

KIM, H.Y., SAHA, B.B., KOYAMA, S., Development of a slug flow absorber working with ammonia–water mixture: part II –data reduction model for local heat and mass transfer characterization. Int. J. Refrigeration 26, (2003), 698–706.

LAESECKE, A.; LUEDDECKE, T. O. D.; HAFER, R. F.; MORRIS, D. J. Viscosity measurements to ammonia, R32, and R134a. Vapor buoyancy and radial acceleration in capillary viscometers. Int. J. Thermophys. 20, (1999), 401-434.

LÁZARO-COLÁN, V. A., Experimental study of an absorption column of water vapor and ammonia in water, PhD thesis (2012) Sao Paulo, Federal University (USP), Sao Paulo, Brazil

LEES, C. H. PHILOS. TRANS. R. On the Thermal Conductivities of Single and Mixed Solids and Liquids and their Variation with Temperature Soc. London, Ser. A 191, (1898), 339-440.

LEITE, B., Modeling of the absorber and the generator of ammonia/water heat absorption refrigeration cycle based on the falling film technology on inclined plates., Master thesis (2015) Sao Paulo, Federal University (USP), Sao Paulo, Brazil.

LIN, P.W., XIA, R.Z, Numerical investigation of a two-stage air-cooled absorption refrigeration system for solar cooling: cycle analysis and absorption cooling performances. *Renew Energy* 36, (2011), 1401–1412.

LIU, J.; WANG, S.; HARTONO, A.; SVENDSEN, H. F. Solubility of N<sub>2</sub>O in and Density and Viscosity of Aqueous Solutions of Piperazine, Ammonia, and Their Mixtures from 283.15 to 323.15 K. *Chen, C. J. Chem. Eng. Data* 57(9), (2012), 2387-2393.

MACRISS, R. A., EAKIN, B. E., ELLINGTON, R. T., Huebler, J., Physical and Thermodynamic Properties of Ammonia-Water Mixtures. *IGT Research Bulletin* 34, (1964).

MERCHAN, V. A., ESCHE, E., FILLINGER, S., TOLKSDORF, G., AND WOZNY, G. Computer-Aided Process and Plant Development – A Review of Common Software Tools and Methods and Comparison against an Integrated Collaborative Approach. *Chemie Ingenieur Technik* 88, (2015), 50-69.

MILLER, W. A., KEYHANI M. The correlation of simultaneous heat and mass transfer experimental data for aqueous lithium bromide vertical falling film absorption. *Journal of Solar Energy Engineering* 123, (2001), 30–42.

MITTERMAIER, M, ZIEGLER, F. Theoretical evaluation of absorption and desorption processes under typical conditions for chillers and heat transformers. *International Journal of Refrigeration* 59, (2015), 91-101.

MOSAIC documentation. (October, 2011). Retrieved from <http://www.mosaic-modeling.de>.

PEREZ-BLANCO, H. A. A model of an ammonia-water falling film absorber, *ASHRAE Trans.* 94 (1), (1988), 467-483.

PERRY, R. H.; GREEN, D. W. (Ed.) *Perry's Chemical Engineers' Handbook*. McGraw-Hill: New York, (1999).

POTNIS, S.V., ANAND, G., GOMEZPLATA, A., ERICKSON, D.C., Papar, R.A., GAX component simulation and validation. *ASHRAE Trans* 1, (1997), 454–459.

PRATA, J. E., Modeling of a falling film absorber for a refrigeration cycle by absorption of ammonia and water. Master thesis (2012) Sao Paulo, Federal University (USP), Sao Paulo, Brazil.

PRAUSNLTZ, J. M., EDWARDS T. J, NEWMAN J., Thermodynamics of Vapor-Liquid Equilibria for the Ammonia-Water System. *Ind. Eng. Chem. Fundam.* 17, (1978), 264-269.

PRETEK, J. and KLOMFAR, J. Simple functions for fast calculations of selected thermodynamic properties of the ammonia-water system: *Int. J. Refrigeration* 18 (1995), 228-234.

ROSA, L.S, PONTES, K.V, PENTEADO A. T, TOLKSDORF, G., ESCHE, E., REPKE, J.-U, Using MOSAIC modeling and CAPE-OPEN interfaces for property calculations in MATLAB. *Blucher* 1, (2018), 4392-4395.

SEADER, D. HENLEY, E. J. Separation process principles. Published. New York : Wiley, (1998).

SIERES, J FERNANDEZ-SEARA J., Modeling of simultaneous heat and mass transfer processes in ammonia–water absorption systems from general correlations. *Heat Mass Transfer* 44, (2007), 113–123.

SIERES, J., FERNÁNDEZ-SEARA, J., UHÍA, F., Analysis of an air cooled ammonia–water vertical tubular absorber. *International Journal of Thermal Sciences* 46, (2007), 93–103.

TIMROT, D. L. PAR VYSOKIH, Steam of high parameters in energetics: Properties of water steam, *Parametrov Energetike* 72, (1950), 767-778.

TOLKSDORF, G.; ESCHE, E.; WOZNY, G.; REPKE, J.-U. Customized code generation based on user specifications for simulation and optimization. *Computers and Chemical Engineering* 121, (2019), 670–684.

TRAUTZ, M.; HEBERLING, R., Viscosity of ammonia & its mixture with hydrogen, nitrogen, ethylene, *ANN. Physik* 10, (1931), 155-177.

TREYBAL, R.E., *Mass Transfer Operations*, McGraw-Hill, New York, (1980).

TRICHÉ D., BONNOTA, S., PERIER-MUZETA, M., BOUDÉHENNA F. DEMASLESA H., CANEY, N. Modeling and experimental study of an ammonia-water falling film Absorber SHC 2015, *International Conference on Solar Heating and Cooling for Buildings and Industry Energy Procedia* 91, (2016), 857 – 867.

TRICHÉ D., BONNOTA, S., PERIER-MUZETA, M., BOUDÉHENNA F. DEMASLESA H., CANEY, N. PERIER-MUZET, M. Experimental and numerical study of a falling film absorber in an ammonia-water absorption chiller. *International Journal of Heat and Mass Transfer* 111, (2017), 374–385.

TRICHÉ, D., Numerical and experimental study of coupled mass and heat transfers in the absorber of an ammonia-water absorption machine. PhD Thesis (2016) Université Grenoble Alpes, France.

VAN BATEN, J., COCO cape open to cape open simulation environment, [www.cocosimulator.org](http://www.cocosimulator.org), (2016).

VAN NESS, H. C., SMITH, J. M., and ABBOTT, M. M., Introduction to Chemical Engineering Thermodynamics, 7th Edition, McGraw Hill Professional, New York, (2007).

VARLASHKIN, P. G.; THOMPSON, J. C. J. Thermal Conductivity of liquid Ammonia Chem. Eng. Data 8, (1963), 526-526.

FLORI, M., VÎLCEANU, L., Performance Characteristics of Vapor Compression Refrigeration Systems. Annals of Faculty Engineering Hunedoara- International Journal of Engineering 2, (2012), 145-148.

VYAZOVOV, V. V. A theory of absorption of slightly soluble gases by liquid films, .I. Tech. Phys 10. (1940), 1519-1532.

WILKE, C.R., CHANG, P., Correlation of diffusion coefficients in dilute solutions, AIChE Journal 1(2), (1955), 264-270.

WILKE, W. Wärmeübergang an Rieselfilme, VDI-Fors-Chungsheft 490 (1962) B28.

XU, F., D. GOSWAMI, Y. Thermodynamic properties of ammonia–water mixtures for power-cycle applications Energy 24, (1999), 525–536.

YIH, S. M., Modeling heat and mass transport in Falling Film Liquid Films, Handbook of heat and Mass Transfer: Mass Transfer and Reactor Design, N. P: Chermisinoff, eds., Gulf Publishing Company 5, (1986), 111-120.

ZIEGLER, B., TREPP, C., Equation of state of ammonia–water mixtures, Int. J. Refrig. 7, (1984), 101–106.

## Appendix A

The following correlations are used to calculate some Thermodynamics and Transport Phenomena Properties of NH<sub>3</sub>, H<sub>2</sub>O and NH<sub>3</sub>/H<sub>2</sub>O mixture, such as: specific heat and binary diffusivity coefficient.

- Specific heat of ammonia and water in vapor phase,  $C_{p_{V,i}}$  (J/mol-K) are calculated by (Van Ness et al., 2007):

$$\frac{C_{p_{V,i}}}{R} = A + BT + CT^2 + DT^{-2} \quad \text{A-1}$$

where  $A, B, C, D$  are parameters (Van Ness et al., 2007),  $T$  (K) is temperature and  $R$  (J/mol-K) is the gas constant.

- Specific heat of ammonia and water in liquid phase (J/mol-K), are respectively computed by (Perry, 1999):

$$C_{p_{L,NH_3}} = \frac{C_1^2}{t} + C_2 - 2C_1 C_3 t - C_1 C_4 t^2 - \frac{C_3^2 t^3}{3} - \frac{C_3 C_4 t^4}{2} - \frac{C_4^2 t^5}{5} \quad \text{A-2}$$

$$C_{p_{L,H_2O}} = C_1 + C_2 T + C_3 T^2 + C_4 T^3 + C_5 T^4 \quad \text{A-3}$$

where  $T$  (K) is temperature,  $C_1, C_2, C_3, C_4$  and  $C_5$  are parameters (Perry, 1999),  $t = 1 - T_r$ .  $T_r, T_r = T/T_c$  and  $T_c$  is critical temperature (K).

- Specific heat of the liquid and vapor mixtures are calculated according to (Conde, 2006; Prata, 2012; Triché, 2016):

$$C_{PL} = x_{NH_3} C_{PL,NH_3} + x_{H_2O} C_{PL,H_2O} \quad \text{A-4}$$

$$C_{PV} = y_{NH_3} C_{PV,NH_3} + y_{H_2O} C_{PV,H_2O} \quad \text{A-5}$$

where  $x$  and  $y$  are mass fractions at the liquid and vapor phase, respectively.

- The binary diffusivity coefficient for the liquid mixture can be calculated by (Conde, 2006):

$$D_L = 117.282 \cdot 10^{-18} T \frac{\sqrt{\Psi_m M_m}}{\mu_m V_{diff}^{0.6}} \quad \text{A-6}$$

where  $T$  (K) is temperature,  $\mu_m$  (Pa-s) is the dynamic viscosity,  $M_m$  (g/mol) is the mixture molecular weight,  $V_{diff}$  (cm<sup>3</sup>/mol) is the molar volume from Conde (2006) and  $\Psi_m$  is the mixture association factor from Wilk and Chang, 1955.

- The binary diffusivity coefficient for the vapor phase can be computed by the Chapman-Enskog equation (Bird *et al.*, 2006):

$$D_V = 0.0018583 \sqrt{T^3 \left( \frac{1}{M_{NH_3}} + \frac{1}{M_{H_2O}} \right) \left( \frac{1}{P \sigma_{NH_3, H_2O} \Omega_D} 10^{-4} \right)} \quad A-7$$

where  $T$  (K) is temperature,  $M_{NH_3}$  and  $M_{H_2O}$  are the molecular weights for ammonia and water, respectively,  $P$  (atm) is pressure,  $\Omega_D$  is a collision integral and  $\sigma_{NH_3, H_2O}$  (Å) is the molecular diameter, both of them from Hirschfelder *et al.* (1954).

### Notation

$A$	Area (m <sup>2</sup> )
$z$	Length (m)
$\delta$	Thickness of the film (m)
$m$	Mass flowrates (kg.s <sup>-1</sup> )
$\dot{m}$	mass flux kg.m <sup>-2</sup> s <sup>-1</sup>
$U$	overall heat transfer coefficient though the wall (W-m <sup>-2</sup> K <sup>-1</sup> )
$q$	Sensible heat flux (W-m <sup>-2</sup> )
$H$	Enthalpy (J-kg <sup>-1</sup> )
$\tilde{h}$	Partial Mass Enthalpy (J-kg <sup>-1</sup> )
$Q$	Heat flux (W-m <sup>-2</sup> )
$L$	Length of the heat and mass exchange area
$P$	Pressure (bar)
$R$	ideal gas constant (cm <sup>3</sup> -atm <sup>-1</sup> mol <sup>-1</sup> )
$T$	Temperature (K)
$d$	Diameter (m)
$x$	Molar/mass fraction at the liquid phase
$y$	Molar/mass fraction at the vapor phase
$\alpha$	heat transfer coefficient (W-m <sup>-2</sup> K <sup>-1</sup> )
$F$	Mass transfer coefficient (kg-m <sup>-2</sup> s <sup>-1</sup> )
$Z$	Mass fraction of ammonia in the absorbed/desorbed flux
$\psi$	Correction factor
$C_p$	Specific heat (J-kg <sup>-1</sup> K <sup>-1</sup> )
$M$	Molecular Weight (g-mol <sup>-1</sup> )
$Sc$	Schmidt number
$Pr$	Prandtl number
$D$	Diffusivity (m-s <sup>-2</sup> )
$\mu$	Viscosity (Pa-s <sup>-1</sup> )
$\lambda$	Thermal conductive (W-m <sup>-1</sup> K <sup>-1</sup> )
$\rho$	Density (kg-m <sup>-3</sup> )
$Re$	Reynolds Number

$H'$	Henry's constant (bar)
$v$	Partial molar volume
$f$	Fugacity (bar)
$\gamma$	Activity Coefficient
$a_{22}$	Parameter of the equation of state
$b$	Parameter of the equation of state
$\phi$	Fugacity Coefficient
$ap$	Correlation composition parameter
$mp$	Correlation composition parameter
$np$	Correlation composition parameter
$nd$	Number of discretization points
$k$	Numbers of parameters at the empirical correlation for bubble point
$j$	Numbers of parameters at the empirical correlation for dew point

*Superscript*

*	Asymmetric convention
$S$	Saturation State
$P_0$	Reference Pressure
$\infty$	Infinite Dilution

*Subscript*

$hv$	Hydraulic diameter of the vapor in the control volume
$0$	Reference State
$L$	Liquid Phase
$V$	Vapor Phase
$c$	Coolant
$i$	component index
$int$	Interface
$W$	Absorber length (m)
$w$	Wall



# CHAPTER IV- TECHNICAL AND ECONOMICAL COMPARISON BETWEEN A FALLING FILM AND A PACKED COLUMN FOR ABSORPTION OF NH<sub>3</sub> BY A NH<sub>3</sub>/H<sub>2</sub>O SOLUTION

---

*“Science is a willingness to accept facts even when they are opposed to wishes”.*

BURRHUS FREDERIC SKINNER

## **IV.1. Initial Considerations**

The absorption of ammonia by a solution of ammonia and water is carried out in falling film and packed columns. This study compares both equipment in terms of absorption capacity, equipment cost and cooling demand based on predictions of rigorous mathematical models validated with experimental data from literature. The packed absorption column is modeled in Aspen Plus, and the falling film, by an equation-oriented approach in Matlab. The UNIQUAC model was used to describe the non-idealities at the liquid phase, and the vapor phase was assumed ideal gas. The results show that the falling film provides a uniform coolant distribution, which favor ammonia absorption. As a consequence, for the same absorption capacity, the falling film allows a reduction of nearly 33.3% in the volume required by the absorption column, at the expense of a capital and installation cost 51% higher. Therefore, the falling film offers a more compact unit but, when space limitation is not an issue, absorption columns might take advantage. As consequence was found that the ammonia mass fraction at the liquid phase, along the absorber length, is slightly higher (4%) than the packed column, showing a greater absorption capacity.

## **IV.2. Introduction**

Absorption refrigeration cycle is commonly used in industry to produce refrigerant at low temperatures. Large absorption-refrigeration systems are found, for

example, in petrochemical plant, where refrigeration capacities up to  $-45^{\circ}\text{C}$  are required for scrubbing processes (Dryden, 1982) or in steelworks sites for cooling prior to liquefaction and separation of gases. In an absorption refrigeration system, the refrigerant (ammonia vapor) is desorbed in an evaporator in a highly endothermic process, which generates the desired refrigeration and the vapor phase is absorbed by a solution in a downstream absorber. The two most common working fluids in absorption refrigeration cycles are LiBr/H<sub>2</sub>O and NH<sub>3</sub>/H<sub>2</sub>O. According to Flores *et al.* (2014), the LiBr/H<sub>2</sub>O fluid presents a risk of crystallization at mass fraction above 68%. On the other hand, the mixture NH<sub>3</sub>/H<sub>2</sub>O is highly stable for a wide range of operating temperatures and pressures (Srikhirin *et al.*, 2001). The absorber is the key unit for a good overall cycle performance (Lázaro-Colán, 2012; Mittermaier e Ziegler, 2015), since the amount of refrigerant absorbed reflects in the refrigeration effect in the evaporator. Therefore, the size, performance and cost of the absorber significantly influences the efficiency of the overall cycle. The design of an absorber must provide sufficient residence time and large contact surface area between solution and vapor to increase the rate of mass and heat transfer, as well as consider minimum size and minimum investment and operating cost (Selim and Elsayed, 1999a).

According to Bahena and Romero (2014) falling film are the most common type of absorbers used in ammonia and water absorption refrigeration cycle. The falling film, depicted in Figure 1a, comprises an array of cooling tubes/plates over which the weak solution is uniformly distributed and flows down by gravity. As the vapor containing the refrigerant flows co-currently or counter-currently to the weak solution, the refrigerant is absorbed by the weak solution. The heat released by absorption is rejected to the coolant flowing upward through the cooling tubes/plates (Bahfar et al. 2014). To ensure a good distribution of the liquid film on each plate and to maximize the surface of the liquid-vapor interface the dispenser has to be carefully chosen.

Several studies in literature report the design of falling film absorbers applied to the ammonia refrigeration absorption cycle. The geometry of the equipment varies from plates (Goel and Goswamy, 2005a) or tubes, which can be vertically or horizontally arranged (Goel and Goswamy, 2005b). Goel and Goswamy, 2005b, concluded that a greater number of tubes with smaller diameter for the cooling fluid is the most efficient configuration as it increases the mass transfer area, while reducing 25% the size of the equipment. Triché *et al.* (2016) presented a prototype plate-type absorber that yielded

26% increase in the mass fraction of ammonia at the liquid phase regarding the feed concentration. The prototype proposed by Aminaravy et al. (2017) consists of a falling film composed of vertical tubes. The tubes are arranged in a column where the cooling fluid (water) flows downward the column co-currently with the vapor and the liquid solution of ammonia and water. The authors observed an outlet mass fraction of ammonia 25% higher than the inlet mass fraction. Among the several configurations presented in the literature for falling film absorbers, Hasenöhr (2011) states that the plate arrangement offers a lower cost and, for a given operating capacity, is more compact than the tubes arrangement.

Packed columns are used in a variety of applications in the chemical process industries. The  $\text{CO}_2$  absorption in packed columns, for example, is a mature technology (Peter, 2013). Some authors report successful application of packed columns for the ammonia absorption by an ammonia and water solution (Selim and Elsayed 1999a, 1999b and Govindaraju, 2005). A typical packed column, depicted in Figure 1b, consists of a vertical, cylindrical shell containing a support plate for the packing material, mist eliminators, as well as a liquid distributing device designed to provide effective irrigation to the packing (Benitez, 2009). The design allows uniform distribution of the solution, and thus provides a large contact area between the liquid and vapor phases. In the packed column, illustrated in Figure 1b, the weak solution with ammonia and water flows downward, while the vapor stream flows from upward. The counter-current flow is more commonly applied because higher mean concentration driving force is achieved compared to that offered by the co-current flow because the contact time and interfacial area between the two phases is decreased, reducing the absorption rate (Shende and Sharma 1974; Govindaraju, 2005). The heat removal in a packed column is not straightforward since the incorporation of cooling coils inside the equipment is not advisable. To overcome this, intercooling is usually applied in the literature (Kvamsdal and Rochelle, 2008, Karimi et. al, 2011, Sachde and Rochelle, 2014 and Oko et. al., 2018). Intercooling is especially useful for systems where the heat of absorption, i.e., heat of solution and/or reaction, results in an increase in temperature of the solvent affecting the vapor pressure of the dissolved species (Plaza et al., 2009). The need to increase heat and mass transfer rates, coupled with the demand for compact and efficient absorbers, stimulates research on design and modeling of various absorber configurations applied to the absorption refrigeration cycle.

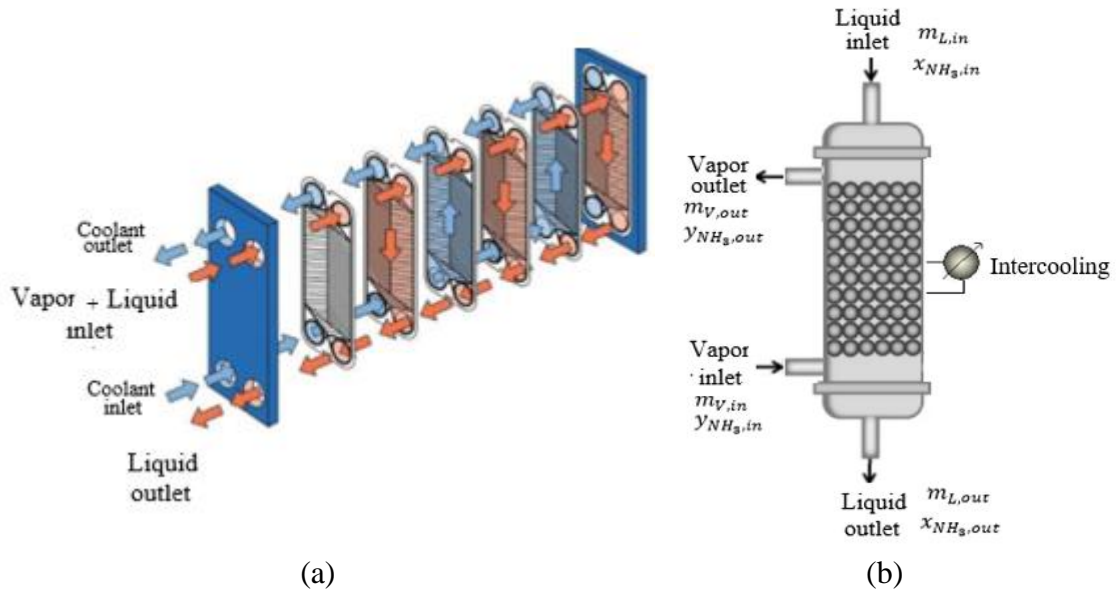


Figure 1- (a) Plate falling film absorber (Cavallo, 2020) e (b) Packed column absorber

Usually for the falling films absorbers, the liquid phase is called *absorbent* and the vapor phase, *refrigerant*. For the packed column, the liquid phase is usually called *solvent* and the vapor phase, *gas*. For the sake of uniformity, this study will adopt the nomenclature liquid and vapor phase to refer the streams of the absorbers. The absorption of ammonia by a solution of ammonia and water is usually carried out in falling film and, less commonly, in packed columns. Each equipment has its specificities, pros and cons regarding, e. g. energy efficiency, adsorption capacity, size and cost. Given the particularities of each technology, a comparative study evidences some key aspects which can support decision making for the industry and meaningful contributions to literature. The equipment modeling become a basic chemical engineering tool for the development of strategies aimed at determining the most efficient technology for a particular application. The study comparing the absorption capacity and installation cost of both technologies for ammonia absorption might give insights about the operation of each equipment and support the choice of the most recommended for the absorption.

The estimation of equipment cost is an important issue for engineering design, but the cost analysis of falling film and packed column for refrigeration cycles has rarely been approached in the literature. Up to the authors knowledge, only Siddiqui (1997) performed an economic analysis of the equipment of an absorption system: falling film tubes, condenser, evaporator, generator, rectifier, pre-cooler and pre-heater. The cost of the entire system was estimated based on empirical correlations, relying on the materials

used, equipment size, installation cost and general expenses. The authors analyzed four refrigerants ( $\text{H}_2\text{O-LiBr}$ ,  $\text{NH}_3\text{-H}_2\text{O}$  and  $\text{NH}_3\text{-LiNO}_3$ ) and concluded that the pair  $\text{NH}_3\text{-H}_2\text{O}$  is 44% more economical than the others. The authors do not attempt to investigate the packed column, therefore, the literature still lacks a techno and economic comparison between the absorbers applied to the absorption system using ammonia and water as a working fluid.

This study aims to perform a techno-economic comparison between falling film and packed column for ammonia absorption by an ammonia and water solution. The technical analysis is based on phenomenological models to predict the efficiency of absorption, monitoring the temperature and mass fraction profiles. The falling film is modeled using a robust equation-oriented approach developed in Chapter III, considering the plates geometry and design parameters in Triche et al. (2016). The packed column is designed by empirical correlations from Norton Chemical Company (Norton, 1977), to achieve the same absorption capacity as the falling film, and modeled in Aspen Plus. The cost estimation of the absorbers is based on the estimation of the investment and installation cost, calculated by empirical correlations from literature by a simplified application of the capital expenditure (CAPEX). The operational expenditure (OPEX) is not considered in this study. The literature lacks a systematic comparison of both equipment regarding the efficiency in terms of ammonia absorption rate, energy consumption, design, operational parameters and cost estimates.

The chapter is organized as follows. Firstly, the absorbers models are presented, followed by the correlations for calculating heat and mass transfer coefficients and the thermodynamic models used to describe the ammonia and water vapor-liquid equilibrium (VLE). Section 3 presents the equipment cost estimation. The results are presented in Section 4: validation of the thermodynamic model with VLE experimental data of ammonia and water, validation of the falling film and packed column model with experimental data from the literature, sensitivity analysis regarding design parameters and operating conditions.

### **IV.3. Modelling of absorbers**

The absorber in an absorption refrigeration cycle aims to concentrate the weak refrigerant solution ( $\text{NH}_3\text{+H}_2\text{O}$ ) by capturing the refrigerant ( $\text{NH}_3$ ) in the vapor stream. The concentration of ammonia in the enriched solution directly influences the heat exchange

in the evaporator where the refrigeration effect happens. The performance of an absorber depends on the rate of absorption, which is determined by the diffusion of ammonia vapor through the liquid phase, and on the phase equilibrium. The next sections present the phenomenological models of the falling film and the absorption column. The steady state models of the absorbers consider unidimensional flow regime, adiabatic equipment and vapor and liquid thermodynamic equilibrium at the interface.

**a. Falling film model**

In the plate falling film absorber, as illustrated in Figure 2, the liquid stream of ammonia and water flows from the top to the bottom, co-currently with the vapor stream (99% wt. ammonia). The cooling fluid is cooling water that flows upstream between the absorber plates. The prototype presented by Triche et al. (2016) is taken as a reference for this comparative study and its dimensions are summarized in Table 1. This falling film consists of 16 plates: 8 channels for the coolant and 7 channels for the liquid and vapor solution, resulting in 14 falling film formed between the plates.

Table 1- Dimensions of the falling film (Triche et al., 2016).

Type of plate material	Liga de metais 316 (Alloy 326)
Plate width	0.111 m
Plate thickness	0.0004 m
Height	0.526 m

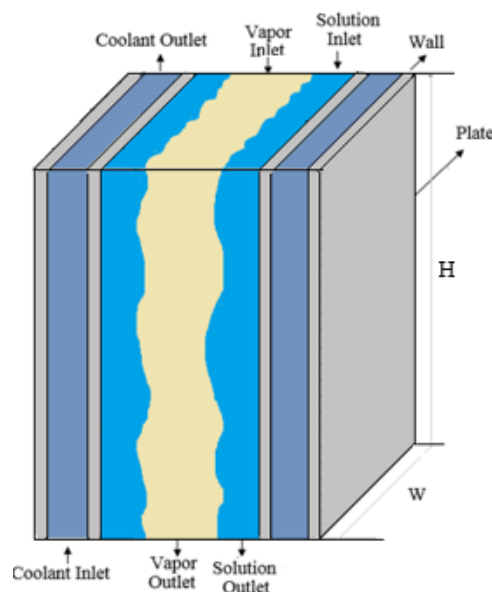


Figure 2- Plate Falling film absorber (Adapted from Triche et al., 2016)

The model of falling film absorber was previously developed (Chapter III) and validated with the experimental data from Triche et al. (2016). It is described by differential mass and energy balances coupled with algebraic equations representing the mass and energy transfer as well as the phase-equilibrium at the interface. The equation-oriented approach ensures robustness and flexibility as it can be extended to other working fluids in a straightforward manner. The mass, component and energy balances for each phase, as well as the coolant together with the mass fluxes of ammonia and water at the interface, are summarized in Table 2. The specific enthalpy of liquid mixture,  $H_L$  (J·kg<sup>-1</sup>), is computed by the correlation proposed by Pretek and Klomfar (1995), as already applied by other authors (Conde, 2006; Triché *et al.*, 2016, 2017). The mass fluxes of ammonia and water,  $\dot{n}_{i,int}$  (kg·m<sup>-2</sup>·s<sup>-1</sup>), are calculated according to Treybal (1968), as also carried out by Goel and Goswami (2005a, 2005b), Lin *et al.* (2011), Sieres and Fernández-Seara (2007).

Table 2- Mathematical model of the falling film.

<b>Vapor phase</b>		
Mass balance	$\frac{dm_V}{dz} = -L \sum_{i=1}^{NC} \dot{n}_{i,int}$	
Component mass balance	$\frac{d(m_V \cdot y_i)}{dz} = \frac{d(m_{V,i})}{dz} = -\dot{n}_{i,int} \cdot L \quad i = 1, \dots, NC$	
Energy balance	$\frac{dH_V}{dz} = \frac{(-\dot{q}_V + H_V \sum_{i=1}^{NC} \dot{n}_{i,int}) \cdot L}{m_V}$	
<b>Liquid phase</b>		
Mass balance	$\frac{dm_L}{dz} = L \sum_{i=1}^{NC} \dot{n}_{i,int}$	
Component mass balance	$\frac{d(m_L \cdot x_i)}{dz} = \frac{d(m_{L,i})}{dz} = \dot{n}_{i,int} L \quad i = 1, \dots, NC$	
Energy balance	$\frac{dH_L}{dz} = \frac{(\dot{q}_L - H_L \sum_{i=1}^{NC} \dot{n}_{i,int}) \cdot L - L_c \cdot U \cdot (T_L - T_c)}{m_L}$	
<b>Coolant</b>		
Energy balance	$\frac{dH_c}{dz} = -\frac{L_c \cdot Q_c}{m_c} = -\frac{L_c \cdot U \cdot (T_L - T_c)}{m_c}$	
<b>Boundary conditions</b>		
$m_L(z = 0) = m_{L0}$	$m_V(z = 0) = m_{V0}$	$H_c(z = L) = H_{cL}$
$x_i(z = 0) = x_{i0}$	$y_i(z = 0) = y_{i0}$	
$H_L(z = 0) = H_{L0}$	$H_V(z = 0) = H_{V0}$	
<b>Heat and mass transfer equations at the interface</b>		
Mass flux at the vapor interface	$\sum_{i=1}^{NC} \dot{n}_{i,int} = K_V \cdot \rho_V \cdot \ln \frac{(FZ - y_{NH_3,int})}{(FZ - y_{NH_3})}$	
Mass flux at the liquid interface	$\sum_{i=1}^{NC} \dot{n}_{i,int} = K_L \cdot \rho_L \cdot \ln \frac{(FZ - x_{NH_3})}{(FZ - x_{NH_3,int})}$	
Heat transfer equation at the interface	$\begin{aligned} \dot{\alpha}_V \cdot (T_V - T_{int}) + \sum_{i=1}^{NC} \dot{n}_{i,int} \cdot \tilde{h}_{V,i} \\ = \dot{\alpha}_L \cdot (T_{int} - T_L) + \sum_{i=1}^{NC} \dot{n}_{i,int} \cdot \tilde{h}_{L,i} \end{aligned}$	

The thermodynamic and transport properties (viscosity, heat capacity, density) are calculated by CAPE-OPEN interfaces using the libraries in TEA (Thermodynamics for Engineering Applications, Van Baten, 2016). The resulting set of equations (mass and energy balances and mass flux at the interface) consists of a non-linear algebraic-



differential system. The differential equations that make up the falling film model were discretized by the finite difference method. The model was implemented in MOSAICmodeling (<http://mosaic-modeling.de/>), a free online modeling environment, capable of automatically generating codes for process simulation and optimization in different programming languages (Merchan et al., 2015 and Tolksdorf et al., 2019). The model is solved in Matlab using the native function *fsolve*, based on the residual minimization method. The falling film model was validated with experimental data from Triche et al (2016) at the operating conditions shown in Table 3.

Table 3- Operating conditions to validate the falling film model at a pressure of 6 bar

Variable	Inlet data		
	Vapor	Liquid	Coolant
Mass flowrate	$5.25 \cdot 10^{-3}$ (kg/s)	$1.67 \cdot 10^{-2}$ (kg/s)	0.326 (kg/s)
Temperature	296.9 (K)	312.0 (K)	300.2 (K)
Mole fraction of NH <sub>3</sub>	0.995	0.46	0
Pressure (bar)	6 bar		
Variable	Outlet data		
Mass flowrate	0	$2.22 \cdot 10^{-2}$ (kg/s)	0.326 (kg/s)
Temperature	–	303.7 (K)	305.8
Mole fraction of NH <sub>3</sub>	0	0.591	0
Pressure (bar)	6 bar		

### ***b. Packed column design***

The absorber column design involves the following steps (Turton et al., 2009): a) selection of the packing type and size; b) determination of the column diameter; c) determination of pressure drop; d) determination of the column height for the required separation; e) selection and design of the column internals (packing support and dispensing liquid). These steps will be described below, except the last one (e), because it might not be included in a preliminary assessment as the proposed in this study.

#### *i. Selection of packing type and size*

The literature reports the use of Berl ceramic saddles and Raschig rings (Selim and Elsayed, 1999a and Selim and Elsayed, 1999b) for the absorption of ammonia by an ammonia and water solution. The height of the column is function of several empirical parameters, some of them related to the packing type. Due to the availability of correlations for Raschig rings by the Norton Chemical Company (Norton, 1977). Raschig rings are,

therefore, used as a packing. The packaging height considered is 0.375 in as recommended by the Norton Chemical Company (Norton, 1977).

*ii. Determination of the column diameter (capacity)*

The dimensioning of the column diameter depends on the vapor flowrate, on the vapor properties and on the ratio between the liquid and vapor flowrates. The diameter can be calculated by several methods, including: recognized pressure drop criterion, flood removal criterion and efficiency criterion (Valez et al. 2013). The recognized pressure drop criterion was proposed by Eckert (1966) and has been used in the literature since its publication to the present date (Bonilla and Klemas 2000, Al-Saidv 2014, Sánchez et al. 2016, Rabelo et al. 2019). Therefore, this method is used to determine the diameter of the packed column,  $\emptyset$ , according to:

$$\emptyset = \sqrt{\frac{4 \cdot A}{\pi}} \quad (1)$$

where  $A$  (ft<sup>2</sup>) is the column cross sectional area, calculated as  $A = m_{V,in}/(I_C G'_f)$  where  $m_{V,in}$  (lb/s) is the mass flowrate of the inlet vapor stream,  $I_C$  the desired percentage of velocity at the flood condition (typically 70% to 80% for packed columns) and  $G'_f$  (lb/ft<sup>2</sup>s) is the surface mass flowrate of the vapor at the flood condition, which can be calculated from generalized correlations, as proposed by Eckert (1970):

$$\begin{aligned} & \log \left( \frac{G'_f{}^2 \cdot PF \cdot \varphi \cdot \mu^{0.2}}{\rho_L \cdot \rho_V \cdot g_c} \right) \\ & = -1.667 - 1.085 \log_{10} FA_{VL} - 0.29655(\log_{10} FA_{VL})^2 \end{aligned} \quad (2)$$

where  $\rho_L$  and  $\rho_V$  (lb/ft<sup>3</sup>) are density of liquid and vapor, respectively, at average temperature between inlet and outlet,  $\varphi$  is the inverse of liquid specific density ( $\rho_{\text{agua}}/\rho_L$ ),  $\mu$  (cP) is liquid viscosity,  $g_c$  (32,3 ft lbm / lbf-sec<sup>2</sup>) is gravity and PF is a packing factor that depends of the packing type and size available in Wankat (2011). For Raschig rings of 0.375 in,  $PF = 1000$ . The units are in the English system because these are empirical correlation, estimated using this set of units.  $FA_{VL}$  is a dimensionless parameter given by:

$$FA_{VL} = \frac{m_{L,in}}{m_{V,in}} \cdot \left(\frac{\rho_V}{\rho_L}\right)^{0,5} \quad (3)$$

where  $m_{L,in}$  (lb/s) and  $m_{V,in}$  (lb/s) are the inlet flowrates of liquid and vapor, respectively.

*iii. Determination of the pressure drop*

The pressure drop in packed columns can be calculated from the empirical correlation proposed by Eckert (1970):

$$\Delta P = \alpha \cdot (10^{\beta \cdot m_{L,in}}) \cdot \left(\frac{G_f'^2}{\rho_V}\right) \quad (4)$$

where  $\alpha$  and  $\beta$  are parameters related to the type of packing, available in Turton et al. (2009),  $m_{L,in}$  (lb/s) is the inlet liquid mass flowrate at the absorber,  $G_f'$  (lb/ft<sup>2</sup>s) is the vapor surface mass flowrate at the flood condition (Eq. 2),  $\rho_V$  (lb/ft<sup>3</sup>) is the vapor density at the average temperature between inlet and outlet conditions and  $\Delta P$  is the pressure drop in inches of H<sub>2</sub>O per feet of column height.

*iv. Determination of the column height required for the specified separation*

The column height calculation is based on mass and energy balances and mass transport coefficients. The literature reports two most common methods for calculating that height: HTU method (Height of a Transfer Unit), based on a mass transfer analysis and HEPT method (Height Equivalent to a Theoretical Plate) based on an analysis of equilibrium stages. The HTU method is extensively used in the literature, however, its great challenge is to obtain the correlations for mass transfer coefficients. In order to overcome this difficulty, several companies that produce packed columns have published empirical correlations for the dimensioning of columns involving the systems of greatest commercial interest. Among these companies, Norton Chemical Company (Norton, 1977) stands out, whose empirical correlations are established and widely used to design absorption columns. Therefore, we consider the correlations proposed by Norton (1977) to calculate the height of the packed absorption column. These correlations from manufacturers provide preliminary estimates of the order of magnitude of the column height, however, in the final design, more rigorous models or specific experimental data must be used. The column height is then be computed according to Norton (1977):

$$Z = \frac{ABS}{(k_{OG}a) \cdot \Delta y_m \cdot P} \quad (5)$$

where  $Z$  (m) is the column height,  $P$  is the column operating pressure (6 bar),  $ABS$  (kmol/s·m<sup>2</sup>) is the rate of solute absorbed by the column per unit of cross section:

$$ABS = \frac{m_{V,in} \cdot y_{in} - m_{V,out} \cdot y_{out}}{A} \quad (6)$$

where  $m_{V,in}$  and  $m_{V,out}$  (kg/s) are the vapor molar flowrates at the inlet and outlet of the column, respectively,  $y_{in}$  and  $y_{out}$  are the ammonia mole fractions of the vapor stream at the inlet (base) and outlet (top) of the column,  $A$  is the column cross sectional area.  $\Delta y_m$  is the logarithmic average of the composition at the vapor phase, calculated by:

$$\Delta y_m = \frac{\Delta y_c - \Delta y_{eq}}{\ln \frac{\Delta y_c}{\Delta y_{eq}}} \quad (7)$$

where  $\Delta y_c = y_{in} - y_{out}$  corresponds to the difference in the mole fraction of the inlet ( $y_{in}$ ) and outlet ( $y_{out}$ ) of vapor phase and  $\Delta y_{eq} = y_{in,eq} - y_{out,eq}$  represents this difference at the equilibrium condition. The equilibrium concentration was determined at the average temperature between the inlet and outlet of the column by VLE formulation as described next.  $k_{OG}a$  is the empirical global coefficient of mass transfer for absorption, calculated by the correlation provided by Norton (1977) for a specific set of systems of great industrial interest, including ammonia and water:

$$k_{OG}a = C_1 \cdot C_2 \cdot V_L^{0,17} \cdot V_G^{C_3} \cdot P^{-0,21} \quad (8)$$

where  $P$  is the operating pressure (6 bar),  $C_1 = 0.012$ ,  $C_2 = 0.85$  e  $C_3 = 0.66$  are constants related to the system and type of packing obtained in Norton (1977),  $V_L$  (m/s) is the average specific velocity of the liquid phase (arithmetic average of inlet and outlet velocities),  $V_V$  (m/s) is the velocity of the vapor phase calculated by:

$$V_V = \frac{m_{V,in}}{A \cdot \rho_V} \sqrt{\rho_V} \quad (9)$$

where  $m_{V,in}$  (kg/s) is the vapor molar flowrate at the inlet of the column,  $A$  is the cross-sectional area and  $\rho_V$  (kg/m<sup>3</sup>) is the density of the vapor phase at the average temperature between inlet and outlet operating conditions.

Given the design parameters, type of packing, height and diameter of the column, the commercial simulator Aspen Plus was used to simulate the packed column for the absorption of ammonia by a solution of ammonia and water. The absorber column is simulated using Radfrac, an Aspen Plus module capable of performing rigorous simulations of multicomponent system in distillation and absorption columns. In the packed column, illustrated in Figure 1b, the liquid stream of ammonia and water flows downward, while the vapor stream (99% of weight of ammonia) flows upward. One intercooling is placed just below the feed, where there is a more pronounced increase in temperature due to the higher concentration gradient. For comparison purpose, the heat duty for the external heat exchanger is the same heat removed by the coolant in the falling film.

The packed column model is firstly validated with experimental data from literature (Fernández-Seara, 2007) and then designed to operate with the same inlet and outlet conditions imposed to the falling film in Table 3 for the sake of comparison. It was assumed that all vapor is absorbed by the liquid solution at the packed column, hence the outlet vapor flowrate is null.

### *c. Heat and mass transfer coefficients*

The process of ammonia absorption by a solution of ammonia and water involves the simultaneous phenomena of heat and mass transfer, then the precise calculation of the mass and heat transfer coefficients are important for the design of the absorber. The correlations used for mass and heat transfer coefficients in packed column and falling film are summarized in Table 4. The heat transfer coefficients in packed column and falling film has been extensively described by the Chilton-Colburn analogy (1934) for the liquid phase (Goel and Goswamy, 2005a, Sieres and Fernández-Seara, 2007, Triché et al., 2016, Aminaravy et al., 2017 and Rosa et al, 2020a) and by the Kakaç et al. (1987) correlation for the vapor phase (Goel and Goswamy, 2005a, Triché et al., 2016, Aminaravy et al., 2017 and Rosa et al, 2020a). The equation proposed by Onda et al. (1968) is recommended by Sieres and Fernández-Seara (2007) for the calculation of the mass transfer coefficient in the packed column. The Yih and Chen (1986) correlation and the Chilton-Colburn analogy (1934) has been frequently used in the falling film to calculate the mass transfer coefficient in the liquid and vapor phase, respectively (Goel and Goswamy, 2005a, Goel and Goswamy, 2005b, Triché et al., 2016, Aminaravy et al., 2017 and Rosa et al., 2020a).

Table 4- Correlations for heat and mass transfer coefficients.

Coefficient	Phase	Equipment	Correlation
Mass Transfer	Liquid	Falling film (Yih and Chen, 1986)	$K_L = 0.01099 \cdot Re_{film}^{0.3955} Sc_L^{0.5} \left( \frac{D_L \cdot \rho_L}{M_L} \right) \left[ \frac{g \cdot \rho_L^2}{\mu_L^2} \right]^{\frac{1}{3}}$
		Packed column (Onda et al., 1968)	$K_L \left( \frac{\rho_L}{\mu_L \cdot g} \right)^{\frac{1}{3}} = 0.0051 \left( \frac{L_W^*}{\mu_L \cdot a_W} \right)^{\frac{2}{3}} \left( \frac{\mu_L}{\rho_L \cdot D_L} \right)^{-\frac{1}{2}} (ad_p)^{0.4}$
	Vapor	Falling film (Chilton-Colburn Analogy, 1934)	$K_V = \frac{\alpha_V}{C_{PV} M_V \left[ \frac{Sc_V}{Pr_V} \right]^{2/3}}$
		Packed column (Onda et al., 1968)	$\frac{K_V RT}{a D_v} = K_5 \left( \frac{V_W^*}{\mu_v \cdot a} \right)^{0.7} \left( \frac{\mu_v}{\rho_v \cdot D_v} \right)^{\frac{1}{3}} (ad_p)^{-2.0}$
Heat Transfer	Liquid	Falling film and Packed column (Chilton-Colburn analogy, 1934)	$\alpha_L = K_L \left( C_{PL} \cdot M_L \left[ \frac{Sc_L}{Pr_L} \right]^{2/3} \right)$
	Vapor	Falling film (Kakaç <i>et al.</i> , 1987)	$\alpha_V = 7.541 \left( \frac{\lambda_V}{d_{hv}} \right)$
		Packed column (Chilton-Colburn analogy, 1934)	$\alpha_V = K_V \left( C_{PV} \cdot M_V \left[ \frac{Sc_V}{Pr_V} \right]^{2/3} \right)$

**d. Selection of thermodynamic models to describe the ELV of the ammonia and water system**

The vapor-liquid equilibrium (VLE) of the mixture ammonia and water must be described to precisely model the ammonia absorption. Table 5 presents thermodynamic models or correlations that have been applied in the literature to describe the VLE for ammonia and water. The models shown in Table 5 do not consider the dissociation of ammonia, following the hypothesis from Prausnitz et al (1975) to neglect ions in the liquid phase when the mole fraction of ammonia is greater than 10<sup>-3</sup>. Some studies do not detail the VLE modeling, other use simplified empirical correlations, as proposed by Pretek and Klomfar (1995) or Perry and Chilton (1984).

For a fair comparison between the investigated equipment, packed column and falling film, the model describing the VLE needs to be the same. Although Rosa et al. (2020) considered Prausnitz *et al.* (1978) to describe the non-idealities of the liquid phase, we choose UNIQUAC (UNIversal QUase Chemical), proposed by Abrams and Prausnitz *et al.* (1975), because Aspen Plus does not offer the thermodynamic model proposed by

Prausnitz *et al.* (1978). Besides that, UNIQUAC has been used by literature (Semenov *et al.*, 2014, Kondrashina *et al.*, 2018, Rosa *et al.* 2021) to describe the ammonia and water VLE. The vapor phase is considered as an ideal gas, since the absorbers operate at a pressure of 6 bar. This model is validated with experimental data from Clifford *et al.* (1932) who reported VLE data at temperatures of 60°C and 90°C for the ammonia and water system (total pressure and mole fraction of ammonia at the vapor phase). The simulations of the NH<sub>3</sub>-H<sub>2</sub>O VLE are carried out in Matlab.

Table 5- Models for the VLE description of the ammonia and water mixture reported in the literature.

Authors	Vapor liquid equilibrium	
	Liquid	Vapor
Selim e Elsayed (1999a)	Not informed	
Selim e Elsayed (1999b)	Empirical correlation from Perry and Chilton (1984) data	
Goel e Goswamy (2005a)	Not informed	
Goel e Goswamy (2005b)	Not informed	
Sieres e Fernández-Seara (2007)	Ziegler e Trepp (1984)	
Semenov <i>et al.</i> (2014)	UNIQUAC	Not informed
Triché <i>et al.</i> (2016)	Empirical correlation from Pretek and Klomfar (1995)	
Aminaravy <i>et al.</i> (2017)	Not informed	
Kondrashina <i>et al.</i> (2018)	UNIQUAC	Not informed
Rosa <i>et al.</i> (2020)	Prausnitz <i>et al.</i> (1978)	Ideal Gas
Rosa <i>et al.</i> (2021)	UNIQUAC	Ideal Gas

### IV.3. Cost estimation of the absorbers

The precise estimate of the investment cost of a chemical plant is dependent on the cost estimate of the individual equipment. According to Sinha (1988) the plant cost accuracy is a function of the precision of the cost correlations available for the individual equipment and of the factors used for translating the equipment cost to the total capital cost. The literature has reported strategies for estimating the cost of absorbers, such as: Towler and Sinnott (2008) empirical correlations (Neagu e Cursaru, 2017 and Pehlan *et al.*, 2017), annualized Capital Cost - CAPEX (Wang *et al.* 2015 and Lukin *et al.*, 2020) and Method of Guthrie (Tall, 2003 and Tsagkari *et al.*, 2016). The investment and

installation costs of the absorbers might be determined from the design parameters of the column and the falling film absorbers. The operational cost will not be estimated because it is usually computed for the complete processes and not only for a singular equipment; then it is out from the scope of this study.

The literature specialized in cost estimates is very broad and has several correlations that allow analyzing the order of magnitude in a preliminary investigation of the costs of an equipment. Therefore, the methodology proposed by Towler and Sinnott (2008), which has been used in the literature (Pehlan et. al, 2017, Bastos et. al, 2018 and Neagu and Cursaru, 2017), is used here to estimate the investment of both absorbers. The following correlation is used to calculate the cost of various components of equipment in the chemical industry:

$$C_c = a + b \cdot S^n \quad (10)$$

where  $C_c$  is the component of the equipment cost,  $a$  and  $b$  are constants available in Towler and Sinnott (2008),  $S$  is the parameter related to the size/capacity and  $n$  is the exponent for the specific type of component. The parameters ( $a$ ,  $b$  and  $n$ ) for the packed column and falling film are shown in Table 6.

According to Pehlan et. al (2017) and Neagu and Cursaru (2017), the cost estimation of an absorbing column,  $C_{col}$ , can be done as a combination of a vertical pressure vessel,  $C_{ves}$ , packing cost,  $C_{pack}$ , and cooling system,  $C_{cool}$ :

$$C_{col} = C_{ves} + C_{pack} + C_{cool} \quad (11)$$

Therefore, to estimate the cost of the column vessel  $C_{ves}$  by Eq. (10), first it is necessary to determinate the size factor,  $S_{ves}$ , which corresponds to the mass of the column vessel ( $m_{ves}$ ), determined by:

$$S_{ves} = m_{ves} = \pi \cdot \emptyset \cdot Z \cdot \varepsilon \cdot \rho \quad (12)$$

where  $\emptyset$  (m) is the external diameter of the column,  $Z$  (m) is the column high,  $\varepsilon$  (m) is the thickness of the vessel wall and the density of the vessel material,  $\rho$ , is 8,000 kg/m<sup>3</sup>, stainless steel 304. The thickness,  $\varepsilon$ , must be calculated from the ASME Code guidelines for Boilers and Pressure Vessels using the equation (ASME, 2007):

$$\varepsilon = \frac{P \cdot \emptyset}{2 \cdot MT \cdot E - 1.2 \cdot P} + CA \quad (13)$$



where  $P$  (kPa) is the design pressure (10% higher than operating pressure),  $\emptyset$  (m) is the column external diameter,  $E$  is the efficiency of the weld. Assuming the welds will be fully radiographed, the weld efficiency is 1.0. The maximum allowable tension for the column made of stainless steel 304 is roughly  $MT = 89,000$  (kPa).  $CA$  is the factor related to corrosion tolerance (0.0035 m).

To calculate the internals cost,  $C_{pack}$  by Eq. (10), the size parameter,  $S_{internals}$ , is given in terms of packing volume, calculated by:

$$S_{internals} = \left( \frac{\pi \cdot \emptyset^2}{4} \right) Z \quad (14)$$

where  $\emptyset$  (m) is the column external diameter and  $Z$  column height.

The cost estimate of the cooling system,  $C_{cool}$  is given in terms of refrigerant flowrate (liters/s) as the size parameter  $S_{cool}$ . This flowrate is determined by operating conditions of the equipment as shown in Table 3.

Towler and Sinnott (2008) show parameters for cost estimation of the plate-type heat exchanger. Since both equipment have a similar design, the falling film investment,  $C_{FF}$ , is estimated based on the proposed parameters for the plate type heat exchanger and the cost of the refrigeration system, as shown below:

$$C_{FF} = C_{TP} + C_{cool} \quad (15)$$

where  $C_{TP}$  is the cost of the local absorber frame in terms of material type and absorber plate area. The size parameter for  $C_{TP}$  is given in terms of area.  $C_{cool}$  is the cost associated with the cooling system given in terms of volumetric coolant flowrate. This flowrate is determined by operating conditions of the falling film.

Table 6- Parameters for cost estimation (Adapted from Towler and Sinnott, 2008)

<b>Equipment</b>	<b>a</b>	<b>b</b>	<b>n</b>	<b>Size Parameter (S)</b>
Vertical pressure vessel	-400	230	0,6	Vessel mass (kg)
Random packing	0	930	1	Volume (m <sup>3</sup> )
Cooling System	61000	650	0,9	Cooling fluid flow (liter/s)
Plate Falling Film (Plate Heat Exchanger);*	1,100	850	0,4	Area (m <sup>2</sup> )

\* material type: stainless steel 304;

The costs are updated according to the inflation by CEPCI (Chemical Engineering Plant Cost Index). These are dimensionless factors used to update the capital costs involved in the design of plants and equipment. They include changes in the value of money due to inflation and deflation, and can be consulted on the CEPCI website (Jenkins, 2020). The updating of costs is carried out by:

$$C_E(\text{Year X}) = C_E(\text{Year Y}) \frac{\text{Index for the year X}}{\text{Index for the year Y}} \quad (16)$$

The costs for absorbers presented by Neagu and Cursaru (2017) are based on the January 2006 corresponding to CEPCI index equal to 478.6. For 2020, the CEPCI index is 607.5.

Most of the data available in relation to equipment cost estimation is presented in the U.S. base Gulf Coast (USGC) or in the European base Northwest Europe (NWE), as these are the areas with the highest concentration of chemical industries. Estimated costs must also be corrected for the intended location, using allocation factors available in Towler and Sinnott (2008). Knowing the appropriate allocation factor, the estimated cost must be corrected by:

$$C_E(\text{region A}) = C_E(\text{USGC}) \cdot LFA \quad (17)$$

where *LFA* is the allocation factor by region. The allocation factor (LFA) in Brazil is 1.14 (Towler and Sinnott, 2008). Brazilian companies have been adopted others values for LFA. Petrobras S.A., example adopts 1.6 whereas Braskem adopts 1.4.

The installation cost of the equipment,  $C_{int}$ , might be computed by:

$$C_{int} = C_E \cdot IF \quad (18)$$

where  $C_E$  is the cost of the equipment and *IF* is the installation factor. According to Neagu and Cursaru (2017), the factor for absorbing columns is 4.0 while for the falling film it is 3.5.

#### IV.4. Results

Firstly, the results of the thermodynamic model for the ammonia and water VLE description are presented, followed by the validation of the absorber models, falling film

and packed column. A sensitivity analysis investigates the influence of the design parameters (diameter and absorbers length) on the amount of ammonia absorbed by the liquid phase. Then, the performance of both absorbers are compared regarding the ammonia mass fraction and temperature profiles along the absorber length. A sensitivity analysis is carried out to investigate the effect of some input variables (liquid temperature, ammonia mass fraction and amount of heat removed) on the mass fraction of ammonia at the outlet liquid stream. Finally, the cost estimation of both absorbers is discussed.

#### IV.4.1 Validation of UNIQUAC model for description of the VLE of the mixture NH<sub>3</sub>-H<sub>2</sub>O

The prediction of the pair UNIQUAC – ideal gas for the mixture ammonia/water was compared with experimental data reported by Clifford et al. (1932) at temperatures of 60°C and 90°C. The results from Aspen Plus are very similar to those obtained from Matlab and are not shown here for the sake of simplicity. Figure 3 indicates that the model can predict with reasonable accuracy the total pressure and ammonia mole fraction at the vapor phase at different ammonia mole fraction in the liquid phase. The mean deviations regarding the total pressure are 4.51% and 3.46% at 60°C and 90°C, respectively. A good accuracy was also observed for the ammonia mole fraction at the vapor phase, as the mean deviations are 4.21% and 4.48% for temperatures of 60°C and 90°C, respectively. Therefore, the UNIQUAC model combined with the ideal gas can accurately describe the ammonia and water VLE.

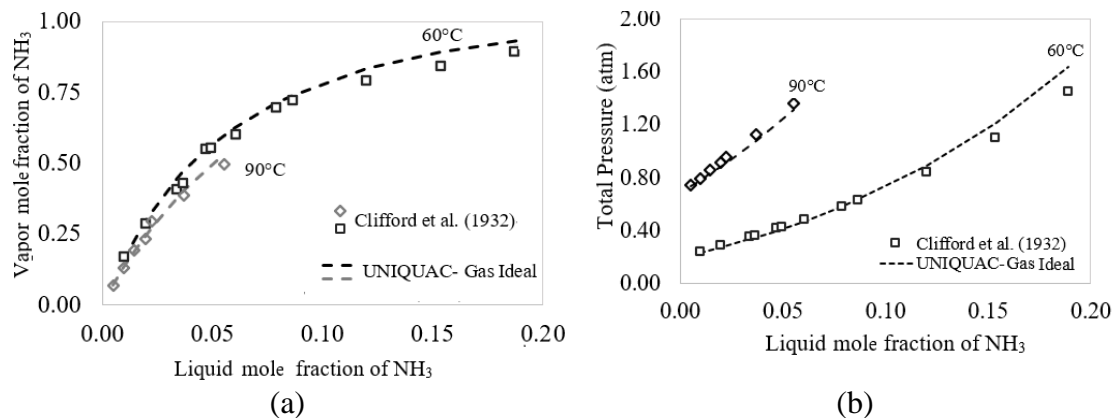


Figure 3- Validation of the UNIQUAC thermodynamic model for the NH<sub>3</sub>-H<sub>2</sub>O VLE (a) ammonia mole fraction at the vapor phase and (b) total pressure.

#### IV.4.2. Validation of the falling film model

Table 7 shows the model validation against experimental data from Triché et al. (2016) at the operating conditions reported in Table 3. The output variables used for validation are: liquid temperature  $T_L$  (K), cooling fluid temperature  $T_C$  (K) and ammonia mass fraction at liquid phase  $x_{NH_3}$ . All output variables are predicted with very good accuracy since low deviations are observed as shown in Table 7, indicating that the model is valid.

Table 7- Validation of the falling film model with experimental data from Triché et al. (2016)

$T_L$ (K)		$T_C$ (K)		$x_{NH_3}$	
Exp	Deviation (%)	Exp	Deviation (%)	Exp	Deviation (%)
303.7	0.09	305.8	0.51	0.591	0.07

#### IV.4.3. Validation of the packed column model

The model of the packed column simulated in Aspen Plus is validated with the experimental data from Sieres and Fernández-Seara (2007) for a packed column where glass Raschig rings with 15 mm is used as packing at the operating conditions shown in Table 8. The working fluid is ammonia and water. The absorbing column from Sieres and Fernández-Seara (2007) has a height of 0.48 meters and diameter of 0.08 meters. The liquid stream flows from the top to the bottom while vapor flows from the bottom to the top of the column. The column is insulated with 55 mm of mineral wool and is considered adiabatic. The pressure drop is approximately 0.01 bar per meter of packed material, thus it is assumed that the column operates at constant pressure.

Table 8- Operating conditions of the packed column at a pressure of 13 bar.

Variable	Inlet vapor data	Inlet liquid data
Mole Flow rate	$8.51 \cdot 10^{-4}$ (kg/s)	$6.81 \cdot 10^{-4}$ (kg/s)
Temperature	273.15 (K)	273.15 (K)
NH <sub>3</sub> mass fraction	0.851	0.994

Table 9 shows the relative deviations of the predicted liquid and vapor outlet temperatures ( $T_L$  and  $T_v$ , respectively) against experimental data from Sieres and Fernández-Seara (2007) for the packed column. The deviations up to 7% reveal that the model is validated and is able to predict the experimental data with reasonable accuracy.

Table 9- Packed column model validation against experimental data from Sieres and Fernández-Seara (2007)

Packing	$T_L$ (K)		$T_v$ (K)	
	Exp.	Deviation (%)	Exp.	Deviation (%)
Glass Raschig rings 15 mm	309.8	6.91	308.4	3.45

#### IV.4.4. Packed column design

The diameter and height of the packed column with Raschig rings 0.375 in of ceramic were designed to meet the outlet conditions shown in Table 3 and the results are summarized in Table 10. The column operates at nearly constant pressure since the pressure drop is very small. The diameter of 0.15 meters is in accordance with the literature recommendation. According to Treybal (1955), Perry and Chilton (1999) and Chavez-Islase Heard (2009), packing column is preferred for diameters lower than 0.60 meters since they are economically more advantageous than trays column. Towler and Sinnott (2008) recommend packings with size < 0.98 in for columns with diameter lower than < 0.3 m because the use of too large packing in a small column can cause poor liquid distribution. Therefore, the packing size of 0.375 in is in agreement with the literature recommendation.

Table 10- Absorption packed column design

Parameter	Value
Type of packing	Ceramic Raschig rings 0.009 m (0.375 in)
Column diameter (m)	0.15 m
Column cross-sectional area (m <sup>2</sup> )	0.0171 m <sup>2</sup>
Column height (m)	0.57 m
Pressure drop (bar)	$6.41 \cdot 10^{-06}$ atm/m of column packed

#### IV.4.5. Evaluation of the design parameters of the absorbers

A sensitivity analysis is carried out to investigate the influence of the design parameters: diameter (Figure 4a) and length (Figure 4b) of the packed column and length of the falling film (Figure 4c) on the amount of ammonia absorbed by the liquid phase. In columns with diameters from 0.1 to 0.2 m, the amount of ammonia absorbed by the liquid stream remains nearly constant because the diameter of the column is defined based on the vapor flow ( $5.25 \cdot 10^{-3}$  kg/s), which is constant. For increasing vapor flow rates,

higher diameter would be required. Figures 4b and 4c reveal that falling film absorber gets higher ammonia mass fraction in shorter equipment length. This behavior may be associated with the greater absorption capacity of the falling film. That is a result of the efficient cooling system, as it will be better explained later.

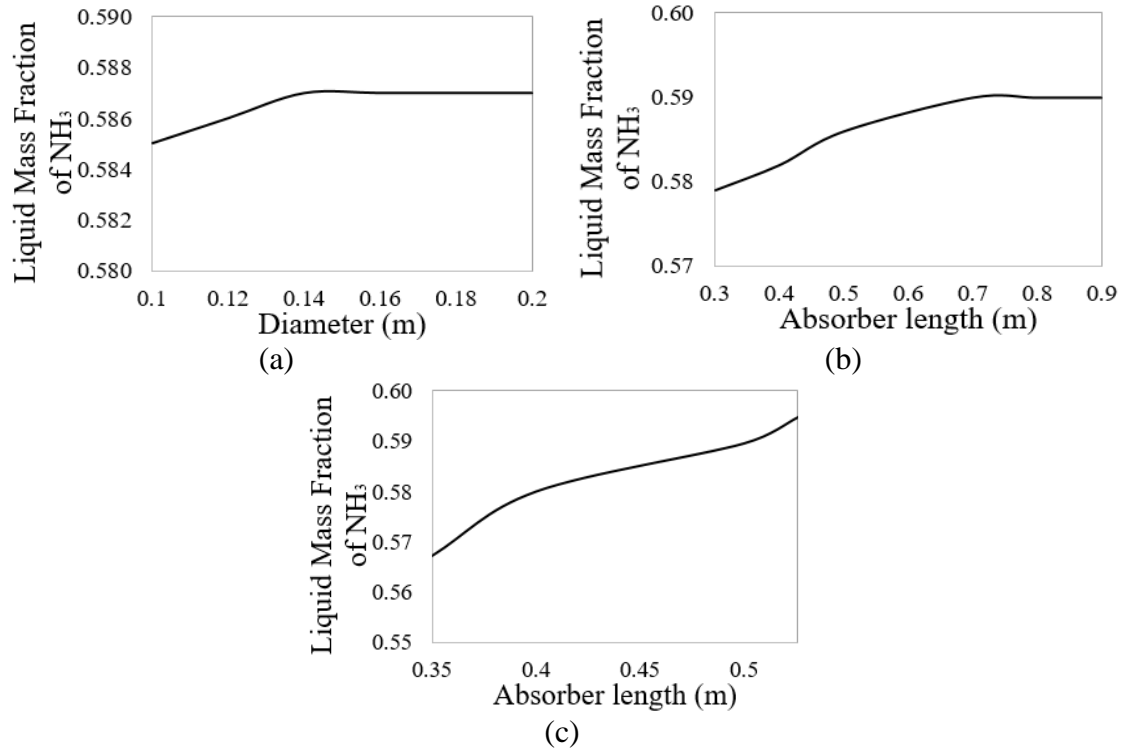


Figure 4- Variation of ammonia mass fraction at the outlet of the liquid (a) packed column diameter, (b) packed column length and (c) falling film length

#### IV.4.6. Analysis of the absorption performance: falling film and packed column

In order to better understand the performance of the falling film and the packed column, simulations for the nominal case presented in Table 3 were performed. Figure 5a shows the ammonia mass fraction and Figure 5b shows the temperature profiles along the absorber length for both equipment. The red line indicates the target outlet liquid mass fraction specified in Table 3 ( $x_{NH_3} = 0.59$ ). The packed column requires 0.57 m to reach the same outlet ammonia mass fraction obtained in the falling film, therefore 8% taller. This fact may be associated with the formation of a high number of films between the absorber plates (14 in total), thus providing an increase in the superficial area for heat and mass transfer. The area occupied by the falling film is 0.06 m<sup>2</sup> whereas the packed column requires an area of 0.28 m<sup>2</sup>. For the conditions evaluated here, the falling film allows a reduction of 33.3% of the equipment volume, then it is much more compact than the packed column.

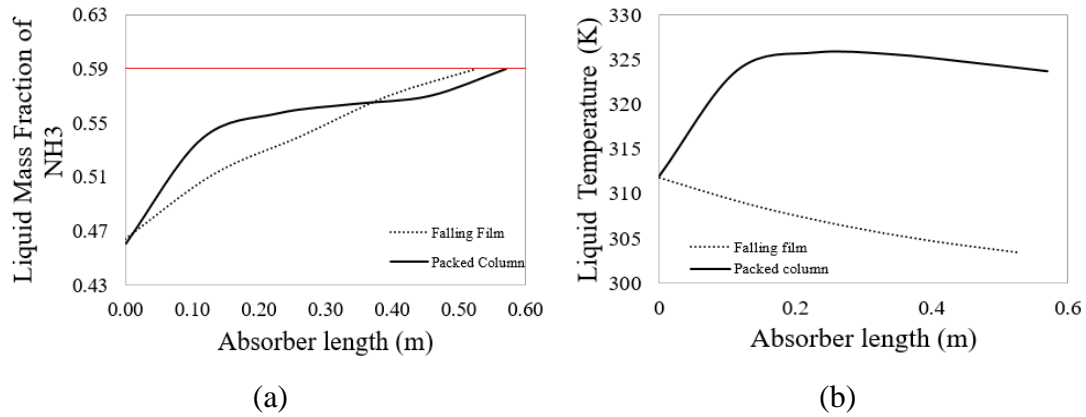


Figure 5- (a) Mass fraction profile: amount of ammonia absorbed in the liquid phase and (b) liquid temperature profile *versus* height of the equipment for the falling film and the packed column.

Analysis of Figure 5a shows that the mass fraction of ammonia increases along the length of the absorbers, indicating that ammonia is continuously absorbed by the liquid phase. In the packed column, the absorption of ammonia in the liquid phase occurs more sharply at the beginning of the absorber, followed by a region of almost stagnation. At the inlet of the absorber, the mass fraction of ammonia in the liquid phase is lower, i. e., the driving force for mass transfer is higher, favoring the absorption process. The sharp ammonia absorption at the inlet results a significant increase in the temperature of the liquid stream in the packed column, as Figure 5b illustrates, because the ammonia absorption is an exothermic process. On the other hand, the temperature of the falling film decreases (Figure 5b), evidencing that its cooling system is effective over its entire length, since the cooling fluid circulates uniformly between the plates of the equipment. Therefore, the heat removal in the column by the intercooling do not achieve an expressive control of the temperature even if it is placed very close to the feed, where the temperature is higher. Therefore, a deeper study on the intercooling scheme might be useful for better understanding its impact on the absorption performance. Due to the higher temperatures achieved, the column begins a stagnation zone, which slows down the absorption rate. This behavior can be better understood with the help of the phase diagram of the ammonia and water mixture (Figure 6). Lower temperatures, afforded by heat removal in the absorber, imply a higher mass fraction of ammonia in the liquid phase at 6 bar. Therefore, cooling causes the temperature of the liquid to decrease and, consequently, the ammonia mass fraction in this phase increases. If the temperature is not well controlled, as show in temperature profile of the column (Figure 5b), the liquid concentration stagnates. Around 0.45m the ammonia mass fraction starts increasing again

due to the counter current vapor flow, as it feed the column at a lower temperature (296.9 K). The temperature change in the absorbers further impacts the thermodynamic and transport properties of the fluids. As a consequence, the equilibrium mass fraction at the interface and heat and mass transfer coefficients change, affecting the mass transfer of ammonia from the vapor to the liquid phase. Then, the falling film has the advantage of a uniform coolant distribution, favoring the ammonia absorption.

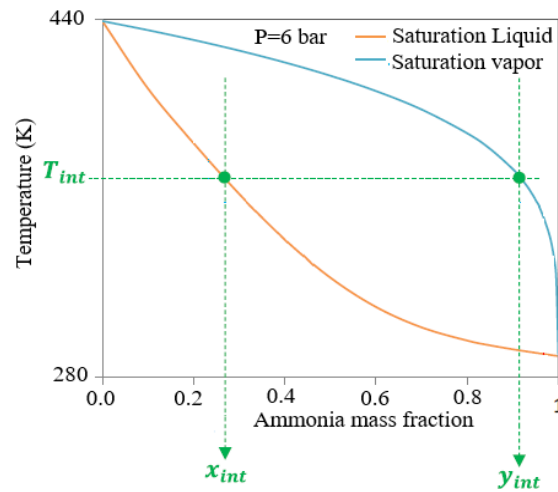


Figure 6- Liquid-vapor phase diagram for NH<sub>3</sub> / H<sub>2</sub>O (Rosa et al., 2020)

#### IV.4.7. Evaluation of the operational parameters of the absorbers

This section investigates the effect of some input variables (ammonia mass fraction and liquid temperature) on the process performance when excited from the base case in Table 3. This analysis can be useful to better understand the variables that most influence the ammonia content in the output stream of the two absorbers. Figure 7 shows the influence of the ammonia inlet mass fraction (Figure 7a) and the liquid temperature (Figure 7b) on the ammonia outlet mass fraction at liquid phase.

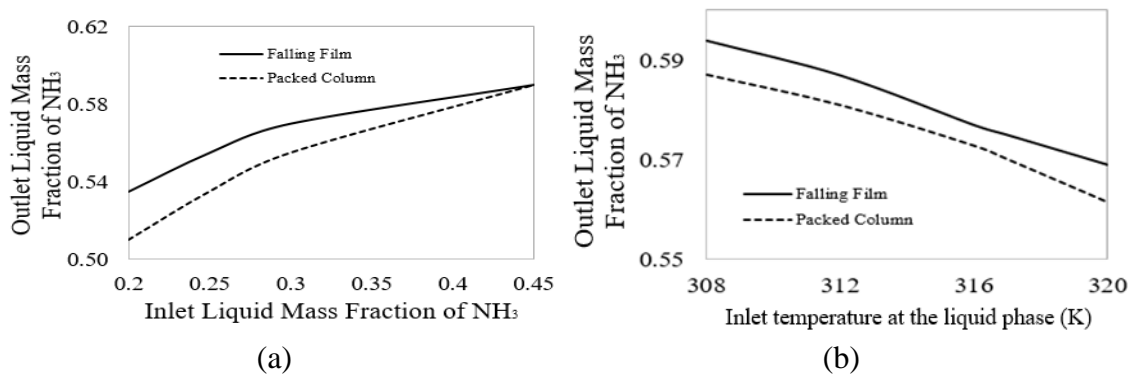


Figure 7- (a) Influence of ammonia inlet mass fraction and (b) liquid inlet temperature



Figure 7a reveals that, for the investigated scenarios, the falling film has ammonia mass fractions slightly higher (4%) at the liquid phase than the packed column, showing a greater absorption capacity, except for the inlet liquid mass fraction of ammonia at the point 0.45, because for this point the column was design to get the same separation of the falling end, as shown in Figure 5a. This fact may be associated with the efficient cooling system of the falling film. Figure 7b shows the influence of the inlet temperature of the liquid stream on the absorption of ammonia. The lower the temperature of the liquid, the higher the ammonia content at the interface, as shown the phase diagram in Figure 6, therefore lower temperatures result in a higher content of the ammonia at the liquid phase.

As show Figure 5.b the heat removal in the packed column by the intercooling do not achieve a significant control of the temperature, so a further study of the influence of the number of intercooling and the amount of the heat removed in the ammonia absorption is shown in Figure 8a and 8b, respectively. Figure 8a reveals that, for a total amount of the heat removed (4 kW), the number of the intercooling does not make difference in the ammonia mass fraction evidencing that the distribution of the heat removed is not effective. Figure 8b depicts that, considering just one intercooling at the middle of the column, increasing the heat removal indeed has a significant influence in the ammonia absorption. This is attributed to the faster diffusion of molecules towards the surface of the packed bed facilitated by heat supply. Moreover, this phenomenon happens for the same reason of the liquid inlet temperature influence as shown in the liquid-vapor phase diagram for  $\text{NH}_3 / \text{H}_2\text{O}$ , for the sake of simplicity, these explanations are not shown here.

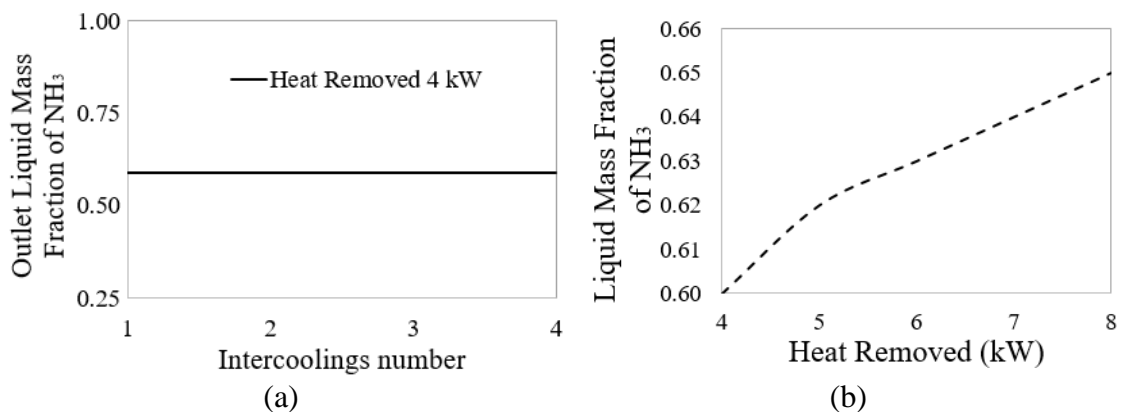


Figure 8- (a) Influence of intercooling numbers and (b) heat removed in packed column

The rate of vapor absorption is partially determined by the physical-chemical thermodynamics (solubility of the gas, diffusivities of the dissolved gas and the reagent in the solution, reaction kinetics) and partially due to the hydrodynamic conditions of the system (flow rates streams, equipment geometry, liquid viscosity and density). Therefore, Figure 9 shows the effect of the ration L/V (L-liquid mass flowrate and V-vapor mass flowrate) on the amount of the ammonia absorbed. For a fixed liquid flowrate, the ammonia mass fraction increases due to an increase in gas flow rate. Evidently, the amount of the ammonia vapor in contact with the liquid phase is higher and therefore more vapor is absorbed to the liquid, increasing the ammonia mass flow rate at the liquid phase.

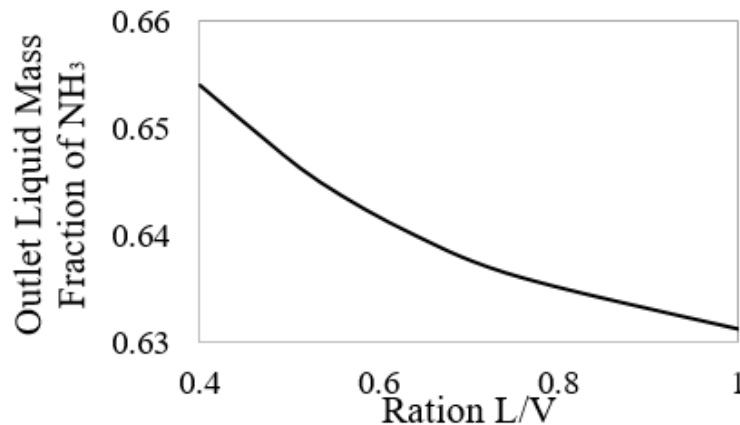


Figure 9- Influence of L/V ratio in the amount of ammonia absorbed

#### ***IV.4.8. Estimation of equipment cost***

An estimate of the absorbers cost was performed based on the design parameters for the packed column (Table 10) and on the design specifications (Table 1). Table 11 shows the estimated component and equipment cost. The final cost of the falling film, including the installation, is 51.38% higher than the packed column, giving an advantage to the packed column. On the other hand, the falling film occupies an volume of 0.006 m<sup>3</sup> whereas the packed column requires volume of 0.009 m<sup>3</sup>. This indicates that the falling film absorber is a more compact device, which may be advantageous for processes where space limitation is an issue. These results are a preliminary estimate just for comparison purposes. For a more detailed analysis, other factors must be taken into account, such as raw material cost, labor, energy cost, but they were not evaluated here because they are beyond the scope of this study.

Table 11- Absorbers cost estimation

Absorbers Components	Size Parameter: <i>S</i>	Component Cost (2006) Eq. 10
Absorber Column Vessel	8.06 kg	\$ 404.58
Packing Cost ( Berl ½ in ceramic saddles )	0.01 m <sup>3</sup>	\$ 8.16
Cooling system	0.33 l/s	\$ 298.03
Plates Falling film	0.06 m <sup>2</sup>	\$ 1,372.86
Final estimate of the cost of absorbers		
	Packed Column	Falling Film
2020 Cost	\$ 902.0	\$ 2,120.91
Brazilian Cost	\$ 1028.51	\$ 2,417.84
Estimated Installation Cost	\$ 4,114.03	\$ 8,462.44

#### IV.5. Conclusion

This study compared falling film absorbers and packed columns for ammonia absorption by NH<sub>3</sub>-H<sub>2</sub>O solution in terms of absorption capacity and equipment cost. For this specific application and operating conditions, the packed column requires 0.57 m to reach the same outlet ammonia mass fraction obtained in the falling film, therefore 8% taller. The volume of the packed column is 0.009 m<sup>3</sup> whereas the falling film is 0.006 m<sup>3</sup>. The falling film is 33.3% more compact than the column, which enables its integration with other equipment by intensify processes. Also, this configuration makes it more versatile in the sense that it can be applied in industrial sectors where there is a limitation of physical space.

Simulations of the falling film and the packed column in different operating conditions reveals that the falling film has ammonia mass fractions, along the absorber, at the liquid phase length is slightly higher (4%) than the packed column, showing a greater absorption capacity. Equipment cost estimation point out that the falling film is more expensive than the packed column. Therefore, the choice of the best equipment for the absorption studied in this work should take into consideration the desired ammonia mass fraction, for a high mass fraction the recommendation is the falling film absorber, if the process requires lower mass fraction the packed column is recommended because the cost is lower. Some hypothesis related to, e.g., the design correlations of the packed column, the packing and liquid distribution, can modify the numerical results and the conclusions herein.

**Notation**

$A$	Area (m <sup>2</sup> )
$\emptyset$	Packed column diameter (m)
$z$	Falling film absorber length (m)
$Z$	Column high (m)
$\delta$	Thickness of the film (m)
$m$	Mass flowrates (kg.s <sup>-1</sup> )
PF	Packing factor
FA	Dimensionless parameter
$\varphi$	Liquid specific density
$U$	Overall heat transfer coefficient though the wall (W-m <sup>-2</sup> K <sup>-1</sup> )
$q$	Sensible heat flux (W-m <sup>-2</sup> )
$H$	Enthalpy (J-kg <sup>-1</sup> )
$\tilde{h}$	Partial Mass Enthalpy (J-kg <sup>-1</sup> )
$Q$	Heat flux (W-m <sup>-2</sup> )
$L$	Length of the heat and mass exchange area
$P$	Pressure (bar)
$R$	Ideal gas constant (cm <sup>3</sup> -atm <sup>-1</sup> mol <sup>-1</sup> )
$T$	Temperature (K)
$d$	Diameter (m)
$x$	Molar/mass fraction at the liquid phase
$y$	Molar/mass fraction at the vapor phase
$\alpha$	heat transfer coefficient (W-m <sup>-2</sup> K <sup>-1</sup> )
$F$	Mass transfer coefficient (kg-m <sup>-2</sup> s <sup>-1</sup> )
$FZ$	Mass fraction of ammonia in the absorbed/desorbed flux
$\psi$	Correction factor
$C_p$	Specific heat (J-kg <sup>-1</sup> K <sup>-1</sup> )
$M$	Molecular Weight (g-mol <sup>-1</sup> )
$Sc$	Schmidt number
$Pr$	Prandtl number
$D$	Diffusivity (m-s <sup>-2</sup> )
$\mu$	Viscosity (Pa-s <sup>-1</sup> )
$\lambda$	Thermal conductive (W-m <sup>-1</sup> K <sup>-1</sup> )
$\rho$	Density (kg-m <sup>-3</sup> )
$Re$	Reynolds Number
$I_c$	Desired percentage of speed in the flood condition
$G'_f$	The surface mass flow of the vapor in the flood condition
$\alpha$	Packing parameters
$\beta$	Packing parameters
$ABS$	The rate of solute absorbed
$k_{OG}a$	Empiric mass transfer coefficient
$C_1$	Packing parameters
$C_2$	Packing parameters
$C_3$	Packing parameters
$V$	Specific velocity (ft/s)
$a_w$	Effective interfacial area of packing per unit volume
$a$	Actual area of packing per unit volume
$L_w^*$	Liquid mass flow rate per unit column cross-sectional area (kg/m <sup>2</sup> s)

$V_W^*$	Liquid mass flow rate per unit column cross-sectional area
$d_p$	Parameter packing size (m)
$K_5$	Parameter packing sizes
$a$	Cost estimation parameter
$b$	Cost estimation parameter
$C$	Equipment cost
$S$	Size/ capacity of the equipment parameter
$n$	Equipment type
$\epsilon$	Thickness of the column (m)
$E$	Welding efficiency
$MT$	Maximum tension allowed (kPa)
$CA$	Corrosion Factor
$IF$	Installation factor
$LFA$	Allocation factor

*Subscript*

$h_v$	Hydraulic diameter of the vapor in the control volume
$L$	Liquid Phase
$V$	Vapor Phase
$c$	Coolant
$i$	component index
$int$	Interface
$W$	Absorber length (m)
$w$	Wall
$VL$	Vapor-liquid

#### IV. References

ABRAMS, D. S., PRAUSNITZ, J. M. Statistical thermodynamics of liquid mixtures: a new expression. For the excess Gibbs energy of partly or completely miscible systems. AICHE J, v.21, pp. 116-128, 1975.

AFKHAMIPOUR, M., AND MOFARAHI, M. Review on the mass transfer performance of CO<sub>2</sub> absorption by amine-based solvents in low- and high-pressure absorption packed columns. RSC Advances, 7(29), 17857–17872, 2017. doi:10.1039/c7ra01352c.

ALI, S., & AKHTAR, J. Hydrodynamics of Packed Bed Column: Study of the Column for the Absorption of CO<sub>2</sub> in Water and its Efficiency. Mass Spectrometry & Purification Techniques, 04 (01), 2018.

AL-SAIDV, M. O. Design and Control of a Packed Absorption Column of H<sub>2</sub>S Form H<sub>2</sub>S–air Gas Mixture : A Case Study of Khartoum Refinery. Nashwa University of Gezira. Department of Applied Chemistry and Chemical Technology Faculty of Engineering and Technology January, 2014

AMINYAVARI, M., APRILE, M., TOPPI, T., GARONE, S., MOTTA, M., A detailed study on simultaneous heat and mass transfer in an in-tube vertical Falling film absorber. *International Journal of Refrigeration* 80: 37–51, 2017.

ASME (American Society of Mechanical Engineering), Section VIII, Division 1. Rules For Construction of Pressure Vessels, 2007.

BECKER, T. M., WANG, M., KABRA, A., JAMALI, S. H., RAMDIN, M., DUBBELDAM, D., VLUGT, T. J. H. Absorption Refrigeration Cycles with Ammonia–Ionic Liquid Working Pairs Studied by Molecular Simulation. *Industrial & Engineering Chemistry Research*, 57(15), 5442–5452, 2018. doi:10.1021/acs.iecr.8b00442

BEHFAR, A., SHEN, Z., LAU, J., & YU, Y. Heat and mass transfer enhancement potential on falling film absorbers for water-LiBr mixtures via a literature review (RP-1462). *HVAC&R Research*, 20(5): 570–580, 2014.

BENITEZ, J. Principles and modern applications of mass transfer operations, 2nd ed. Hoboken, U.S.A: John Wiley and Sons, 2009.

CHAVEZ-ISLAS, L. M. AND HEARD, C. L. Design and Analysis of an Ammonia/Water Absorption Refrigeration Cycle by Means of an Equation-Oriented Method. *Ind. Eng. Chem. Res.* 48, 1944–1956, 2009.

CHILTON, T.H., COLBURN, A.P., Mass transfer (absorption) coefficients prediction from data on heat transfer and fluid friction. *Ind. Eng. Chem.*, 26 1183–1187, 1934.

CLIFFORD, I. L., HUNTER, E., The system ammonia-water at temperatures up to 150°C and at pressures up to twenty atmospheres, *J Phys Chem*, 37 i01-118, 1932.

CONDE, M., Thermophysical properties of ammonia-water mixtures for the industrial design of absorption refrigeration equipment, M. CONDE Engineering, 2006.

DRYDEN, I.G.C. The Efficient Use of Energy, Heat salvage, Butterworth-Heinemann, Pages 366-391, ISBN 9780408012508, 1982. <https://doi.org/10.1016/B978-0-408-01250-8.50025-8>.

ECKERT, J. S. Selecting the Proper Distillation Column Packing, *Chem. Eng. Prog.* 66, no. 3: 39–44, 1970.

EDGE Guidance Document for the Building Sector based on the Montreal Protocol Version 1, Refrigerants and Materials Selection to Reduce Climate Impact, Published: April 3, 2017.

FOLGER, P. Carbon Capture: A Technology Assessment Congressional Research Service, 7-5700 November 5, 2013

GOEL, N, GOSWAMI DY. A compact Falling Film Absorber. *Journal of Heat Transfer* 127, 957-965, 2005b.

GOEL, N, GOSWAMI DY. Analysis of a counter-current vapor flow absorber. *International Journal of Heat and Mass Transfer* 48, 1283-1292, 2005a.

GOVINDARAJU, S. D. Analysis of absorber operations for the 5 kw ammonia/water combined cycle. Master Thesis. University of Florida, 2005.

KAKAÇ, S., AUNG, W., SHAH, R.K. *Handbook of Single-phase Convective Heat Transfer*. Wiley NewYork, 1987.

KARIMI, M., HILLESTAD, M., SVENDSEN, H.F. Investigation of intercooling effect in CO<sub>2</sub> capture energy consumption. *Energy Procedia*. 4: p. 1601-1607, 2011.

KOHL, A. L. "Absorption and Stripping." *Handbook of Separation Process Technology*. Ed. Ronald W. Rousseau. New York: John Wiley & Sons, 340-344, 385-387, 1987.

KONDRASHINA, K A., A A Kozlova, A N Petukhov, D N Shablikin, M M Trubyanov and I V Vorotyntsev1 Thermodynamic modelling of VLE behaviour at the high purification of R717 refrigerant by highpressure batch distillation. *Journal of Physics, Conf. Ser.* 1134 012060, 2018.

KVAMSDAL H. M, ROCHELLE G. T. Effects of the Temperature Bulge in CO<sub>2</sub> Absorption from Flue Gas by Aqueous Monoethanolamine. *Industrial Engineering and Chemistry Research*. p. 867-875, 2008.

LÁZARO-COLÁN, V. A., Experimental study of an absorption column of water vapor and ammonia in water, PhD thesis, Sao Paulo, Federal University (USP), Sao Paulo, Brazil, 2012.

LIN, P.,W., XIA. R.Z, Numerical investigation of a two-stage air-cooled absorption refrigeration system for solar cooling: cycle analysis and absorption cooling performances. *Renew Energy* 36, 1401–1412, 2011.

LUKIN, I., PIETZKA, L., GROß, K., GÓRAK, A., & SCHEMBECKER, G. Economic evaluation of rotating packed bed use for aroma absorption from bioreactor off-gas. *Chemical Engineering and Processing - Process Intensification*, 154, 108011, 2020. doi:10.1016/j.cep.2020.108011.

MERCHAN, V. A., ESCHE, E., FILLINGER, S., TOLKSDORF, G., AND WOZNY, G. Computer-Aided Process and Plant Development – A Review of Common Software Tools and Methods and Comparison against an Integrated Collaborative Approach. *Chemie Ingenieur Technik* 88, 50-69, 2015.

MITTERMAIER, M, ZIEGLER, F. Theoretical evaluation of absorption and desorption processes under typical conditions for chillers and heat transformers. *International Journal of Refrigeration* 59, 91-101, 2015.

MORISON, K. R., WORTH, Q. A. G., and O'DEA, N. P. Minimum Wetting and Distribution Rates in Falling Film Evaporators. *Food and Bioproducts Processing*, 84(4), 302–310, 2006. doi:10.1205/fbp06031

MOSAIC documentation. Retrieved from <http://www.mosaic-modeling.de>, 2011.

MUSTAFA, N. F. A., SHARIF, M. F. A., TAY, W. H., ABDUL HALIM, H. N., and MHD YUSOF, S. M. Mass Transfer Performance Study for CO<sub>2</sub> Absorption into Non-Precipitated Potassium Carbonate Promoted with Glycine Using Packed Absorption Column. *Sustainability*, 12(9), 3873, 2020. doi:10.3390/su12093873.

NAIR, P.S. and SELVI, P.P. Absorption of Carbon dioxide in Packed Column *International Journal of Scientific and Research Publications*, Volume 4, Issue 4, 2014.

NEAGU M. and CURSARU, D. L. Technical and economic evaluations of the triethylene glycol regeneration processes in natural gas dehydration plants. *Journal of Natural Gas Science and Engineering* 37, 327-340, 2017.

NEAGU, M. AND CURSARU, D. L. Technical and economic evaluations of the triethylene glycol regeneration processes in natural gas dehydration plants. *Journal of Natural Gas Science and Engineering*, 37, 327–340, 2017.

Norton Chemical Company, Design Information for Packed Towers, Bulletin DC-II, Akron, OH: Norton Chemical Company, 1977.

OKO, E., RAMSHAW, C., and WANG, M. Study of intercooling for rotating packed bed absorbers in intensified solvent-based CO<sub>2</sub> capture process. *Applied Energy*, 223: 302–316, 2018.

ONDA, K., TAKEUCHI, H. AND OKUMOTO, Y. Mass transfer coefficient between gas and liquid phases in packed columns. *J. Chem. Eng. Jpn.* 1, 56, 1968.

PERRY RH, GREEN D. *The chemical engineers' handbook* Chapters 3, 14 and 18. 6th ed., New York: McGraw-Hill, 1984.

PERRY, R. H.; GREEN, D. W. (Ed.) *Perry's Chemical Engineers' Handbook*. McGraw-Hill: New York, 1999.

PLAZA, J. M., CHEN, E., and ROCHELLE, G. T.. Absorber intercooling in CO<sub>2</sub> absorption by piperazine-promoted potassium carbonate. *AIChE Journal*, 2009. doi:10.1002/aic.12041.

PRAUSNLTZ, J. M., EDWARDS T. J, NEWMAN J., *Thermodynamics of Vapor-Liquid Equilibria for the Ammonia-Water System*. *Ind. Eng. Chem. Fundam.* 17, 264-269, 1978.

EDWARDS, T. J.; NEWMAN, J.; PRAUSNITZ, J. M. *Thermodynamics of aqueous solutions containing volatile weak electrolytes*, *AIChE J.*, v. 21, pp. 248-259, 1975.

PRETEK, J. and KLOMFAR, J. Simple functions for fast calculations of selected thermodynamic properties of the ammonia-water system. *Int. J. Refrigeration* 18: 228-234, 1995.

ROSA, L. P. S., PONTES, K. V., COSTA, G. M. N., PENTEADO, A. T., ESCHE, E., & REPKE, J.-U.. An equation-oriented novel approach for modeling the falling film



absorber using rigorous thermodynamic and transport description. *Chemical Engineering Research and Design*, 159: 179–194, 2020.

SACHDE, D. and ROCHELLE, G. T. Absorber Intercooling Configurations using Aqueous Piperazine for Capture from Sources with 4 to 27% CO<sub>2</sub> / *Energy Procedia* 63:1637 – 1656, 2014.

SÁNCHEZ, P.; SÁNCHEZ, E. J. P.e SILVA. R. S. Design Of A Packed-Bed Absorption Column Considering Four Packing Types And Applying Matlab. *Nexo Revista Científica* Vol. 29, No. 02, pp. 83-104: 2017.

SELIM, A M., ELSAYED, M M. Interfacial Mass Transfer and Mass Transfer Coefficient in Aqua Ammonia Packed Bed Absorber. *International Journal of Refrigeration*, Vol. 22: 263-274, 1999a.

SELIM, A.M. E ELSAYED, M.M. Performance of a packed bed absorber for aqua ammonia absorption refrigeration system. *International Journal of Refrigeration* 22: 283–292, 1999b.

SEMENOV, I. A., UL'YANOV, B. A., DUBROVSKII, D. A., & KULOV, N. N. Simulation of a distillation column with nonequimolar mass transfer in the production of methylamines. *Theoretical Foundations of Chemical Engineering*, 48(5), 644–649, 2014.

SHENDE, B. W., & SHARMA, M. M. Mass transfer in packed columns: co-current operation. *Chemical Engineering Science*, 29(8), 1763–1772, 1974.

SIDDIQUI M., A., Economic Analyses Of Absorption Systems: Part A-Design And Cost Evaluation. *Energy Convers. Mgmt.*, 38(9): 889-904, 1997.

SIERES, J., & FERNÁNDEZ-SEARA, J. Experimental investigation of mass transfer performance with some random packings for ammonia rectification in ammonia–water absorption refrigeration systems. *International Journal of Thermal Sciences*, 46(7): 699–706, 2007.

SRIKHIRIN, P., APHORNRATANA, S., CHUNGAIBULPATANA, S. A review of absorption refrigeration Technologies. *Renewable and Sustainable Energy Reviews*, 5: 343–372, 2001.

TAAL, M. . Cost estimation and energy price forecasts for economic evaluation of retrofit projects. *Applied Thermal Engineering*, 23(14), 1819–1835, 2003. doi:10.1016/s1359-4311(03)00136-4.

TAN, L. S., SHARIFF, A. M., LAU, K. K., and BUSTAM, M. A. Factors affecting CO<sub>2</sub> absorption efficiency in packed column: A review. *Journal of Industrial and Engineering Chemistry*, 18(6), 1874–1883, 2012. doi:10.1016/j.jiec.2012.05.013.

TOLKSDORF, G.; ESCHE, E.; WOZNY, G.; REPKE, J.-U. Customized code generation based on user specifications for simulation and optimization. *Computers and Chemical Engineering* 121: 670–684, 2019.

- TOWLER, G. e SINNOTT R., Chemical Engineering Design - Principles, Practice and Economics of Plant and Process Design, 2nd Ed, (pp. Capítulos 1, 7, 8 e 9), Elsevier, 2008.
- TREYBAL, R. E. Mass Transfer Operations. Mc Graw Hill publications, New York, 1955.
- TRICHÉ D., BONNOTA, S., PERIER-MUZETA, M., BOUDÉHENNA F. DEMASLESA H., CANEY, N. Modeling and experimental study of an ammonia-water Falling film Absorber. International Conference on Solar Heating and Cooling for Buildings and Industry Energy Procedia 91: 857 – 867, 2016.
- TSAGKARI, M., COUTURIER, J.-L., KOKOSSIS, A., & DUBOIS, J.-L. Early-Stage Capital Cost Estimation of Biorefinery Processes: A Comparative Study of Heuristic Techniques. ChemSusChem, 9(17), 2284–2297, 2016. doi:10.1002/cssc.201600309.
- TURTON R, BAILIE R, WHITING W, SHAEIWITZ JA, BHATTACHARYYA D. Analysis, Synthesis, and Design of Chemical Processes. 4th; Prentice Hall, 2013.
- VALENZ, L., VACLAV, L. and HAIDL, J. The Effect of Column Diameter and Packing Height on the Pressure Drop and on the HETP of Structured Packings. Industrial & Engineering Chemistry Research 52(17):5967–5974, 2013.
- VAN BATEN, J., COCO CAPE OPEN to CAPE OPEN simulation environment, www.cocosimulator.org, 2016.
- WANG, C., SEIBERT, A. F., & ROCHELLE, G. T. Packing characterization: Absorber economic analysis. International Journal of Greenhouse Gas Control, 42, 124–131, 2015. doi:10.1016/j.ijggc.2015.07.027.
- WANKAT, P., Separation Processes. Includes Mass Transfer Analysis, 4th ed., Prentice Hall, Upper Saddle River, NJ., Inc., New York, NY, 2011.
- WILKE, C.R., CHANG, P., Correlation of diffusion coefficients in dilute solutions, AIChE Journal 1(2): 264-270, 1955.
- YEH, J. T., PENNLINE, H. W. and RESNIK, K. P. Study of CO<sub>2</sub> Absorption and Desorption in a Packed Column. Energy & Fuels, 15(2): 274–278, 2001. doi:10.1021/ef0002389.
- ZIEGLER, B., TREPP, C., Equation of state of ammonia–water mixtures, Int. J. Refrig. 7: 101–106, 1984.

# CHAPTER V- A COMPARATIVE STUDY OF THERMODYNAMIC MODELS TO DESCRIBE THE VLE OF THE H<sub>2</sub>O, CO<sub>2</sub> AND NH<sub>3</sub> MIXTURE

---

*“The only thing permanent is change.”*

IMMANUEL KANT

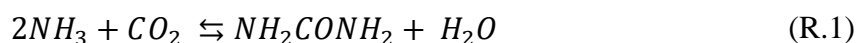
## **V.1. Initial Considerations**

Due the flexibility of the falling film model proposed in the Chapter III, it can be applied to others fluids. However, the thermodynamic equilibrium at the interface of the mixture has to be well established, especially if the mixture is complex as electrolyte system. So, this study aims to ascertain the influence of the activity coefficient model and equation of state for predicting the vapor-liquid equilibrium (VLE) of the multi-electrolyte H<sub>2</sub>O-NH<sub>3</sub>-CO<sub>2</sub> system. The non-idealities of the liquid phase are described by the eUNIQUAC and eNRTL models. The vapor phase is modeled by the Nakamura equation, which is compared with the ideal gas assumption. The models are validated with experimental data from literature on total pressure and ammonia partial pressure. Results show that the models UNIQUAC and NRTL without dissociation can only reproduce the experimental conditions in the absence of CO<sub>2</sub>. When the electrolyte term is considered, the eUNIQUAC model is able to reproduce the experimental data with greater accuracy than the eNRTL. The equation of state which describes the vapor phase plays no major role in the accuracy of the VLE prediction in the operating conditions evaluated here. Indeed, the accuracy relies on the activity coefficient, therefore the ideal gas equation can be considered if the non-idealities of the liquid phase are described by a well-tuned model. These findings could be useful for equipment design, flowsheet simulations and large-scale simultaneous optimization problems.

## V.2. Introduction

Vapor-liquid equilibrium (VLE) of electrolyte systems are usually found in several segments of the chemical industry, such as reaction and separation stages in the urea synthesis process; absorption process to remove  $CO_2$  and  $H_2S$  from gaseous streams; extractive crystallization to precipitate salts using organic solvents. In separation units of the synthesis of urea, for example, the description of phase equilibria of the  $H_2O - NH_3 - CO_2$  mixture plays a key role. According to Ramasamy (1988), a better understanding of the VLE allows for i) energy integration towards self-sufficient processes, since accurate predictions of process streams enthalpies are required, ii) a reduction in energy expenditure when designing condenser and absorbers because the equilibrium temperature and composition are more precisely predicted. Experimental data at industrial scale are rarely available because the sampling process is usually complex, either due to the severe temperature and pressure conditions, or due to the dissociation of molecules into ions. Thermodynamic models able to describe the equilibrium conditions of ionic mixtures, therefore, are of paramount importance for the process design and operation.

The industrial production of urea occurs by the reaction between ammonia and carbon dioxide under certain temperature and pressure conditions, according to (Bhaskar and Chander Das, 2007):



In fact, numerous reactions take place simultaneously due to the chemical balance between water, carbon dioxide and ammonia (Lemkowitz et al., 1972), as Figure 1 depicts. The molecular species in the solution dissociate themselves generating ions, which in turn can react to produce urea. In the literature, different reaction schemes have been proposed to describe the species dissociation which occurs in the context of reaction R.1, as Table 1 summarizes. The reaction VI (Figure 1) represents the formation of urea which is neglected by Bernardis et al. (1989b), Goppert and Maurer (1988), Kurz et al. (1995), Freitas et al. (2013) and Jilvero et al. (2015), because its rate is so low that the time needed to achieve the equilibrium conditions is much longer than the residence time in most equipment in a urea plant. As a result, urea is considered an inert component and the system is represented by the ternary mixture  $H_2O - NH_3 - CO_2$ . Bernardis et al. (1989b) further neglect the formation of solid  $NH_4HCO_3$  (bicarbonate) and its

CHAPTER V- A comparative study of thermodynamic models to describe the VLE of the  $H_2O$ ,  $CO_2$  and  $NH_3$  mixture

dissociation (reaction VII, Figure 1) because they observe that the corresponding thermodynamic equilibrium constant is very small and thus the concentration of the carbonate ion is always very small. This study, therefore, considers the reactions I, II, III and IV. There are other reactions in the solid-liquid equilibrium than an ammonium bicarbonate formation: ammonium carbonate, ammonium carbamate and ammonium sesquicarbonate. However, it is known that ammonium bicarbonate is dominant ammonia salt because  $CO_2$  absorption reaches steady state (Kim et al., 2008; Park et al., 2008).

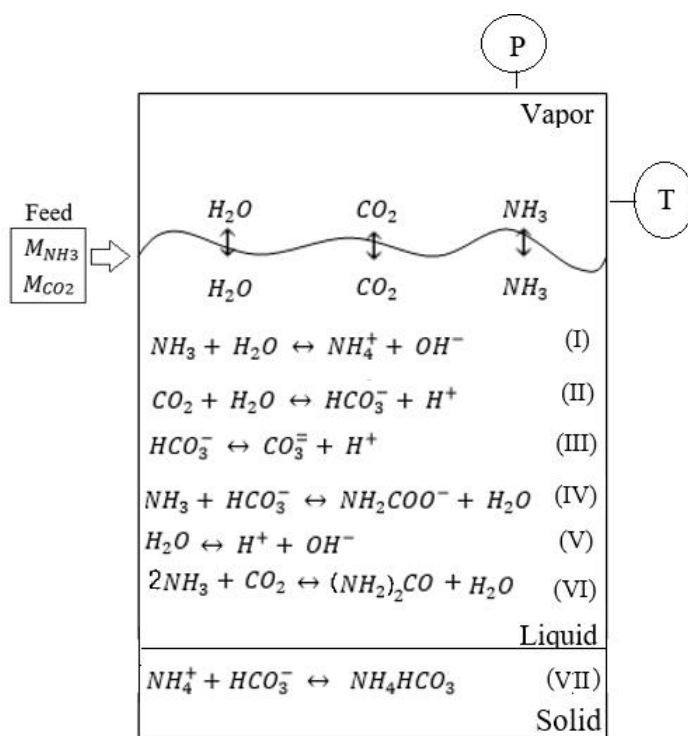


Figure 1- Ionic dissociation in the ternary system  $H_2O - NH_3 - CO_2$

In the 1970s, Edwards (1975) proposed a thermodynamically consistent method to describe the VLE of volatile weak electrolytes in dilute aqueous solutions, including ammonia, carbon dioxide, hydrogen sulfide, sulfur dioxide, and hydrogen cyanide. This model considers mass and charge balances, chemical equilibrium and phase equilibrium. To calculate the VLE in aqueous solution, activity coefficients for the solute and the solvent (water) as well as fugacity coefficients are required to describe the liquid and vapor phases, respectively. Although the activity and fugacity models are system dependent, Edwards' method was used by many authors in the literature as the basis for describing the VLE of electrolyte systems (Kurz et al., 1995; Goppert and Maurer, 1988;

Darde et al., 2010; Que and Chen, 2011; Freitas et al., 2013; Jilvero et al., 2015). According to Edwards et al. (1978), the presence of ions in the vapor phase should only be considered at very high temperatures, consequently the choice of the fugacity model for the vapor phase is not so stiff. On the other hand, the presence of charge in the liquid phase, as shown in Figure 1, causes a great deviation from ideality, therefore the activity model should be carefully chosen. The rigorous modeling of electrolyte systems, therefore, is not a trivial task.

The thermodynamic models most frequently used in literature to describe the VLE of the ternary system  $H_2O - NH_3 - CO_2$  are summarized in Table 1. The non-idealities of the liquid phase were firstly described by the Pitzer model which is able to describe both weak and strong electrolytes based on a complex virial model with numerous parameters. Goppert and Maurer (1988) and Kurz et al. (1995) validated the Pitzer model against experimental data and observed that it can predict the VLE data reasonably well at low solute concentrations (molalities of ammonia 2.8 mol/kg at 393.15 K and 3.1-3.8 mol/kg at 373.15 K), but large deviations are observed near the minimum total pressure and at very high solute molalities (molalities of ammonia 12.2 mol/kg at 393.15 K and 12.3 mol/kg at 373.15 K). Later, semi-empirical thermodynamic models for electrolyte solutions based on the concept of local composition, eUNIQUAC (Sandler, 1984; Sandler et al., 1986) and eNRTL (Chen and Evens, 1986), were proposed to describe the activity coefficient for electrolyte solutions. The eUNIQUAC, unlike the Pitzer model, considers the water dissociation and has a significantly lower number of temperature dependent parameters (Jaworski et al., 2011), which have to be obtained experimentally. Bernardis et al. (1989a) applied eUNIQUAC to describe the liquid phase of the ternary system  $H_2O - NH_3 - CO_2$  and, later, Bernardis et al. (1989a) included urea in the system, considering it an inert component. Darde et al. (2010) extended the validation of the eUNIQUAC model, modified by Thomsen and Rasmussen (1999), to a wider range of temperature and pressure. The eNRTL relies on much more complicated expressions and requires greater computational effort. Due to species dissociation, the models which describe the liquid phase become too complex, hindering the use of the model for design, operation and large-scale flowsheet optimizations. The knowledge of when the dissociation of species might be neglected is therefore important because it enables model simplification, encouraging its further use on industrial scale. Although different models for describing the non-idealities of the liquid and vapor phases of the ternary system

$H_2O - NH_3 - CO_2$  have been used in literature, there is no agreement about which is the best model to describe this system. Jilvero et al. (2015) and Darde et al. (2012) compared the models eUNIQUAC and eNRTL to describe the liquid phase: Jilvero et al. (2015) observed no significant difference in accuracy, whereas Darde et al. (2012) concluded that the eUNIQUAC can more satisfactorily describe the experimental data. The comparison between the thermodynamic models under different operating conditions is crucial to evaluate the predictive capabilities of each model and to define which is the best for a particular application.

As the presence of ions in the vapor phase might be neglected (Edwards et al., 1978), the literature usually employs equations of state without ion specifications. The presence of polar species in the vapor mixture of the system  $H_2O - NH_3 - CO_2$  have been described by several models such as PC-SAFT (Perturbed-Chain Statistical Associating Fluid Theory, Gross and Sadowski, 2001), Nakamura (Nakamura et al., 1976) and SRK (Soave-Redlich-Kwong, Soave, 1972), as can be seen in Table 1. The PC-SAFT equation of state is based on statistical thermodynamics and can be applied for polar and non-polar mixtures. The Nakamura equation, although less complex than the PC-SAFT, still considers the presence of polar and non-polar molecules in the vapor phase. The SRK equation of state, proposed by Soave (1972), on the other hand, requires a modification in the temperature-dependent attractive term to be applied to polar substances and their mixtures (Yesavage et al., 1986). There is also no agreement in the literature about the most suitable model to describe the vapor-phase and its influence on the overall accuracy of the model.

This study aims to ascertain the best pair of activity coefficient and fugacity models for predicting the vapor-liquid equilibrium of the  $H_2O - NH_3 - CO_2$  system. The eUNIQUAC and eNRTL models are compared for describing the liquid phase. The model from Pitzer (1980) is not used for comparison due to the huge number of parameters which would hinder its practical implementation. A modified Pitzer activity coefficient model was developed by Xu et al. (2014), which needs significantly less parameters to be adjusted than the traditional model and showed to be accurate over a wide range of temperatures and concentrations. In an attempt to investigate the need and the effect of considering the electrolytes in the liquid phase, the extended models eUNIQUAC and eNRTL are compared to the conventional UNIQUAC and NRTL models. The vapor phase is described by the Nakamura equation as well as by the ideal gas equation. The

first is chosen to compute the non-idealities of the vapor phase because it can describe polar species with a reasonable level of complexity. The present study, however, suggests that the ideal gas hypothesis might be valid if a more rigorous model, which considers the presence of electrolytes, describes the liquid phase because there is a synergy between the phases. The model predictions are validated with experimental data available in the literature. The findings of the present study might be useful for further studies, such as equipment design, optimization and control of process in the field of CO<sub>2</sub> capture, utilization and storage (CCUS) and urea synthesis, for example.



Table 1. Summary of the models most frequently used to describe the VLE of the H<sub>2</sub>O – NH<sub>3</sub> – CO<sub>2</sub> system.

AUTHOR	REACTIONS CONSIDERED	TEMPERATURE, PRESSURE AND CONCENTRATION RANGE	THERMODYNAMIC MODEL	
			LIQUID PHASE	VAPOUR PHASE
Bernardis <i>et al.</i> (1989a)	$NH_3 + H_2O \rightleftharpoons NH_4^+ + OH^-$ $CO_2 + H_2O \rightleftharpoons H^+ + HCO_3^-$ $NH_3 + HCO_3^- \rightleftharpoons NH_2COO^- + H_2O$ $H_2O \rightleftharpoons H^+ + OH^-$	Temperature: 414 < T < 473 K Pressure: 7 kPa < P < 20 MPa Molality: $m_{NH_3}$ from 3.85 to 18.3 mol/kg and $m_{CO_2}$ up to 14 mol/kg	eUNIQUAC (from Sandler <i>et al.</i> , 1986)	Nakamura
Bernardis <i>et al.</i> (1989b)	$NH_3 + H_2O \rightleftharpoons NH_4^+ + OH^-$ $CO_2 + H_2O \rightleftharpoons H^+ + HCO_3^-$ $NH_3 + HCO_3^- \rightleftharpoons NH_2COO^- + H_2O$ $H_2O \rightleftharpoons H^+ + OH^-$	Temperature: 414 < T < 473 K Pressure: 7 kPa < P < 20 MPa Concentration: not defined	eUNIQUAC (from Sandler <i>et al.</i> , 1986)	Nakamura
Goppert and Maurer (1988)	$NH_3 + H_2O \rightleftharpoons NH_4^+ + OH^-$ $CO_2 + H_2O \rightleftharpoons H^+ + HCO_3^-$ $HCO_3^- \rightleftharpoons H^+ + CO_3^{2-}$ $NH_3 + HCO_3^- \rightleftharpoons NH_2COO^- + H_2O$	Temperature: 333.15 < T < 443.15 K Pressures ≤ 69 atm Molality: $m_{NH_3} = 16$ mol/kg and $m_{CO_2} = 13$ mol/kg	Pitzer	Nakamura
Kurz <i>et al.</i> (1995)	$NH_3 + H_2O \rightleftharpoons NH_4^+ + OH^-$ $CO_2 + H_2O \rightleftharpoons H^+ + HCO_3^-$ $HCO_3^- \rightleftharpoons H^+ + CO_3^{2-}$ $NH_3 + HCO_3^- \rightleftharpoons NH_2COO^- + H_2O$ $H_2O \rightleftharpoons H^+ + OH^-$	Temperature: 313 < T < 353 K Pressure: ≤ 6.90 atm Molality: $m_{NH_3} = 6$ and 12 mol/kg and $m_{CO_2} \leq 10$ mol/kg	Pitzer	Nakamura
Darde <i>et al.</i> (2010)	$NH_3 + H_2O \rightleftharpoons NH_4^+ + OH^-$ $CO_2 + H_2O \rightleftharpoons H^+ + HCO_3^-$ $HCO_3^- \rightleftharpoons H^+ + CO_3^{2-}$ $NH_3 + HCO_3^- \rightleftharpoons NH_2COO^- + H_2O$ $HCO_3^- + NH_4^+ \rightleftharpoons NH_4HCO_3$ $NH_2COO^- + NH_4^+ \rightleftharpoons NH_2COONH_4$ $CO_3^{2-} + 2NH_4^+ + H_2O \rightleftharpoons CO_3(NH_4)_2 \cdot H_2O$	Temperature: 273 < T < 333 K Pressure: ≤ 98.7 atm Molality: $m_{NH_3} = 80$ mol/kg	eUNIQUAC (Darde <i>et al.</i> 2010 that is an upgraded of the version proposed by Thomsen and Rasmussen, 1999)	Soave-Redlich-Kwong (SRK) equation
Que and Chen (2011)	$NH_3 + H_2O \rightleftharpoons NH_4^+ + OH^-$ $CO_2 + 2H_2O \rightleftharpoons H_3O^+ + HCO_3^-$ $HCO_3^- \rightleftharpoons H_3O^+ + CO_3^{2-}$ $NH_3 + HCO_3^- \rightleftharpoons NH_2COO^- + H_2O$ $NH_4HCO_3 \rightleftharpoons HCO_3^- + NH_4^+$ $2H_2O \rightleftharpoons H_3O^+ + OH^-$	Temperature: T > 473 K Pressures ≤ 6.90 atm Concentration: $w_{NH_3} = 0.30$ and $0 \leq w_{CO_2} \leq 1$	eNRTL	PC-SAFT

CHAPTER V- A comparative study of thermodynamic models to describe the VLE of the H<sub>2</sub>O, CO<sub>2</sub> and NH<sub>3</sub> mixture

AUTHOR	REACTIONS CONSIDERED	TEMPERATURE, PRESSURE AND CONCENTRATION RANGE	THERMODYNAMIC MODEL	
			LIQUID PHASE	VAPOUR PHASE
Darde <i>et al.</i> (2012)	eUNIQUAC: $NH_3 + H^+ \rightleftharpoons NH_4^+$ $CO_2 + H_2O \rightleftharpoons H^+ + HCO_3^-$ $HCO_3^- \rightleftharpoons H^+ + CO_3^{2-}$ $NH_3 + HCO_3^- \rightleftharpoons NH_2COO^- + H_2O$ eNRTL: $2H_2O \rightleftharpoons H_3O^+ + OH^-$ $CO_2 + H_2O \rightleftharpoons H^+ + HCO_3^-$ $HCO_3^- \rightleftharpoons H^+ + CO_3^{2-}$ $NH_3 + HCO_3^- \rightleftharpoons NH_2COO^- + H_2O$ $NH_3 + H_2O \rightleftharpoons NH_4^+ + OH^-$ $HCO_3^- + NH_4^+ \rightleftharpoons NH_4HCO_3$	Temperature: $273 < T < 473$ K Pressure: $0 < P < 139$ atm Molality: $m_{NH_3}$ up to 14.3 mol/kg	eNRTL  eUNIQUAC (from Darde <i>et al.</i> 2010 that is an upgraded of the version proposed by Thomsen and Rasmussen, 1999)	Soave-Redlich-Kwong (SRK) equation
Freitas <i>et al.</i> (2013)	$NH_3 + H_2O \rightleftharpoons NH_4^+ + OH^-$ $CO_2 + H_2O \rightleftharpoons H^+ + HCO_3^-$ $HCO_3^- \rightleftharpoons H^+ + CO_3^{2-}$ $NH_3 + HCO_3^- \rightleftharpoons NH_2COO^- + H_2O$ $H_2O \rightleftharpoons H^+ + OH^-$	Temperature: $313 < T < 473$ K Pressure: $\leq 69$ atm Molality: $m_{NH_3} = 16$ mol/kg and $m_{CO_2} \leq 13$ mol/kg	eUNIQUAC (from Thomsen <i>et al.</i> 1996 and Thomsen 1997)	Nakamura
Jilvero <i>et al.</i> (2015)	$NH_3 + H_2O \rightleftharpoons NH_4^+ + OH^-$ $CO_2 + 2H_2O \rightleftharpoons H_3O^+ + HCO_3^-$ $HCO_3^- \rightleftharpoons H_3O^+ + CO_3^{2-}$ $NH_3 + HCO_3^- \rightleftharpoons NH_2COO^- + H_2O$ $H_2O \rightleftharpoons H^+ + OH^-$	Temperature: $283.15 < T < 310.15$ K Pressures: $1.13 < P < 1.23$ atm Concentration: $w_{NH_3} = 0.05$ and $0.10$ and $0.15 \leq w_{CO_2} \leq 0.75$	eNRTL  eUNIQUAC (from Darde <i>et al.</i> 2010 that is an upgraded of the version proposed by Thomsen and Rasmussen, 1999)	PC-SAFT  Soave-Redlich-Kwong (SRK) equation

### V.3. Thermodynamic model for the VLE of electrolyte systems

The electrolyte method proposed by Edwards (1975) considers that chemical and phase equilibria occur simultaneously. The chemical equilibrium in the liquid phase occurs due to the dissociation of the species in aqueous solution. The phase equilibrium occurs between the remaining molecular species in the liquid phase and the species in the vapor phase. At very high temperatures, Edwards et al. (1978) suggest that electrolytes are also present in the vapor phase and therefore should be considered in the phase equilibrium. For the application in this study the temperature range is from 313 to 353 K. At this condition there is simultaneous solubility of ammonia and carbon dioxide in water so the ions in the vapor phase can be neglected.

The first step when modeling electrolyte systems is to determine the dissociation reactions (Edwards, 1975). As previously discussed, reactions I to IV (Figure 1) are considered. Therefore, the ionic species are  $HCO_3^-$ ,  $CO_3^{2-}$ ,  $NH_4^+$ ,  $NH_2COO^-$ ,  $OH^-$  and  $H^+$ , and the molecular species,  $H_2O$ ,  $NH_3$  and  $CO_2$ . To describe phase equilibrium in electrolyte systems according to the phase rule, the temperature and total feed of molecular solutes ( $M_{NH_3}$ ,  $M_{CO_2}$ ) are usually specified. Firstly, the chemical equilibrium has to be ensured through component mass balance and charge balance so that the molalities of ions and molecular species in the liquid phase are computed ( $m_{NH_3}$ ,  $m_{CO_2}$ ,  $m_{H_2O}$ ,  $m_{NH_4^+}$ ,  $m_{HCO_3^-}$ ,  $m_{CO_3^{2-}}$ ,  $m_{H^+}$ ,  $m_{OH^-}$ ,  $m_{NH_2COO^-}$ ). Secondly, the molalities of the molecular species are converted into molar fractions ( $x_{NH_3}$ ,  $x_{CO_2}$ ,  $x_{H_2O}$ ). Finally, the thermodynamic equilibrium is solved by the determination of the molar fraction in the vapor phase ( $y_{NH_3}$ ,  $y_{CO_2}$ ,  $y_{H_2O}$ ) and the total pressure,  $P$ . The chemical and phase equilibrium for the system  $H_2O - NH_3 - CO_2$  is detailed below.

#### i) Chemical equilibrium

The equilibrium constant of the dissociation reactions (I to IV, according to Figure 1) are defined by:

$$K_i(T) = \frac{\prod_{i=1}^{NP} (\gamma_i m_i)^{v_i}}{\prod_{i=1}^{NR} (\gamma_i m_i)^{v_i}} \quad i = 1, \dots, 4 \quad (1)$$

where  $K_i$  is the chemical dissociation constant of reaction  $i$ ,  $v_i$  is the stoichiometric coefficient of component  $i$ ,  $NP$ , the number of the species formed in reaction,  $NR$ , the number of the species in the reagents of reactions,  $m$  are the molalities of ionic and

molecular species and  $\gamma$  is the activity coefficient of ionic and molecular species calculated by the thermodynamic models. The correlations for  $K_i$  for the system  $H_2O - NH_3 - CO_2$  are reported by Edwards *et al.* (1978).

ii) *Phase Equilibrium*

At phase equilibrium, the fugacity of each component in the vapor phase ( $\hat{f}_i^V$ ) is equal to the fugacity in the liquid phase ( $\hat{f}_i^L$ ). For the water, which is considered the solvent, the equilibrium is expressed by:

$$\hat{\phi}_{H_2O}^V y_{H_2O} P = a_{H_2O} f_{H_2O}^L \quad (2)$$

where  $\hat{\phi}_{H_2O}^V$  is the fugacity coefficient,  $y_{H_2O}$  is the molar fraction of water in the vapor phase,  $P$  is pressure,  $a_{H_2O}$  is the activity of water, which is given by  $a_{H_2O} = x_{H_2O} \gamma_{H_2O}$ , where  $x_{H_2O}$  is the molar fraction of water in the liquid phase and  $\gamma_{H_2O}$ , its activity coefficient, and  $f_{H_2O}^L$  is the fugacity of the water in the liquid at the reference, given by:

$$f_{H_2O}^L = \phi_{H_2O}^{sat} P_{H_2O}^{sat} \theta_{H_2O}^* \quad (3)$$

where  $\phi_{H_2O}^{sat}$  is the fugacity coefficient of water at the system temperature and at the water saturation pressure ( $P_{H_2O}^{sat}$ ) calculated by Antoine's equation and  $\theta_{H_2O}^*$  is the Poynting correction factor for pressure, computed by  $\int_{P_s^{sat}}^{Pr} \frac{\bar{v}_{i,s}^\infty}{RT} dP$ . The fugacity coefficient is computed by an equation of state, such as the Nakamura equation. If ideal gas is assumed, then  $\hat{\phi}_{H_2O}^V = 1$ . The activity coefficient ( $\gamma_{H_2O}$ ) is computed, for example, by eUNIQUAC and eNRTL.

The VLE for the solutes  $NH_3$  and  $CO_2$  are given by:

$$\hat{\phi}_i^V y_i P = m_i \gamma_i^{(m)} H_{i,s}^{Pr,m} \quad i \in \{NH_3, CO_2\} \quad (4)$$

where  $m_i$  is the molality of component  $i$ ,  $\gamma_i^{(m)}$  is its activity coefficient on the molal scale and  $H_{i,s}^{Pr,m}$  is its Henry constant in the solvent  $s$  (water) at the reduced pressure, given by:

$$H_{i,s}^{Pr,m} = H_{i,s}^{Psat} \exp \left( \int_{P_s^{sat}}^{Pr} \frac{\bar{v}_{i,s}^\infty}{RT} dP \right) \quad (5)$$

CHAPTER V- A comparative study of thermodynamic models to describe the VLE of the H<sub>2</sub>O, CO<sub>2</sub> and NH<sub>3</sub> mixture

where  $\bar{v}_{i,s}^{\infty}$  is the partial molar volume at the infinite dilution of component  $i$  in the solvents (water), available in Krichevsky and Kasamovsky (1935),  $R$  is the universal gas constant,  $T$  is temperature,  $P$  is pressure, which is integrated from the saturation pressure  $P_s^{sat}$  to the reduced pressure  $P_r$  and  $H_{i,s}^{psat}$  is the Henry constant for component  $i$  in solvent  $s$  (water) at the solvent saturation pressure, given by:

$$\ln H_{i,s}^{psat} = a_i + b_i/T + c_i \ln T + d_i T + e_i/T^2 \quad (6)$$

where  $a_i, b_i, c_i, d_i, e_i$  are parameters of component  $i$ , which are reported by Edwards *et al.* (1978).

The resulting mathematical model consists of two subsystems: chemical equilibrium and thermodynamic equilibrium. The first subsystem consists of  $n = 7$  algebraic equations given by the mass and charge balances as well as chemical equilibrium. Given the solute inlet molalities  $M_{NH_3}$  and  $M_{CO_2}$  as well as the temperature, the molalities for all components are calculated ( $m_{NH_3}, m_{CO_2}, m_{H_2O}, m_{NH_4^+}, m_{HCO_3^-}, m_{CO_3^{2-}}, m_{NH_2COO^-}$ ). The second subsystem is composed of 4 equations (Eq. 2, Eq. 4 and  $\sum_{i=1}^3 x_i = 1$ ) which enables the calculation of the composition in the vapor phase ( $y_{NH_3}, y_{H_2O}, y_{CO_2}$ ) and the total pressure ( $P$ ) for a given inlet temperature and liquid molar fraction.

As shown in Table 1 the eUNIQUAC and the eNRTL models have been used in the literature to describe the non-idealities for the liquid phase in phase equilibrium for the electrolyte system  $H_2O - NH_3 - CO_2$ . To describe the vapor phase, the ideal gas model is compared with the Nakamura equation, which takes into account polar and non-polar compounds. The following sections briefly describe the thermodynamic models used here.

*a. Extended UNIQUAC - eUNIQUAC*

The eUNIQUAC model is an extension of the original UNIQUAC model (Abrams and Prausnitz, 1975) to further consider electrolyte systems by adding the Debye-Hückel term, which describes the long-range interactions between the species in solution. Sandler *et al.* (1986) proposes the eUNIQUAC, which was later upgraded by Thomsen (1997) according to:

$$\ln \gamma_i(T, x) = \ln \gamma_i^C(x) + \ln \gamma_i^R(T, x) + \ln \gamma_i^{DH}(T, x) \quad (7)$$

where  $i$  is the specie, either molecular or ionic,  $\ln \gamma_i^C(x)$  is the combinatorial term,  $\ln \gamma_i^R(T, x)$ , the residual and  $\ln \gamma_i^{DH}(T, x)$ , the Debye-Hückel contributions. To calculate the combinatorial term, the pure component parameters, volume ( $r_i$ ) and surface ( $q_i$ ), must be known. The residual term further needs binary interaction parameters:  $u_{ij}^0$  and  $u_{ij}^t$ , where  $u_{ij}^0$  does not depend on temperature and  $u_{ij}^t$  does. The pure component and the binary interaction parameters required by the eUNIQUAC model for the system H<sub>2</sub>O – NH<sub>3</sub> – CO<sub>2</sub> are taken from Darde et al. (2010), who reported parameters for temperatures up to 423 K. Table 2 to Table 4 show the parameters required by the extended UNIQUAC model for the system H<sub>2</sub>O – NH<sub>3</sub> – CO<sub>2</sub>.

Table 2. Pure component parameters for the extended UNIQUAC model (Darde *et al.* 2010)

	$r$	$q$
H <sub>2</sub> O	0.92	1.4
NH <sub>3</sub>	1.6292	2.9852
CO <sub>2(aq)</sub>	0.75	2.45
NH <sub>4</sub> <sup>+</sup>	4.8154	4.6028
H <sup>+</sup>	0.1378	1x10 <sup>-16</sup>
OH <sup>-</sup>	9.3973	8.8171
CO <sub>3</sub> <sup>2-</sup>	10.828	10.769
HCO <sub>3</sub> <sup>-</sup>	8.0756	8.6806
NH <sub>2</sub> COO <sup>-</sup>	4.3022	4.1348

Table 3. Binary interaction parameters ( $u_{ij}^0$ ) for the extended UNIQUAC model (Darde et al. 2010).

	H <sub>2</sub> O	NH <sub>3</sub>	CO <sub>2(aq)</sub>	NH <sub>4</sub> <sup>+</sup>	H <sup>+</sup>	OH <sup>-</sup>	CO <sub>3</sub> <sup>2-</sup>	HCO <sub>3</sub> <sup>-</sup>	NH <sub>2</sub> COO <sup>-</sup>
H <sub>2</sub> O	0								
NH <sub>3</sub>	594.72	1090.8							
CO <sub>2(aq)</sub>	8.8383	2500	302.25						
NH <sub>4</sub> <sup>+</sup>	52.7305	785.98	-424.01	0					
H <sup>+</sup>	10000	10 <sup>9</sup>	10 <sup>9</sup>	10 <sup>9</sup>	0				
OH <sup>-</sup>	600.5	1733.9	2500	1877.9	10 <sup>9</sup>	1562.9			
CO <sub>3</sub> <sup>2-</sup>	361.39	524.13	2500	226.6	10 <sup>9</sup>	1588	1458.3		
HCO <sub>3</sub> <sup>-</sup>	577.05	534.01	526.305	505.55	10 <sup>9</sup>	2500	800.01	771.04	
NH <sub>2</sub> COO <sup>-</sup>	28.2779	498.15	2500	44.849	10 <sup>9</sup>	2500	2500	613.25	3343.1

Table 4. Binary interaction parameters ( $\mathbf{u}_{ij}^t$ ) for the extended UNIQUAC model (Darde et al. 2010).

	H <sub>2</sub> O	NH <sub>3</sub>	CO <sub>2(aq)</sub>	NH <sub>4</sub> <sup>+</sup>	H <sup>+</sup>	OH <sup>-</sup>	CO <sub>3</sub> <sup>2-</sup>	HCO <sub>3</sub> <sup>-</sup>	NH <sub>2</sub> COO <sup>-</sup>
H <sub>2</sub> O	0								
NH <sub>3</sub>	7.1827	7.0912							
CO <sub>2(aq)</sub>	0.86293	0	0.3587						
NH <sub>4</sub> <sup>+</sup>	0.50922	6.1271	8.6951	0					
H <sup>+</sup>	0	0	0	0	0				
OH <sup>-</sup>	8.5455	0.1364	0	0.34921	0	5.6169			
CO <sub>3</sub> <sup>2-</sup>	3.3516	4.9305	0	4.0555	0	2.7496	-1.3448		
HCO <sub>3</sub> <sup>-</sup>	-0.38795	5.3111	-3.734	-0.00795	0	0	1.7241	-0.01981	
NH <sub>2</sub> COO <sup>-</sup>	8.0238	6.6532	0	12.047	0	0	0	3.058	-15.92

The electrostatic term is computed by the Debye-Hückel equation. For the molecular compounds, including the solvent (water), this term is given by:

$$\ln \gamma_i^{DH}(T, x) = \frac{2A_\gamma M_i}{b^3} \left[ 1 + bI^{0.5} - \frac{1}{1 + bI^{0.5}} - 2 \ln(1 + bI^{0.5}) \right] \quad (8)$$

where  $M_i$  is the molecular weight of component  $i$ ,  $b = 1.5 (\text{kg/mol})^{0.5}$ ,  $A_\gamma$  is the Debye-Hückel parameter given by Sandler et al. (1986) and  $I$  is the ionic strength of the solution, which are respectively given by:

$$A_\gamma = 1.131 + 1.335 \cdot 10^{-3}T(^{\circ}\text{C}) + 1.164 \cdot 10^{-5}T(^{\circ}\text{C})^2 \quad (9)$$

$$I = \frac{1}{2} \sum m_i z_i^2 \quad (10)$$

where  $m_i$  is the molality of the ionic species and  $z_i$  is the charge of specie  $i$ . The Debye-Hückel contribution for the ionic compounds ( $\text{HCO}_3^-$ ,  $\text{CO}_3^{2-}$ ,  $\text{NH}_4^+$ ,  $\text{NH}_2\text{COO}^-$ ) is computed according to:

$$\ln \gamma_i^{DH}(T, x) = -\frac{z_i^2 A_\gamma I^{0.5}}{1 + bI^{0.5}} \quad (11)$$

The activity coefficients of the ionic compounds are required by the chemical equilibrium described in Eq. (1).

*b. Electrolyte-NRTL model*

The species in electrolyte systems can be classified into molecular, cationic and anionic. The eNRTL (Non-Random, Two Liquids) model was proposed by Chen et al. (1982) and is based on the local composition model as well as on the like-ion repulsion and on local electro-neutrality assumptions. As presented by Chen and Evans (1986), the Gibbs free energy for aqueous electrolyte solution takes into account two contributions: the long-range ion-ion interactions which exist beyond the immediate vicinity of the ionic species; the local interactions which exist in the local vicinity of every specie, as shown Figure 2.

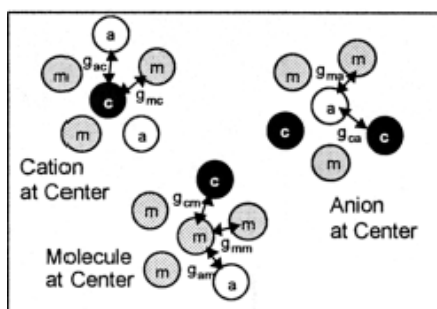


Figure 2- Interactions considered by the eNRTL model (Chen et al., 2001)

Chen and Evans (1986) state that the long-range ion-ion interactions are computed by the asymmetric expression from Pitzer (1980) whereas the local interactions are computed by the NRTL equation. The representation of  $\ln \gamma_i$  is given by a combination of the long-range (DH) and the short-range (SR) contribution, as given by:

$$\ln \gamma_i^{ex*} = \ln \gamma_i^{DH} + \ln \gamma_{i,SR}^{ex*} \quad (12)$$

where the superscript  $ex *$  means the excess property in the asymmetric convention.

The term  $\ln \gamma_i^{DH}$  is computed by the Pitzer-Debye- Hückel equation and represents the long-range ion-ion interactions, according to:

$$\ln \gamma_i^{DH}(T, x) = - \left( \frac{1000}{M_s} \right)^{1/2} \frac{A_\gamma}{3} \left[ \frac{2 z_i^2}{\rho} \ln \left( 1 + \rho I_x^{1/2} \right) + \frac{z_i^2 I_x^{1/2} - 2 I_x^{3/2}}{1 + \rho I_x^{1/2}} \right] \quad (13)$$

where  $M_s$  is the solvent molecular weight,  $\rho$  is the specific mass,  $z_i$  is the charge of specie  $i$  and  $A_\gamma$  is the Debye-Hückel parameter, computed by Eq. (9). The ionic strength  $I_x$  is calculated according to (Pitzer, 1993):



$$I_x = \frac{1}{2} \sum x_i z_i^2 \quad (14)$$

where  $x_i$  is the molar fraction of the ionic species and  $z_i$  is the charge of specie  $i$ .

The short range term  $\ln \gamma_{i,SR}^*$  is computed by NRTL, as described by Song *et al.* (2009). Table 5 shows the interacting parameters as provided by Chen *et al.* (2011). They cover a wide temperature range from 200 to 600 K.

Table 5.  $\tau_{ij}$  and  $\alpha_{ij}$  (Chen *et al.* 2011)

Component i	Component j	$\tau_{1,ij}$	$\tau_{2,ij}$	$\alpha_{ij}$
H <sub>2</sub> O	NH <sub>3</sub>	0.5275	-1022.3	0.1
NH <sub>3</sub>	H <sub>2</sub> O	3.0173	-726.72	0.1
H <sub>2</sub> O	NH <sub>4</sub> <sup>+</sup> , HCO <sub>3</sub> <sup>-</sup>	-3.9505	2860.2	0.2
NH <sub>4</sub> <sup>+</sup> , HCO <sub>3</sub> <sup>2-</sup>	H <sub>2</sub> O	3.4774	-1850.6	0.2
H <sub>2</sub> O	NH <sub>4</sub> <sup>+</sup> , CO <sub>3</sub> <sup>2-</sup>	3.4273	0	0.2
NH <sub>4</sub> <sup>+</sup> , CO <sub>3</sub> <sup>2-</sup>	H <sub>2</sub> O	-2.7182	0	0.2
H <sub>2</sub> O	NH <sub>4</sub> <sup>+</sup> , NH <sub>2</sub> COO <sup>-</sup>	9.7292	0	0.2
NH <sub>4</sub> <sup>+</sup> , NH <sub>2</sub> COO <sup>-</sup>	H <sub>2</sub> O	-4.3814	0	0.2
NH <sub>3</sub>	NH <sub>4</sub> <sup>+</sup> , NH <sub>2</sub> COO <sup>-</sup>	7.3696	0	0.1
NH <sub>4</sub> <sup>+</sup> , NH <sub>2</sub> COO <sup>-</sup>	NH <sub>3</sub>	-4.8826	0	0.1

### c. Nakamura Equation

Nakamura (1976) proposed an equation of state with perturbation in the rigid sphere term for gaseous mixtures containing polar and non-polar components. The model was developed from the equation of state from Carnahan and Starling (1972) and is represented as:

$$P = \frac{RT}{v} \left[ \frac{1 + \xi + \xi^2 + \xi^3}{(1 - \xi)^3} \right] - \frac{a^*}{v(v + c^*)} \quad (15)$$

where  $P$  is pressure,  $v$  is molar volume,  $T$  is temperature,  $R$  is the ideal gas constant,  $a^*$  represents the length of attractive forces,  $c^*$  is a parameter independent from temperature, defined solely for the polar compounds,  $\xi$  is the reduced density, which is given by:

$$\xi = \frac{b^*}{4v} \quad (16)$$

where the parameter  $b^*$  refers to the size of the rigid nucleus of the molecule. The value of  $c^*$  has to be slightly greater than zero and less than  $b^*$ . The parameters  $a^*$  and  $b^*$  depend on the temperature, according to:

$$a^* = \alpha + \frac{\beta}{T} \quad (17)$$

$$\log b^* = -\gamma - \delta T \quad (18)$$

where  $\alpha$ ,  $\beta$ ,  $\gamma$  and  $\delta$  are empirical constants.

For mixtures, the parameters  $a^*$ ,  $b^*$  and  $c^*$  are replaced by the mixture parameters  $a_m$ ,  $b_m$  and  $c_m$ , which are functions of the pure component parameters, according to:

$$a_m = \sum_{i=1}^{NC} \sum_{j=1}^{NC} y_i y_j a_{ij} \quad (19)$$

$$b_m = \sum_{i=1}^{NC} y_i \cdot b_i \quad (20)$$

$$c_m = \sum_{i=1}^{NC} y_i \cdot c_i \quad (21)$$

where  $NC$  represents the number of components,  $y_i$  is the molar fraction of component  $i$  and  $a_{ij}$  is given by:

$$a_{ij} = \alpha_{ij} + \frac{\beta_{ij}}{T} \quad (22)$$

$$\alpha_{ij} = \alpha_{ij}^0 + \alpha_{ij}^1 \quad (23)$$

$$\beta_{ij} = \beta_{ij}^0 + \beta_{ij}^1 \quad (24)$$

where the parameters  $\alpha_{ij}$  and  $\beta_{ij}$  represent intramolecular attraction forces between molecules  $i$  and  $j$ .

The fugacity coefficient,  $\hat{\phi}_i^v$ , can be determined by the Nakamura equation according to:

$$\ln \hat{\phi}_i^v = \frac{4\xi - 3\xi^2}{(1 - \xi)^2} + \frac{b_i}{b_m} \left( \frac{4\xi - 2\xi^2}{(1 - \xi)^3} \right) + \frac{-2}{RTv} \cdot \sum_{j=1}^{NC} y_j a_{ij} \cdot \sum_{k=1}^5 \frac{(-1)^k}{(k+1)} \left( \frac{c_m}{v} \right)^k + 1 + \frac{a_m c_i}{RTv^2} \cdot \sum_{k=1}^4 \frac{(-1)^k (k+1)}{(k+2)} \left( \frac{c_m}{v} \right)^k + 0.5 - \ln Z \quad (25)$$

where  $\xi$  is the reduced density;  $a, b, c$  are model parametrs;  $R$  gases universal constant;  $v$  is molar mixture volume,  $Z$  is the compressibility factor. The parameters used by the Nakamura equation for the system  $H_2O - NH_3 - CO_2$  are available in Nakamura et al. (1976) for a wide temperature range (273 K – 1023 K) and for pressures up to 344,73 bar psia. Table 6 to 7 show the parameters used by the Nakamura equation for the system NH<sub>3</sub>-CO<sub>2</sub>-H<sub>2</sub>O.

Table 6. Pure component parameters for the Nakamura Equation (Nakamura et al. 1976)

	$c^*$	$a^*$	$\beta$	$\gamma$	$\delta$
H <sub>2</sub> O	0.01	3.1307	1161.7	1.5589	5.93x10 <sup>-5</sup>
NH <sub>3</sub>	0.01	2.6435	561.63	1.3884	4.67x10 <sup>-5</sup>
CO <sub>2</sub>	0.00	3.1693	253.17	1.2340	1.47x10 <sup>-4</sup>

Table 7. Mixture parameters for the Nakamura Equation (Nakamura et al. 1976)

	$\alpha^0$	$\alpha^1$	$\beta^0$	$\beta^1$
H <sub>2</sub> O	1.06	2.07	8.40	1153.30
NH <sub>3</sub>	1.83	0.81	13.30	548.30
CO <sub>2</sub>	3.17	0.00	253.17	0.00

Table 8. Binary interaction parameters for the Nakamura Equation (Nakamura et al. 1976)

	$\alpha_{ij}^0$		
	H <sub>2</sub> O	NH <sub>3</sub>	CO <sub>2</sub>
H <sub>2</sub> O	1.06	1.40	4.36
NH <sub>3</sub>	1.40	1.83	3.10
CO <sub>2</sub>	4.36	3.10	3.17

*d. Preliminary evaluation of extended UNIQUAC and NRTL equations for electrolytes*

In order to study the quality of eUNIQUAC and eNRTL in the description of ionic behavior of electrolyte solutions, we carried out a preliminary evaluation of the thermodynamic methods using experimental data of average ionic activity coefficient for

CHAPTER V- A comparative study of thermodynamic models to describe the VLE of the  $H_2O$ ,  $CO_2$  and  $NH_3$  mixture

the salts  $NaCl$ ,  $KNO_3$ ,  $HCl$  and  $NaNO_3$ , reported by Hamer and Wu (1972). The parameters for the eUNIQUAC and the eNRTL equations are available at Chen (1986) and Thomsen (1997), respectively. Figure 3 and 4 show the results of the average ionic activity coefficient *versus* the molality for the above-mentioned salts at  $25^\circ C$ . The predictions of both equations are very close to the experimental data so that the equations are valid. At low and moderate molalities, both equations describe the system accurately with average deviations around 5%. At high molalities, though, the eNRTL slightly deviates from some experimental data, suggesting a superiority prediction capacity of the eUNIQUAC.

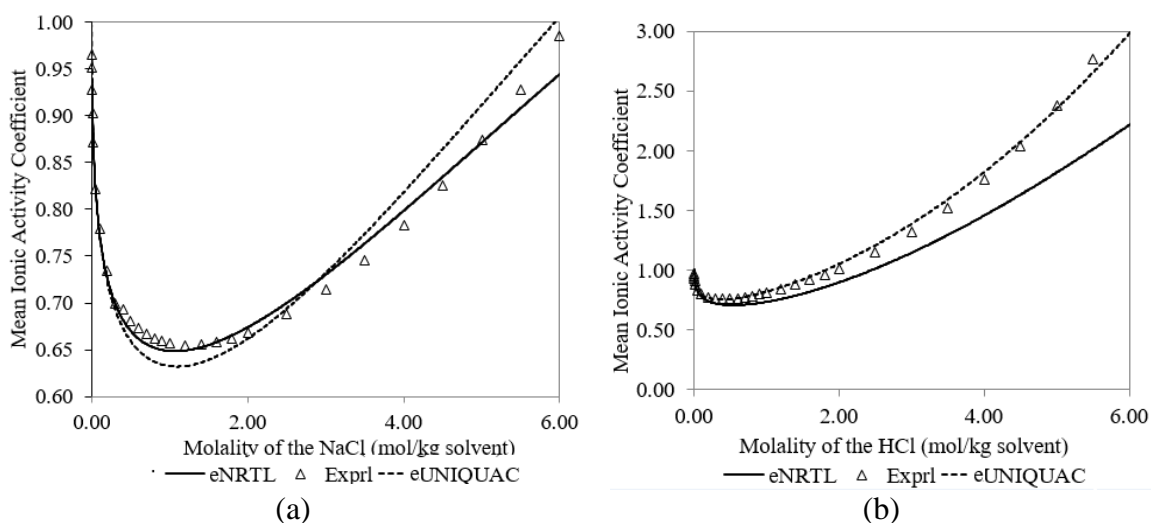


Figure 3. Average ionic activity coefficient for a)  $NaCl$  and b)  $HCl$ .

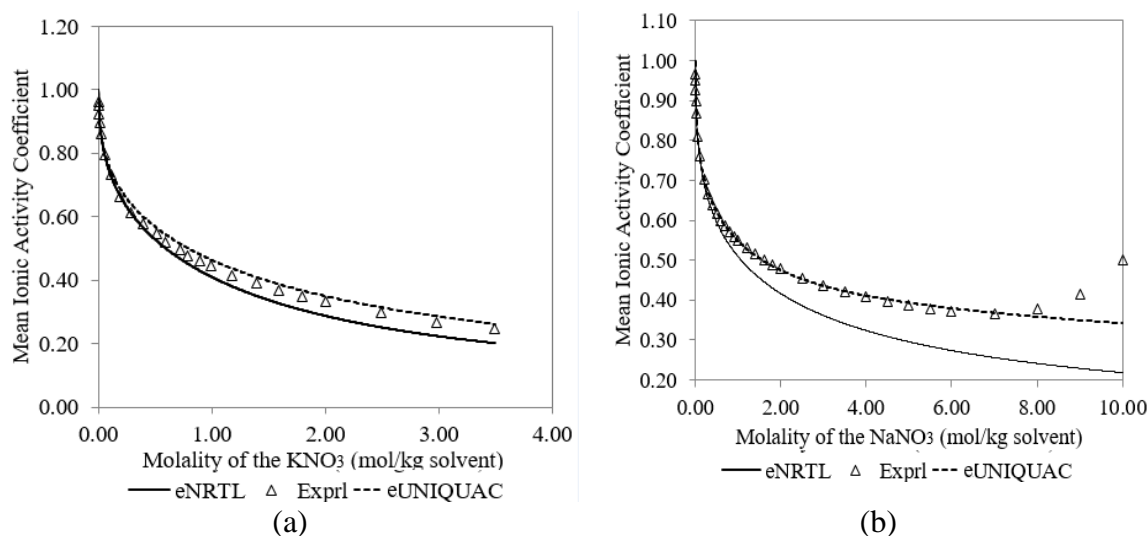


Figure 4. Average ionic activity coefficient for a)  $KNO_3$  and b)  $NaNO_3$ .

e. Validation procedure

The thermodynamic models investigated to describe the VLE for the electrolyte system  $H_2O - NH_3 - CO_2$  are compared with the experimental data from Kurz *et al.*

(1995). The authors reported the total pressure and partial pressure for the system  $H_2O - NH_3 - CO_2$  up to 6.9 atm for different temperatures and molalities, as summarized in Table 9. Kurz *et al.* (1995) show experimental data of VLE and solid precipitation as well, here just VLE data are used for the model validation.

Table 9-The inlet experimental conditions reported by Kurz et al. (1995).

Temperature (K)	Molalities Range	
	$M_{NH_3}$	$M_{CO_2}$
313 K	6.33 and 11.83 molal	0 to 5.38 molal
333 K	6.05 and 11.96 molal	0 to 4.44 molal
353 K	6.83 and 12.00 molal	0 to 3.43 molal

The models were simulated in Matlab® using an Intel (R), Core (TM) i3-3217U, 4.00GB RAM computer with operational system 64 bits. The algebraic equations are then solved in Matlab using the native function *fsolve*, which is based on the residual minimization method. Although the eNRTL model is available in Aspen, all the simulations were carried out in Matlab because the eUNIQUAC and the Nakamura models are not available in this commercial simulator. The models developed here can be used for modeling equipment which is not available in the Aspen database.

#### V.4. Results and Discussion

Firstly, the influence of the species dissociation into ions in the VLE of the system  $H_2O - NH_3 - CO_2$  is investigated. The conventional UNIQUAC and NRTL models, i.e. Eq. (7) and (13) without the Debye-Hückel term, are employed to predict the activity coefficient in the liquid phase, and the fugacity of the vapor phase is predicted by the Nakamura equation and the ideal gas law. To ascertain the most suitable thermodynamic models to describe the VLE of the ternary system, the activity coefficient models which take into account the electrolyte terms, eUNIQUAC and eNRTL, are compared.

##### a. VLE description without species dissociation (UNIQUAC and NRTL)

The activity coefficients are predicted by the UNIQUAC and NRTL models, and the fugacity by the Nakamura equation and ideal gas law. Therefore, four scenarios are investigated: UNIQUAC and Nakamura (U+Nk); UNIQUAC and ideal gas (U+Ig); NRTL and Nakamura (N+Nk); NRTL and ideal gas (N+Ig). Table 10 shows the deviation

CHAPTER V- A comparative study of thermodynamic models to describe the VLE of the H<sub>2</sub>O, CO<sub>2</sub> and NH<sub>3</sub> mixture

between the predicted and experimental total pressure ( $P_T$ ) and ammonia partial pressure ( $P_{NH_3}$ ) at different temperatures and molalities of ammonia in the absence of CO<sub>2</sub>,  $m_{CO_2} = 0$ . The model predictions are in good agreement with the experimental data provided by Kurz et al. (1995). The UNIQUAC model is more accurate than the NRTL, regardless the models describing the vapor phase. Higher inlet molalities of ammonia results in higher deviations due to the greater ionic concentration in solution as result of the more pronounced dissociation of ammonia. The deviations tend to decrease with increasing temperature because it weakens intermolecular forces so that more molecules leave the liquid phase, decreasing the rate of dissociation reactions and the concentration of ions. As a consequence, it reduces the non-ideality of the mixture. If just a small amount of CO<sub>2</sub> is present, e.g., 0.72 molal of CO<sub>2</sub> at 6.33 molal of NH<sub>3</sub> and 313 K, the deviations are higher than 40%. Then, the results are not shown here for the sake of simplicity. This indicates that the CO<sub>2</sub> strongly increases the non-ideality of the mixture, then the dissociation of the species has to be considered to accurately describe the VLE of the system H<sub>2</sub>O – NH<sub>3</sub> – CO<sub>2</sub> under the operating conditions presented in Table 9.

Table 10- Relative deviations (%) of total and ammonia partial pressure when the species dissociation is neglected<sup>[1]</sup>.

Molal of NH <sub>3</sub> , $M_{NH_3}$	$P_T$ (atm)				$P_{NH_3}$ (atm)			
	U+Nk	U+Ig	N+Nk	N+Ig	U+Nk	U+Ig	N+Nk	N+Ig
Deviation (%) for 313 K								
6.33	3.20	3.00	3.15	2.96	4.29	4.11	4.19	4.12
11.83	4.26	3.90	11.29	10.89	6.10	5.76	14.14	13.75
Deviation (%) for 333 K								
6.06	1.64	1.28	0.97	1.31	2.42	2.12	1.12	1.40
11.96	2.23	1.58	2.94	2.29	3.90	3.29	4.82	4.20
Deviation (%) for 353 K								
6.83	0.39	0.29	0.92	1.11	0.43	0.99	1.03	1.45
12.00	1.89	0.77	3.42	3.96	4.23	3.23	4.13	4.51

<sup>[1]</sup>U+Nk: Uniquac and Nakamura; U+Ig: Uniquac and ideal gas; N+Nk: NRTL and Nakamura; N+Ig: NRTL and ideal gas.

*b. VLE description with species dissociation (eUNIQUAC and eNRTL)*

When the species dissociation into ions is considered, the electrolyte term in the activity coefficient model has to be taken into account. As a result, the following pairs of models are considered: eUNIQUAC and Nakamura (eU+Nk); eUNIQUAC and ideal gas (eU+Ig); eNRTL and Nakamura (eN+Nk); eNRTL and ideal gas (eN+Ig). The simulations are carried out over a wide range of CO<sub>2</sub> and NH<sub>3</sub> compositions at three temperatures, according to the experimental conditions from Kurz (1995) summarized in Table 9. The predicted total pressure at 313K and 333K is compared with the experimental data in Figure 5 for increasing molalities of CO<sub>2</sub>. The results at 353K are very similar to the lower temperatures and are not shown here for the sake of simplicity. The eUNIQUAC is able to predict the experimental data reasonably well over a wide range of compositions, regardless of the choice of the equation of state, unlike the eNRTL, as confirmed by the relative deviations which can be seen in Table 11. Greater deviations are observed at higher molalities CO<sub>2</sub>, a condition which is associated with more pronounced interactions between the pairs molecule-molecule, molecule-ion and ion-ion. The stronger the interaction, the more complex the system, compromising the prediction of the thermodynamic model. Despite the non-linearity of the liquid phase, the results indicate that the model describing the vapor phase plays no major role. When the ideal gas law is assumed, the results from eUNIQUAC corroborate the experimental data, indicating that the activity model can capture the non-idealities of the liquid phase. Although the deviations of eNRTL are higher than eUNIQUAC, the fugacity model does not change the model prediction significantly. The ideal gas assumption is therefore valid if the liquid phase is described by eUNIQUAC.

Although the eNRTL does not fit the experimental data from Kurz et al. (1995), as illustrated in Figure 5 and Table 11, Que and Chen (2011) and Jilvero et al. (2015) successfully apply the eNRTL model to describe the non-idealities of the liquid phase of the same ternary system. These authors simulate the VLE using Aspen Plus, which estimates the parameters of the eNRTL model so that lower deviations are obtained. The parameters of the eNRTL used for the simulations presented here, however, are taken from the literature (Que and Chen, 2011) since the parameter estimation is beyond the scope of this study. Despite this feature of the commercial simulator, its database does not offer either eUNIQUAC nor the Nakamura equation of state, which is why another simulation platform was used here. More accurate predictions could be obtained if the

CHAPTER V- A comparative study of thermodynamic models to describe the VLE of the  $H_2O$ ,  $CO_2$  and  $NH_3$  mixture

parameters of the eNRTL were estimated from experimental data, as carried out by Prudente et al. (2019).

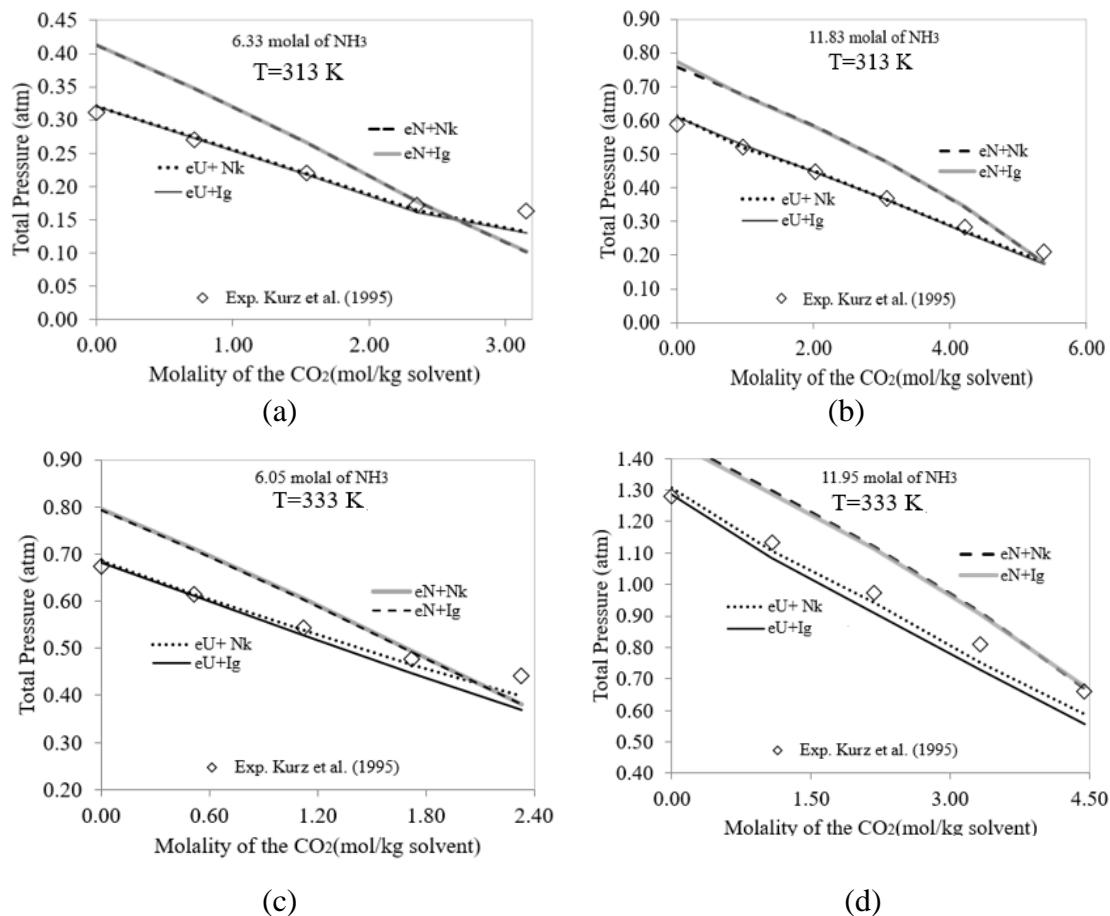


Figure 5- Total pressure of the system  $H_2O - NH_3 - CO_2$  predicted by eN+Nk and eN+Ig and by eU+Nk and eU+Ig at  $T=333\text{ K}$  a) at 6.33 molal  $NH_3$  and b) at 11.83 molal  $NH_3$  and at 333 K c) at 6.05 molal  $NH_3$  and d) at 11.95 molal  $NH_3$ .

Figure 5 indicates that increasing the  $CO_2$  concentration causes a drop in the total pressure of the system. A higher  $CO_2$  content favors chemical dissociation reactions in the liquid phase, decreasing the concentration of molecular species that vaporize, reducing the vapor pressure. These findings are in accordance with the literature (Göppert and Maurer, 1988; Pereda *et al.*, 2000). These authors report pressure decreases until the ammonia in the liquid phase is totally consumed by the dissociation reactions. From that point on, the additional  $CO_2$  stays in the molecular form and can vaporize, thus contributing to the increase in the total pressure. In these conditions, carbon dioxide has to be physically dissolved in an aqueous, nearly non-reactive solution. The results of ammonia partial pressure are very similar to those in Figure 5, so for the sake of simplicity they are not shown here.



Table 11: Average relative deviation (%) of total pressure when species dissociation is considered.

Molal of NH <sub>3</sub>	eU+Nk	eU+Ig	eN+Nk	eN+Ig
Average Deviation (%) T=313 K				
6.33	6.62	6.42	21.05	20.78
11.83	4.39	5.46	22.79	20.87
Average Deviation (%) T=333 K				
6.06	2.91	5.38	12.20	12.53
11.96	5.16	7.29	11.22	11.57
Average Deviation (%) T=353 K				
6.83	5.66	6.05	9.29	9.13
12.00	7.72	8.02	8.35	7.17

Table 11 shows that the deviation of eNRTL decreases at high temperatures, when the molecular forces between the molecules are weakened, consequently, more species tends to stay in molecular form and the non-ideality of the liquid phase decreases. The deviations from eUNIQUAC, though, does not show dependence on temperature, probably because it has less temperature dependent parameters.

## V.5. Conclusion

This study investigates the ability of different thermodynamic models to predict the VLE for the H<sub>2</sub>O – NH<sub>3</sub> – CO<sub>2</sub> system. In the absence of CO<sub>2</sub>, the dissociation into ions can be neglected without loss of accuracy because the conventional UNIQUAC and NRTL models are able to describe the VLE for the mixture ammonia and water. When CO<sub>2</sub> is added to the system, however, the ionic dissociation has to be considered, therefore the extension models for electrolytes, eUNIQUAC and the eNRTL have to be employed to satisfactorily predict the activity coefficient of the liquid phase. The results show that the fugacity model, which represents the vapor phase, plays no major role at low pressures (<7 bar) because, for a given activity coefficient model, both Nakamura and the ideal gas law results in similar predictions. Therefore, there is no need to use complex equations of state, such as PC-SAFT, to describe the vapor phase, as has been suggested in the literature. The activity coefficient model is indeed important and can capture the non-idealities of the liquid phase. The eUNIQUAC model is simpler and more precise than the eNRTL, even when its parameters are not previously adjusted to the experimental data. Therefore, the pair eUNIQUAC with Nakamura or with the ideal gas

CHAPTER V- A comparative study of thermodynamic models to describe the VLE of the  $H_2O$ ,  $CO_2$  and  $NH_3$  mixture

to predict the VLE of the  $H_2O - NH_3 - CO_2$  system is recommended. These findings might be useful for the formulation of less complex models for the design and operation of processes which involve ionic species.

## V.6. References

ABRAMS, D. S. and PRAUSNITZ, J. M. Statistical thermodynamics of liquid mixtures: a new expression. For the excess Gibbs energy of partly or completely miscible systems. *AIChE J*, v.21, pp. 116-128, 1975.

BERNARDIS, M.; CARVOLI, G.; SANTINI, M. UREA- $NH_3$ - $CO_2$ - $H_2O$  VLE Calculations using an extended UNIQUAC equation. *Fluid Phase Equilibria*, v. 53, pp. 207-218, 1989b.

BERNARDIS, M., CARVOLI, G., & DELOGU, P.  $NH_3$ - $CO_2$ - $H_2O$  VLE calculation using an extended UNIQUAC equation. *AIChE Journal*, 35(2), 314–317, 1989a.

BHASKAR, K. and CHANDRA DAS, P. Manufacture of Urea. Bachelor Thesis from Department of Chemical Engineering, National Institute of Technology Rourkela, 2007.

CARNAHAN, N. F. C and STARLING, K. E. Intermolecular repulsions and the equation of state for fluids *AIChE J.*; v. 18, pp. 1184–1189, 1972.

CHEN, C. C. and EVANS, L. B. A Local Composition Model for the Excess Gibbs Energy of Aqueous Electrolyte Systems *AIChE J.*, v. 32, pp. 444, 1986.

CHEN, C. C.; BRITT, H. I.; BOSTON, J. F.; EVANS, L. B. Local composition model for excess Gibbs energy of electrolyte systems. Part I: Single solvent, single completely dissociated electrolyte systems. *AIChE J.*, v. 28, pp. 588-596, 1982.

DARDE, V.; WELL, W. J. M. V.; TENBY, E. H. S. and THOMSEN, K. Modeling of Carbon Dioxide Absorption by Aqueous Ammonia Solutions Using the Extended UNIQUAC Model. *Ind. Eng. Chem. Res.*, v. 49, pp. 12663-12674, 2010.

DARDE, V., THOMSEN, K., VAN WELL, W. J. M., BONALUMI, D., VALENTI, G., and MACCHI, E. Comparison of two electrolyte models for the carbon capture with aqueous ammonia. *International Journal of Greenhouse Gas Control*, 8, 61–72, 2012.

CHAPTER V- A comparative study of thermodynamic models to describe the VLE of the H<sub>2</sub>O, CO<sub>2</sub> and NH<sub>3</sub> mixture

EDWARDS, T. J.; MAURER G.; NEWMAN, J.; PRAUSNITZ, J. M. Vapor-Liquid Equilibria in Multicomponent Aqueous Solutions of Volatile Weak Electrolytes. *AIChE J.*, v. 24, pp. 966-976, 1978.

EDWARDS, T. J.; NEWMAN, J.; PRAUSNITZ, J. M. Thermodynamics of aqueous solutions containing volatile weak electrolytes, *AIChE J.*, v. 21, pp. 248-259, 1975.

FREITAS, D. A., COSTA, G. M. N., GUERRIERI, Y. Expanding Aspen Plus® applications with the use of external models, case study: thermodynamic models for electrolyte solutions. In: Proceedings of the 13th International Conference on Properties and Phase Equilibria for Products and Process Design, 26 – 30 May 2013, Iguazu Falls, Argentina – Brazil.

GOPPERT, U. and MAURER, G. Vapor-liquid equilibria in aqueous solutions of ammonia and carbon dioxide at temperatures between 333 and 393 K and pressures up to 7 MPa; *Fluid Phase Equilib.*, v. 41, pp. 153-185, 1988.

GROSS, J.; SADOWSKI, G. Perturbed-Chain SAFT: An Equation of State Based on a Perturbed Theory for Chain Molecules. *Ind. Eng. Chem. Res.*, v. 40, pp. 1244-1260, 2001.

HAMER, W.J, and WU Y.-C. Osmotic coefficients and Mean Activity Coefficients of Uni-Univalent Electrolytes in Water at 25°C, *J. Phys. Chem. Ref. Data*, volume 1, pp. 1047-1099, 1972.

JAWORSKI, Z.; CZERNUSZEWICZ, M., GRALLA, Ł. comparative study of thermodynamic electrolyte models applied to the solvay soda system. *Chem. Proc. Eng.*, v. 32, pp. 135-154, 2011.

JILVERO, H.; JENS, K. J.; NORMANN, F.; ANDERSSON, K.; HALSTENSEN, M.; EIMER, D.; JOHNSON, F. Equilibrium measurements of the NH<sub>3</sub>-CO<sub>2</sub>-H<sub>2</sub>O system – measurement and evaluation of vapor-liquid equilibrium data at low temperatures. *Fluid Phase Equilib.*, v. 385, pp. 237-247, 2015.

Kim, Y. J., You, J. K., Hong, W. H., Yi, K. B., Ko, C. H., and J.- Kim, N., “Characteristics of CO<sub>2</sub> absorption into aqueous ammonia,” *Separation Science and Technology*, vol. 43, no. 4, pp. 766-777, 2008.

KRICHEVSKY, I. R. and KARSAMOVSKY, J. S. Thermodynamic Calculation of Solubilities of Nitrogen and Hydrogen in Water at High Pressures, v. 57, pp. 2168, 1935.

CHAPTER V- A comparative study of thermodynamic models to describe the VLE of the H<sub>2</sub>O, CO<sub>2</sub> and NH<sub>3</sub> mixture

KURZ, F.; RUMPF, B. and MAURER, G.. Vapor-liquid-solid equilibria in the system NH<sub>3</sub>-CO<sub>2</sub>-H<sub>2</sub>O from around 310 to 470 K: New experimental data and modeling. Fluid Phase Equilib., v. 104: pp. 261-275, 1995.

LEMKOWITZ, S. M.; DE COOKER, M. G. R. T.; VAN DEN BERG P. J. Some fundamental aspects of urea technology. The international Fertiliser Society. London, 1972.

NAKAMURA, R.; BREEDVELD, G. J. F.; PRAUSNITZ, J. M. Thermodynamic Properties of Gas Mixtures Containing Common Polar and Nonpolar Components. Ind. Eng. Chem. Proc. Des. Dev., v. 15, pp. 557–564, 1976.

PEREDA, S., THOMSEN, K., & RASMUSSEN, P. Vapor–liquid–solid equilibria of sulfur dioxide in aqueous electrolyte solutions. Chemical Engineering Science, 55 (14), 2000.

PITZER, K.S. Electrolytes: From dilute solutions to fused salts. J. Am. Chem. Soc, v. 102, pp. 2902-2906, 1980.

PITZER, K. S. Electrolytes.: From Dilute Solutions to Fused Salts. Molecular Structure and Statistical Thermodynamics, 512–517, 1993.

PRUDENTE, A. N. ; SANTANA, D. D. ; PONTES, K. V. ; LOUREIRO, J. M. ; RIBEIRO, A. M. ; NOGUEIRA, I. Parameter Estimation of a Liquid-Liquid Equilibrium for the Quaternary Mixture N-Propanol, Propanoic Acid, Propyl Propionate And Water Through Exploration And Exploitation Technique. In: Proceedings of the Congress on Numerical Methods in Engineering, 2019, Guimarães, p. 1097-1107, 2019.

QUE, H and CHEN, C.C. Thermodynamic modeling of the NH<sub>3</sub> – CO<sub>2</sub> – H<sub>2</sub>O system with Electrolyte NRTL Model. Ind. Eng. Chem. Res., v. 50, pp. 11406-11421, 2011.

RAMASAMY, K. A Study of the Vapour-Liquid Equilibria of the System Ammonia - Carbon Dioxide – Water in Relation to the Synthesis of Urea. Thesis from Delft University of Technology, Faculty of Industrial and Design Engineering Holand, 1988.

SANDLER B. Extended UNIFAC/UNIQUAC Models for (1) Gas Solubilities and (2) Electrolyte Solutions”. Ph.D. Thesis, Department of Chemical Engineering, Technical University of Denmark, DK-2800 Lyngby Denmark, 1984.

CHAPTER V- A comparative study of thermodynamic models to describe the VLE of the H<sub>2</sub>O, CO<sub>2</sub> and NH<sub>3</sub> mixture

---

SANDLER, B.; FREDENSLUND, A.; RASMUSSEN, P. Calculation of vapour-liquid equilibria in mixed solvent/salt systems using an extended UNIQUAC equation. Chem. Eng. Sci., v. 41, pp. 1171–1183, 1986.

SOAVE, G. Equilibrium constants from a modified Redlich-Kwong equation of state. Chem. Eng. Sci., Vol. 27, pp. 1197-1203, 1972.

SONG, Y.; CHEN, C.-C. Symmetric electrolyte non-random two liquid activity coefficient model. Ind. Eng. Chem. Res., v. 48, pp. 7788-7797, 2009.

THOMSEN, K. Aqueous electrolytes: model parameters and process simulation, Ph.D Thesis - Department of Chemical Engineering Technical University of Denmark DK-2800 Lyngby, Denmark, 1997.

THOMSEN, K., RASMUSSEN, P. Modeling of vapor–liquid–solid equilibrium in gas–aqueous electrolyte system. Chem. Eng. Sci. 54, 1787–1802, 1999.

XU, Y., WANG, Z., LIU, X., AND JIN, B. Modeling of the NH<sub>3</sub>-CO<sub>2</sub>-H<sub>2</sub>O vapor-liquid equilibria behavior with species-group Pitzer activity coefficient model. Int. J. Greenh. Gas Control, 31:113, 2014.

YESAVAGE, V. F; KLDNAY, J. and SANDARUSL, A. A Compilation of Parameters for a Polar Fluid Soave-Redlich-Kwong Equation of State. Chemical Engineering and Petroleum Refining Department, Colorado School of Mines, Golden, Colorado 80401, 1986.

# CHAPTER VI- CONCLUSIONS AND SUGGESTIONS FOR FUTURE WORKS

---

*“The ideas that revolutionized the world are advancing at a small step.”*

GEORG WILHELM FRIEDRICH HEGEL

## **VI.1. Conclusions**

This thesis aimed to propose a rigorous and flexible phenomenological model for a falling film absorber and to carry out a comparative study of its efficiency with a packed column. The falling film model is described by differential mass and energy balances coupled with algebraic equations representing the mass and energy balances as well as the phase-equilibrium at the interface. This thesis also investigates a rigorous thermodynamic description for the system  $\text{NH}_3\text{-H}_2\text{O}$  and for the electrolyte system  $\text{NH}_3\text{-H}_2\text{O-CO}_2$ . The system  $\text{NH}_3\text{-H}_2\text{O}$  is applied to the falling film model for refrigeration cycle and the  $\text{NH}_3\text{-H}_2\text{O-CO}_2$  can be integrating to the falling film model for further applications, such as:  $\text{CO}_2$  capture and utilization and urea synthesis. The mathematical modeling proposed here, therefore, has enormous industrial importance because it allows process monitoring and optimization in a systematic approach.

The rigorous falling film model proposed was successfully validated with data from literature. The results, for the specific operating conditions, indicate that the overall resistance for mass transfer along the falling film absorber is controlled by the liquid phase whereas the heat transfer is controlled by the coolant side. Unlike the usual approach in literature, a rigorous modeling of the vapor-liquid equilibrium at the interface is successfully proposed. The results show that the proposed modeling approach can efficiently solve the falling film equation system on the basis of a unique set of differential algebraic equations, being more efficient than the literature approach. Therefore, the

falling film model proposed is more robust and more flexible since it can be extended to other mixtures and integrated to a process flowsheet or optimization problems.

The findings of the comparative study between a falling film absorber and a packed column reveals that the falling film type absorber has greater absorption capacity and it is 33,3% more compact, in terms of special area, than the packed column. But the falling film cost is almost the double of the packed column. Therefore, the choice of the best equipment for ammonia absorption should take into consideration the desired ammonia concentration. For a high concentration, the recommendation is for the falling film absorber, if the process requires lower concentrations, the packed column is recommended because of its lower cost.

The falling film model proposed here is flexible and can be applied to other working fluids by changing the thermodynamics models and the TPPs calculations. For further applications of the model to industrial process containing  $\text{NH}_3\text{-H}_2\text{O-CO}_2$ , such as  $\text{CO}_2$  capture and utilization and urea synthesis the results of the thermodynamic description show that the fugacity model for the vapor phase plays no major role at low pressures. The activity coefficient model to capture the non-idealities of the liquid phase is indeed important. The eUNIQUAC model has more accuracy and simplicity than the eNRTL, even when its parameters are not previously adjusted to the experimental data. Therefore, the pair eUNIQUAC with Nakamura or with the ideal gas is recommended, for low pressures, to describe the VLE of the electrolyte system  $\text{H}_2\text{O} - \text{NH}_3 - \text{CO}_2$ .

## VI.2. Suggestions for future work

The findings of this thesis can be deployed in future works, therefore, the following suggestions can be cited:

- Develop an optimization problem aiming to find the best operating conditions of the falling film absorber applied to the ammonia and water refrigeration cycle;
- Compare the geometry of the falling film, demonstrating the flexibility of the proposed model: vertical and horizontal pipes and bubble and evaluate their performance in the ammonia and water refrigeration cycle;

- Evaluate the influence of different thermodynamics models, such as: NRTL and PC-SAFT in the ammonia and water falling film absorber performance;
- Apply the falling film absorber model for CO<sub>2</sub> capture process and urea syntheses by integrating thermodynamics model for the electrolyte system NH<sub>3</sub>-H<sub>2</sub>O-CO<sub>2</sub> and calculating the thermodynamic and transport properties for this system;
- Export the falling film model to Aspen Plus and integrate it with a packed column, to assess whether a combination of them in the same equipment improves absorption performance.



# APPENDIX A- FALLING FILM MODEL FOR ABSORPTION / DESORPTION PROCESS

## 1. Introduction

This Appendix has the goal to show the mass and energy balance equations for the falling film which is used for absorption and desorption processes. Figure A.1 illustrates a differential control volume, CV, where the mass balances, species balances, energy balances are to be developed. The positive sign convention for heat and mass fluxes is adopted, meaning that the heat and mass fluxes flow from the vapor phase to the liquid phase and heat from the liquid phase to the coolant. The vapor and liquid streams are fed at the top, flowing down through gravity. When the liquid and vapor phases come into contact, the absorption/desorption occurs. Since the process is exothermic or endothermic, heating or cooling are needed. In the CV in Figure A.1, coolant is fed counter-current from the bottom to the top of the equipment.

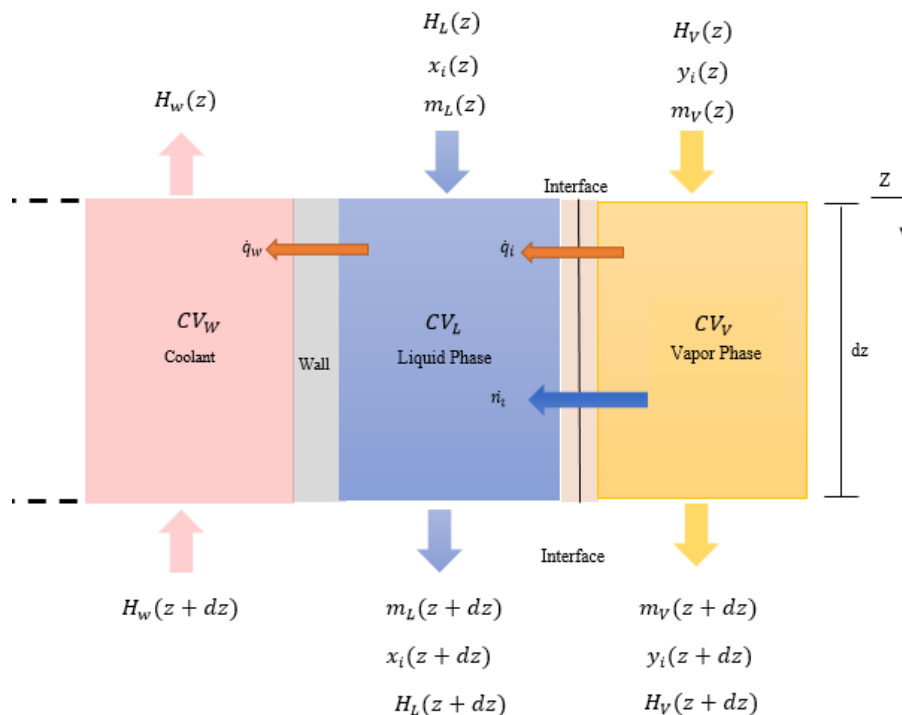


Figure A.1- Differential control volume with the positive sign.

Figure A.1 represents the differential control volume for  $CV_L$ ,  $CV_V$   $CV_w$  where  $dA_i$  is the lateral transfer area,  $m_L$  is the liquid flowrate (kg/s)  $x_i$  is molar fraction of component  $i$  in the liquid phase,  $n_i$  is the mass flux of component  $i$ ,  $H_L$  (J/kg) is the specific enthalpy of the liquid phase,  $Q_w$  (J/m<sup>2</sup>-s) is heat flux from the bulk liquid to the coolant,  $Q_L$  (J/m<sup>2</sup>-s) is the heat flux from the vapor to the bulk liquid,  $m_V$  is the vapor flowrate (kg/s),  $H_V$  (J/kg) is the specific enthalpy in vapor bulk,  $Q_V$  (J/m<sup>2</sup>-s) is heat flux from the vapor bulk to the to the liquid bulk,  $m_w$  is the coolant flowrate (kg/s),  $H_w$  (J/kg) is the enthalpy specific enthalpy of the coolant. The next sections will show the energy, component and mass balances developed at the control volumes shown in Figure A.1.

Two geometries of falling film absorbers are studied in this work: plaques (Figure A.2) and pipes (Figure A.3). The mass and energy balances are written for an infinitesimal volume with length  $\Delta z$ . The infinitesimal area of the interface where mass and heat transfer between liquid and vapor occurs is given by:

$$dA_i = L \cdot dz \tag{A.1}$$

where  $L$  is the length of the heat and mass exchange area and  $dz$  is the height of the infinitesimal element. If the falling-film is constituted by pipes (Figure A.2),  $L = \pi(d - 2\delta)$ , where  $d$  is inner diameter of the pipe,  $\delta$  is thickness of the film. If the falling-film is made of plates (Figure A.3),  $L = wth$ , where  $wth$  is width of the plaque. It is worth to mention that the heat and mass transfer coefficients can be changed according the absorber geometry.

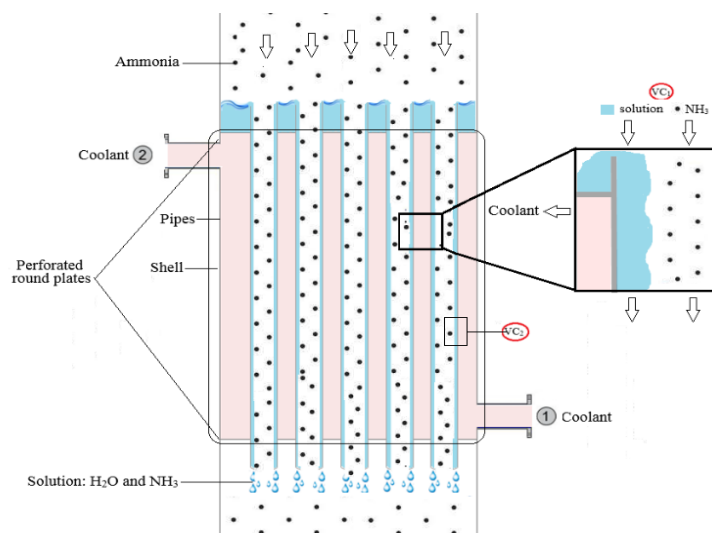


Figure A.2- Tubes falling film absorber

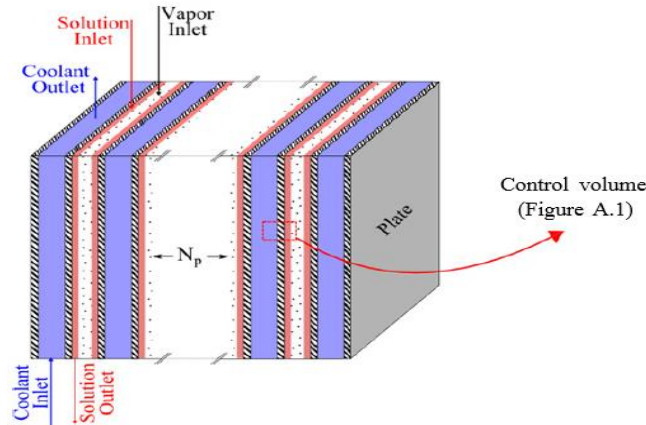


Figure A.3- Plates falling film absorber (Triche et al., 2016)

## 2. Mass, component and energy balances

The mass, component and energy balances at the CV are developed for each phase (liquid and vapor). Alternatively, it is possible to develop the balance for one phase, either liquid or vapor, and the global balance.

### 2.1 Mass balance

The mass balance is developed for the liquid and the vapor phase for differential control volume (Figure A.1).

#### *i. Mass balances for the Liquid Phase*

A differential global mass balance in the liquid  $VC_L$  (Figure A.1), where there is no mass accumulation, is represented by the expression:

$$m_L(z + \Delta z) = m_L(z) - \sum_{i=1}^{NC} \dot{n}_{i,int} dA_i \quad (A.2)$$

Substituting  $dA_i$  from Equation A.1 and recalling the definition of the derivative at the limit when  $\Delta z \rightarrow 0$ , Equation A.2 may be rewritten as:

$$\frac{dm_L}{dz} = -L \sum_{i=1}^{NC} \dot{n}_{i,int} \quad (A.3)$$

where  $L$  is the length of the heat and mass exchange area,  $NC$  is the number of components,  $z$  is the length (m),  $m_L$  is the liquid flowrate (kg/s) and  $n_i$  is the mass flux (kg/m<sup>2</sup>-s) of the component  $i$ .

*ii. Component mass balances for the Liquid Phase*

The mass balance for the component  $i$  in the liquid mixture (Figure A.1) can be represented by:

$$m_L(z + \Delta z)x_i(z + \Delta z) = m_L(z)x_i(z) - \dot{n}_{i,int}dA_i \quad (A.4)$$

At the limit when  $\Delta z \rightarrow 0$  and recalling Equation A.1:

$$\frac{d(m_L x_i)}{dz} = -\dot{n}_{i,int}L \quad (A.5)$$

In order to escape some numerical problems and to simplify the mathematical modeling, the component mass balance in equation A.5 may be written in terms of the flowrate of component  $i$ ,  $m_{L,i} = m_L x_i$ :

$$\frac{dm_{L,i}}{dz} = -\dot{n}_{i,int}L \quad (A.6)$$

*iii. Mass Balance for the Vapor Phase*

A differential global mass balance for the vapor  $VC_V$  (Figure A.1), where there is no mass accumulation, is represented by:

$$m_V(z) = m_V(z + \Delta z) - \sum_{i=1}^{NC} \dot{n}_{i,int}dA_i \quad (A.7)$$

At the limit where  $\Delta z \rightarrow 0$  and recalling the definition at equation A.1, equation A.7 may be rewrite as:

$$\frac{dm_V}{dz} = -L \sum_{i=1}^{NC} \dot{n}_{i,int} \quad (A.8)$$

where  $L$  is the length of the heat and mass exchange area,  $NC$  is the number of components,  $z$  is the length (m),  $m_V$  is the vapor flowrate (kg/s) and  $n_i$  is the mass flux kg/m<sup>2</sup>-s of component  $i$ .

*iv. Component mass balances for the Vapor Phase*

The mass balance for the component  $i$  in the vapor mixture (Figure A.1) can be represented by:

$$m_V(z)y_i(z) = m_V(z + \Delta z)y_i(z + \Delta z) - n_i dA_i \quad (\text{A.9})$$

At the limit where  $\Delta z \rightarrow 0$  and recalling the definition at equation A.1, equation A.9 may be rewritten as:

$$\frac{dm_V y_i}{dz} = -\dot{n}_{i,int} L \quad (\text{A.10})$$

In order to escape some numerical problems and to simplify the mathematical modeling, the component mass balance in equation A.11 may be written in terms of the flowrate of component  $i$ ,  $m_{V,i} = m_V y_i$ :

$$\frac{dm_{V,i}}{dz} = -\dot{n}_{i,int} L \quad (\text{A.11})$$

## 2.2 Energy balances

The energy balances for each phase at CV (Figure A.3) are shown in this section. Alternatively, it is possible to develop the balance for one phase, either liquid or vapor, and the global balance.

*i. Energy balance for the Liquid Phase*

The energy balance for the CV<sub>L</sub> (Figure A.1), may be written as:

$$H_L(z)m_L(z) + Q_L dA_i = H_L(z + \Delta z)m_L(z + \Delta z) + Q_w dA_c \quad (\text{A.12})$$

where  $dA_c$  is the coolant heat transfer area. If the falling-film is constituted by pipes,  $dA_c = \pi d_w dz$ , where  $d_c$  is external diameter of the pipe. If the falling-film is made of plaques,  $dA_c = wth dz$ , where  $wth$  is width of the plaque.

At the limit where  $\Delta z \rightarrow 0$  and recalling the definition at equation A.1, equation A.12 may be rewritten as:

$$\frac{dm_L H_L}{dz} = Q_L L - Q_w d_c \quad (\text{A.13})$$

Detailing the derivative form Equation A.13:

$$H_L \frac{dm_L}{dz} + m_L \frac{dH_L}{dz} = Q_L L - Q_w d_c \quad (\text{A.14})$$

Substituting equation A.3 into equation A.14:

$$m_L \frac{dH_L}{dz} = Q_L L - H_L L \sum_{i=1}^{NC} \dot{n}_{i,int} - Q_w d_c \quad (\text{A.15})$$

The heat fluxes at the liquid interface are composed of two parts: the convective heat transfer due to the temperature gradient between the liquid phase and the interface and the sensible heat transfer due to the mass transfer across the interface (Triche et al. 2016):

$$Q_L = \alpha_L \psi_{hL} (T_{int} - T_L) + \sum_{i=1}^{NC} \dot{n}_{i,int} \tilde{h}_{L,int} \quad (\text{A.16})$$

where  $\alpha_L$  is the liquid heat transfer coefficient,  $\psi_{hL}$  is the heat correction factor,  $\tilde{h}_{L,i}$  is the molar partial enthalpy for the component  $i$  in liquid phase. It is worth to mention that Equation A.16 represents that the heat flows from the gas phase to interface and from the interface to the liquid phase.

Substituting equations A.16 into equation A.15:

$$\begin{aligned} \frac{dH_L}{dz} & \quad (\text{A.17}) \\ & = \frac{(\alpha_L \psi_{hL} (T_{int} - T_L) + \sum_{i=1}^{NC} \dot{n}_{i,int} \tilde{h}_{L,i} - H_L \sum_{i=1}^{NC} \dot{n}_{i,int}) L - Q_w d_c}{m_L} \end{aligned}$$

where  $Q_w$  indicates the heat flux from the liquid phase to the coolant, which can be calculated by:

$$Q_w = U_{Total} (T_L - T_w) \quad (\text{A.18})$$

where  $T_L$  is the bulk liquid temperature,  $T_w$  is the coolant temperature and  $U_{Total}$  is the overall heat transfer coefficient through the wall.

### ii. *Energy balance for the Vapor Phase*

The energy balance for the  $CV_V$  may be written as:

$$H_V(z) m_V(z) = H_V(z + \Delta z) m_V(z + \Delta z) + Q_V dA_i \quad (\text{A.19})$$

At the limit where  $\Delta z \rightarrow 0$  and recalling the definition at equation A.1, equation A.19 may be rewritten as:

$$\frac{dm_V H_V}{dz} = -Q_V L \quad (\text{A.20})$$

Detailing the derivative form Equation A.20:

$$H_V \frac{dm_V}{dz} + m_L \frac{dH_V}{dz} = -Q_V L \quad (\text{A.21})$$

Replacing equation A.8 into equation A.21:

$$H_V \left( -L \sum_{i=1}^{NC} \dot{n}_{i,int} \right) + m_V \frac{dH_V}{dz} = -Q_V L \quad (\text{A.22})$$

$$m_V \frac{dH_V}{dz} = -Q_V L + H_V L \sum_{i=1}^{NC} \dot{n}_{i,int} \quad (\text{A.23})$$

The heat fluxes at the liquid interface are composed of two parts: the convective heat transfer due to the temperature gradient between the two phases and the sensible heat transfer due to the mass transfer across the interface:

$$Q_V = \alpha_V \psi_{hV} (T_V - T_{int}) + \sum_{i=1}^{NC} \dot{n}_{i,int} \tilde{h}_{V,i} \quad (\text{A.24})$$

where  $\alpha_V$  is the vapor heat transfer coefficient,  $\psi_{hV}$  is the heat correction factor,  $\tilde{h}_{V,i}$  is the molar partial enthalpy for the component  $i$  in vapor phase. It is worth noting that in equation A.24 heat from the gas phase to interface and from the interface to the liquid phase.

Inserting equations A.24 into equation A.23:

$$\frac{dH_V}{dz} = \frac{-(\alpha_V \psi_{hV} (T_V - T_{int}) + \sum_{i=1}^{NC} \dot{n}_{i,int} \tilde{h}_{V,i})L + H_V L \sum_{i=1}^{NC} \dot{n}_{i,int}}{m_V} \quad (\text{A.25})$$

### iii. Energy Balance for the Coolant

The energy balance for the  $CV_L$  may be written as:

$$H_w(z)m_w = dA_w Q_w + H_w(z + \Delta z)m_w \quad (\text{A.26})$$

At the limit where  $\Delta z \rightarrow 0$  and recalling the definition at equation A.1, equation A.26 may be rewritten as:

$$\frac{dH_w}{dz} = -\frac{\pi d_e Q_w}{m_w} = -\frac{\pi d_e U (T_L - T_w)}{m_w} \quad (\text{A.27})$$

### 3. Summary of Mass, component and energy balances at CV

The mass, component and energy balances for each phase at CV, developed in section 2, are summarized in Table A.1.

Table A.1-Mass, component and energy balances at CV

<b>Vapor phase</b>	
Mass balance	$\frac{dm_V}{dz} = -L \sum_{i=1}^{NC} \dot{n}_{i,int}$
Component mass balance	$\frac{d(m_V y_i)}{dz} = \frac{d(m_{V,i})}{dz} = -\dot{n}_{i,int} L \quad i = 1, \dots, NC$
Energy balance	$\frac{dH_V}{dz} = \frac{-(\alpha_V \psi_{hV}(T_V - T_{int}) + \sum_{i=1}^{NC} \dot{n}_{i,int} \tilde{h}_{V,i})L + H_V L \sum_{i=1}^{NC} \dot{n}_{i,int}}{m_V}$
<b>Liquid phase</b>	
Mass balance	$\frac{dm_L}{dz} = L \sum_{i=1}^{NC} \dot{n}_{i,int}$
Component mass balance	$\frac{d(m_L x_i)}{dz} = \frac{d(m_{L,i})}{dz} = \dot{n}_{i,int} L \quad i = 1, \dots, NC$
Energy balance	$\frac{dH_L}{dz} = \frac{(\alpha_L \psi_{hL}(T_{int} - T_L) + \sum_{i=1}^{NC} \dot{n}_{i,int} \tilde{h}_{L,i} - H_L \sum_{i=1}^{NC} \dot{n}_{i,int})L - Q_w d_c}{m_L}$
<b>Coolant</b>	
Energy balance	$\frac{dH_w}{dz} = -\frac{\pi d_e Q_w}{m_w} = -\frac{\pi d_e U(T_L - T_w)}{m_w}$

Table A. 2 summarizes the boundary conditions for the ordinary differential equation system shown in Table A.1. The inlet liquid and vapor streams as well as the inlet coolant stream, which flows counter-current, specifies the contour conditions.



Table A. 2- Boundary conditions

Inlet liquid	Inlet vapor	Coolant
$m_L(z = 0) = m_{L0}$	$m_V(z = 0) = m_{V0}$	$H_w(z = L) = H_{wL}$
$x_i(z = 0) = x_{i0}$	$y_{NH_3}(z = 0) = y_{NH_30}$	
$H_L(z = 0) = H_{L0}$	$H_V(z = 0) = H_{V0}$	

It is worth to mention that the  $n_i$  and  $q$  are the mass and heat flux at the interface. The model to calculate them are shown in the next section.

#### 4. Interface Equations

Due to concentration and temperature gradients at the interface between the liquid and the vapor phases there are two mass transfer resistances. The first resistance is between the vapor phase and the interface in a limit layer with thickness  $\delta_V$ . The second one is between the interface and the liquid phase in a limit layer with thickness  $\delta_L$ . Figure A.4 shows a schematic of the limit layer at the interface where  $\zeta$  is the interface direction.

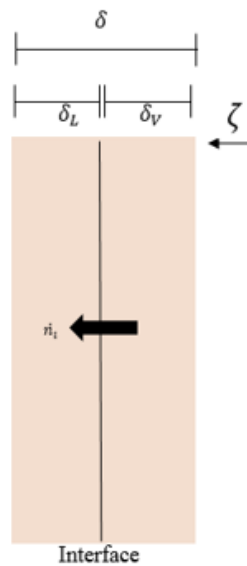


Figure A.4- Schematic of the interface between vapor and liquid

The variation in concentration of each component near the interface induces a phenomenon of mass diffusion of ammonia and water through the interface. As heat is also transferred due to mass transfer, the absorption phenomenon involves coupled mass

and heat transfers at the liquid-vapor interface. The next subsections show the heat and mass transfer equations at the interface for a binary system.

#### 4.1. *Mass flux at the interface*

Mass diffusion and bulk transport of the components across the liquid-vapor interface involve mass transfer between the liquid and the vapor phase. Then, mass transfer equations at the vapor-liquid interface are shown in this section.

##### *i. Mass flux at the interface at the liquid phase*

The mass fluxes of the component  $i$  entering the liquid phase ( $n_{i,L}$ ) and leaving the vapor phase ( $n_{i,v}$ ) is composed for two contributions: convective and diffusive according to Treybal (1968), which has a negative sign to indicate that the flux is from the more concentrated side of the specie  $i$  to the less concentrated side:

$$\dot{n}_{i,L} = x \sum_{i=1}^{NC} \dot{n}_{i,L} - \rho_L D_L \left( \frac{dx}{d\zeta} \right) \quad (\text{A.28})$$

where  $D_L$  (m<sup>2</sup>/s) is the coefficient of the massic diffusion,  $\rho_L$  (kg/m<sup>3</sup>) is the specific mass of the liquid phase.

We might define  $Z$  as the ratio between the flux of the component  $i$  and the total surface mass flow absorbed or desorbed at the liquid-vapor interface:

$$Z = \frac{\dot{n}_{i,L}}{\sum_{i=1}^{NC} \dot{n}_{i,L}} \quad (\text{A.29})$$

or

$$Z \sum_{i=1}^{NC} \dot{n}_{i,L} = \dot{n}_{i,L} \quad (\text{A.30})$$

Replacing Equation A.30 into Equation A.28:

$$Z \sum_{i=1}^{NC} \dot{n}_{i,L} = x \sum_{i=1}^{NC} \dot{n}_{i,L} - \rho_L D \left( \frac{dx}{d\zeta} \right) \quad (\text{A.31})$$

$$(Z - x) \sum_{i=1}^{NC} \dot{n}_{i,L} = -\rho_L D \left( \frac{dx}{d\zeta} \right) \quad (\text{A.32})$$

Equation A.32 is a differential separable equation that can be written as:

$$\sum_{i=1}^{NC} \int_0^{\delta_L} n_{i,L} d\zeta = -\rho_L D \int_{x_{i,int}}^{x_i} \frac{dx}{(Z-x)} \quad (\text{A.33})$$

By integrating Equation A.33 between the interface ( $\zeta = 0$  and  $x = x_{int}$ ) and the limit of the boundary layer of vapor diffusion ( $\zeta = \delta_L$  and  $x = x_i$ ) and considering  $F_L = \rho_L D / \delta_L$ , the equation of the mass flux is obtained:

$$\sum_{i=1}^{NC} n_{i,L} = F_L \ln \frac{(Z-x_i)}{(Z-x_{int})} \quad (\text{A.34})$$

where  $F_L$  is the mass transfer coefficient (m/s) between the liquid phase and the interface, obtained from the correlation developed by Yih (1987). It may be calculated by:

$$F_{Li} = 0.01099 Re_{film}^{0.3955} Sc_L^{0.5} \left( \frac{D_L \rho_L}{M_L} \right) \left[ \frac{g \rho_L^2}{\mu_L^2} \right]^{\frac{1}{3}} \quad (\text{A.35})$$

where  $Re_{film}$  is the Reynolds number for the liquid film,  $Sc_L$  Schmidt number for the liquid phase,  $M_L$  is the molecular weight (kg/mol),  $D_L$  is diffusivity,  $\mu_L$  is viscosity (Pa/s),  $\rho_L$  is density (kg-m<sup>-3</sup>). This equation is only valid in a falling film with a Reynolds number between 49 and 300 and in fully developed conditions (Yih, 1987).

*ii. Mass flux at the interface at the vapor phase*

Like in the liquid phase, the mass fluxes of the component  $i$  leaving the vapor phase ( $n_{i,V}$ ) and entering the liquid phase is composed by two contributions: convective and diffusive according to Treybal (1968), which has a positive sign because the flux is from the less concentrated side of the specie  $i$  to the more concentrated side:

$$n_{i,V} = y \sum_{i=1}^{NC} n_{i,V} + \rho_V D_V \left( \frac{dy}{d\zeta} \right) \quad (\text{A.36})$$

where  $D_V$  (m<sup>2</sup>/s) is the coefficient of the massic diffusion,  $\rho_V$  (kg/mol) is the specific mass of the vapor phase.

Considering the ratio  $Z$  which is the ratio between the surface mass flow rate of the component  $i$  and the total surface mass flow absorbed or desorbed at the liquid-vapor interface:

$$Z = \frac{n_{i,V}}{\sum_{i=1}^{NC} n_{i,V}} \quad (\text{A.37})$$

or

$$Z \sum_{i=1}^{NC} n_{i,V} = n_{i,V} \quad (\text{A.38})$$

Replacing Equation A.37 into Equation A.36:

$$Z \sum_{i=1}^{NC} n_{i,V} = y \sum_{i=1}^{NC} n_{i,V} + \rho_V D \left( \frac{dy}{d\zeta} \right) \quad (\text{A.39})$$

$$\sum_{i=1}^{NC} \int_0^{\delta_V} n_{i,V} d\zeta = \rho_V D \int_{x_{i,int}}^{y_i} \frac{dy}{(Z-y)} \quad (\text{A.40})$$

By integrating Equation A.40 between the interface ( $\zeta = 0$  and  $y = y_{int}$ ) and the limit of the boundary layer of vapor diffusion ( $\zeta = \delta_V$  and  $y = y_i$ ) and considering  $F_V = \rho_V D / \delta_V$ , the equation of the total surface mass flux is obtained:

$$\sum_{i=1}^{NC} n_{i,V} = F_V \ln \frac{(Z - y_{i,int})}{(Z - y_i)} \quad (\text{A.41})$$

where  $F_V$  mass transfer coefficient for the vapor phase, which is calculated by applying the Chilton-Colburn (1934) analogy:

$$F_V = \left( \frac{\alpha_V}{C_{PV} M_V \left[ \frac{Sc_V}{Pr_V} \right]^{2/3}} \right) \quad (\text{A.42})$$

where  $Pr_V$  Prandtl number ( $Pr_V = \frac{\mu_V C_{PV}}{\lambda_V}$ ),  $Sc_V$  Schmidt number ( $Sc_V = \frac{\mu_V}{D_V \rho_V}$ ),  $C_{PV}$  (J·kg<sup>-1</sup>·K<sup>-1</sup>) specific heat, molecular weight  $M_V$  (kg/mol) and  $\alpha_V$  (m·s<sup>-1</sup>) heat transfer coefficient for the vapor phase. In the Prandtl and Schmidt number for the vapor phase,  $D_V$  is diffusivity from Wilke and Chang (1955),  $\mu_V$  is viscosity (Pa·s<sup>-1</sup>),  $\lambda_V$  is thermal conductive,  $\rho_V$  (kg·m<sup>-3</sup>) is density.

Since it is assumed that there is no chemical reaction is taking place at the interface and taking into account that the interface itself contains no significant mass (Bird et al., 2006), continuity of the total mass flux at the interface might be assumed for any species being transferred. So, the following equation might be written for the mass flux equations:

$$n_{i,L} = n_{i,V} = n_{i,int} \quad (\text{A.43})$$

#### 4.2. Heat flux at the interface

The heat fluxes at the interface are composed of two parts: the convective heat transfer due to the temperature gradient between the two phases and the sensible heat transfer due to the mass transfer across the interface (Bird *et al.*, 2006):

$$q = \alpha \nabla T + \sum_{i=1}^{NC} n_{i,int} \tilde{h}_i \quad (\text{A.44})$$

where  $\tilde{h}$  is the partial molar enthalpy of specie  $i$  (J/kg),  $n_i$  is the molar flux of specie  $i$ ,  $\alpha$  (W/m<sup>2</sup>-K) is the heat transfer coefficient and  $\psi$  is a the corrector factor. The heat fluxes at the liquid and vapor interfaces are then compute as:

$$Q_L = \alpha_L \psi_L (T_{int} - T_L) + \sum_{i=1}^{NC} n_{i,int} \tilde{h}_i \quad (\text{A.45})$$

$$Q_V = \alpha_V \psi_V (T_V - T_{int}) + \sum_{i=1}^{NC} n_{i,int} \tilde{h}_i \quad (\text{A.46})$$

where the subscripts  $L$  and  $V$  indicate the liquid and vapor interface, respectively. The heat transfer coefficient for the liquid phase,  $\alpha_L$  (W-m<sup>-2</sup>K<sup>-1</sup>) can calculate by using Chilton-Colbum (1934) analogy:

$$\dot{\alpha}_L = \psi_{hL} \alpha_L \quad (\text{A.47})$$

$$\alpha_L = \psi_{hL} F_L \left( C_{PL} M_L \left[ \frac{Sc_L}{Pr_L} \right]^{2/3} \right) \quad (\text{A.48})$$

where  $Pr_L$  Prandtl number ( $Pr_L = \frac{\mu_L C_{PL}}{\lambda_L}$ ),  $Sc_L$  Schmidt number ( $Sc_L = \frac{\mu_L}{D_L \rho_L}$ ),  $C_{PL}$  (J·kg<sup>-1</sup>K<sup>-1</sup>) specific heat, molecular weight  $M_L$  (kg/mol) and  $F_L$  (m·s<sup>-1</sup>) mass transfer coefficient for the liquid phase. In the Prandtl and Schidt number for the liquid phase,  $D_L$  is diffusivity from Wilke and Chang (1955),  $\mu_L$  is viscosity (Pa·s<sup>-1</sup>),  $\lambda_L$  (W·m<sup>-1</sup>K<sup>-1</sup>) is thermal conductive,  $\rho_L$  (kg·m<sup>-3</sup>) is density. The correction factors,  $\psi_{hL}$ , take account the finite mass transfer effect. It can be calculated by (Triché, 2016):

$$\psi_{hL} = \frac{\left( \frac{\sum_{i=1}^{NC} n_{i,int} \tilde{c}_{pL,i}}{\alpha_L} \right)}{1 - e^{\left( -\frac{\sum_{i=1}^{NC} n_{i,int} \tilde{c}_{pL,i}}{\alpha_L} \right)}} \quad (\text{A.49})$$

The heat transfer coefficient for the vapor phase,  $\alpha_V$  (W·m<sup>-2</sup>K<sup>-1</sup>) can be calculated by using the correlation give at Kakaç *et al.* (1987):

$$\dot{\alpha}_V = \psi_{hV} \alpha_V \quad (\text{A.50})$$

$$\alpha_V = 7.541 \left( \frac{\lambda_V}{d_{hv}} \right) \quad (\text{A.51})$$

where  $\lambda_V$  ( $\text{W}\cdot\text{m}^{-1}\text{K}^{-1}$ ) is the thermal conductive in vapor phase,  $d_{hv}$  (m) is hydraulic diameter of the vapor in the control volume. The correction factors ( $\psi_{hV}$ ), from Triché et. al (2016) can be calculated by:

$$\psi_{hG} = \frac{\left( \frac{\sum_{i=1}^{NC} n_{i,int} \tilde{C}_{pV,i}}{\alpha_V} \right)}{1 - e^{\left( -\frac{\sum_{i=1}^{NC} n_{i,int} \tilde{C}_{pV,i}}{\alpha_V} \right)}} \quad (\text{A.52})$$

The heat flux between the bulk gas and the liquid solution at the interface,  $Q_{int}$ , can be calculated considering the energy continuity across the gas–liquid interface:  $Q_{int} = Q_L = Q_V$ . Then, Equations A.45 and A.46 can be written as:

$$\alpha_V \psi_V (T_V - T_{int}) + \sum_{i=1}^{NC} n_{i,int} \tilde{h}_{V,i} = \alpha_L \psi_L (T_{int} - T_L) + \sum_{i=1}^{NC} n_{i,int} \tilde{h}_{L,i} \quad (\text{A.53})$$

#### 4.3. Summary: heat and mass transfer equations at interface

The heat and mass transfer equations at the vapor-liquid interface, developed in subsections 4.1 and 4.2, are summarized in Table 3.

Table A.3- Heat and mass transfer equations at interface in CV

Mass Flux at the vapor interface	$\sum_{i=1}^{NC} n_{i,int} = \dot{F}_V \ln \frac{(Z - y_{i,int})}{(Z - y_i)}$
Mass Flux at the liquid interface	$\sum_{i=1}^{NC} n_{i,int} = \dot{F}_L \ln \frac{(Z - x_i)}{(Z - x_{int})}$
Heat transfer equation at the interface	$\alpha_V \psi_V (T_V - T_{int}) + \sum_{i=1}^{NC} n_{i,int} \tilde{h}_{V,i} = \alpha_L \psi_L (T_{int} - T_L) + \sum_{i=1}^{NC} n_{i,int} \tilde{h}_{L,i}$

The molar fluxes of each specie at the interface and the temperature at the interface can be computed by the system of algebraic equations in Table 3 which, together with the

differential equations, shown in Table A.1, compose the differential algebraic equation (DAE) system that represents the falling film model. The vector  $X$  represents the algebraic and differential states of the DAE system:

$$X = [n_{NH_3}, n_{H_2O}, H_{in}, H_L, H_v, H_w, \mathbf{x}, \mathbf{y}, m_L, m_V] \quad (A.54)$$

As Table A. 2 shows, the coolant specifies a contour condition at  $z = L$ , unlike the other differential equations which provide the supplementary condition at  $z = 0$ . To solve this problem, then, the finite differences method is applied to discretize the equations in Table A.1. The detailed discretization will be discussed in the next section.

Enthalpies of ammonia and water liquid mixture,  $H_L$  ( $J \cdot kg^{-1}$ ), are computed by the correlations proposed by Pretek and Klomfar (1995), as already used by some authors in literature (Conde (2006), Goel and Goswami, 2005; Fernández-Seara et al., 2007; Triché et al., 2016, Triché et al., 2017 and Aminyavari *et al.*, 2017), whereas the mixture enthalpy for the vapor ( $H_V$ ) phase is consider as ideal gas, as recommended by Triche *et. al* (2016, 2017). The mass partial enthalpies for the component  $i$  in vapor and liquid phase,  $\tilde{h}_{V,i}$  and  $\tilde{h}_{L,i}$  ( $J \cdot kg^{-1}$ ) are computed by correlations from Ziegler and Trepp (1984). Regarding the composition at the interface, they are calculated by empirical correlations from Pretek and Klomfar (1995).

## 5. Discretization of the energy and mass balances equations

The differential Equations (Table A.1) that represent the energy and mass balance in the liquid and vapor bulk are discretized by finite differences method. Figure A.5 shows the schematic representation of the discretization along one pipe among the pipes bundle, if the falling film absorber is composed by pipes.

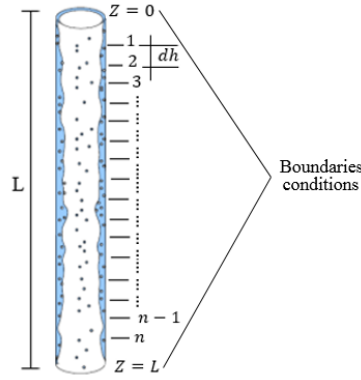


Figure A.5- Schematic Representation of the Discretization along the tube

As the boundaries conditions for the mass and energy balances for the liquid and vapor bulks are specified at  $z = 0$ , the backward finite differences approximation is applied. The energy balance of the coolant, though, specifies the boundary condition at  $z = L$ , then the forward finite differences approximation is applied as shown Figure A.5.

Table A.4- Discretized differential equation system

<b>Vapor phase</b>	
Mass balance	$\frac{dm_V}{dz} = -L \sum_{i=1}^{NC} n_{i,int} = f_{MV} \rightarrow \left( \frac{dm_V}{dz} \right)_{z=j} \approx \frac{m_{V,j} - m_{V,(j-h)}}{h} = f_{MV,j}$
Component mass balance	$\frac{d(m_{V,i})}{dz} = -n_{i,int}L = f_{CV} \rightarrow \left( \frac{d(m_{V,i})}{dz} \right)_{z=j} \approx \frac{m_{L,j} - m_{L,(j-h)}}{h} = f_{ML,j}$
Energy balance	$\frac{dH_V}{dz} = \frac{-(\alpha_V \psi_{hV}(T_V - T_{int}) + \sum_{i=1}^{NC} n_{i,int} \tilde{h}_{V,i})L + H_V L \sum_{i=1}^{NC} n_{i,int}}{m_V} = f_{EV} \rightarrow \left( \frac{dH_V}{dz} \right)_{z=j} \approx \frac{H_{V,j} - H_{V,(j-h)}}{h} = f_{EV,j}$
<b>Liquid phase</b>	
Mass balance	$\frac{dm_L}{dz} = L \sum_{i=1}^{NC} n_{i,int} = f_{ML} \rightarrow \left( \frac{dm_L}{dz} \right)_{z=j} \approx \frac{m_{L,j} - m_{L,(j-h)}}{h} = f_{ML,j}$
Component mass balance	$\frac{d(m_{L,i})}{dz} = n_{i,int}L = f_{CL} \rightarrow \left( \frac{d(m_{L,i})}{dz} \right)_{z=j} \approx \frac{m_{L,i,j} - m_{L,i,(j-h)}}{h} = f_{CL,j}$
Energy balance	$\frac{dH_L}{dz} = \frac{(\alpha_L \psi_{hL}(T_{int} - T_L) + \sum_{i=1}^{NC} n_{i,int} \tilde{h}_{L,i} - H_L \sum_{i=1}^{NC} n_{i,int})L - Q_w d_c}{m_L} = f_{EL} \rightarrow \left( \frac{dH_L}{dz} \right)_{z=j} \approx \frac{H_{L,(j)} - H_{L,(j-h)}}{h} = f_{EL,j}$
<b>Coolant</b>	
Energy balance	$\frac{dH_w}{dz} = -\frac{LQ_w}{m_w} = -\frac{LU(T_L - T_w)}{m_w} = f_w \rightarrow \left( \frac{dH_w}{dz} \right)_{z=j} \approx \frac{H_{w,(j+h)} - H_{w,(j)}}{h} = f_{w,j}$
$j= 1$ : Discretized points and $i= 1$ : Components number	



## 6. References

AMINYAVARI, M., APRILE, M., TOPPI, T., GARONE, S., MOTTA, M. A detailed study on simultaneous heat and mass transfer in an in-tube vertical falling film absorber, *International Journal of Refrigeration* 80, 2017, 37–51

BIRD, B., STEWART, W., LIGHTFOOT, E. *Transport Phenomena*, Revised second ed. JohnWiley & Sons, Inc., 2006

CHILTON, T.H., COLBURN, A.P., Mass transfer (absorption) coefficients prediction from data on heat transfer and fluid friction. *Ind. Eng. Chem.*, 1934. 26, 1183–1187.

CONDE, M, Thermophysical properties of ammonia-water mixtures for the industrial design of absorption refrigeration equipment, M. CONDE Engineering, 2006.

SIERES, J FERNANDEZ-SEARA J., Modeling of simultaneous heat and mass transfer processes in ammonia–water absorption systems from general correlations. *Heat Mass Transfer*, 2007, 44:113–123

GOEL N, GOSWAMI DY. A compact Falling Film Absorber. *Journal of Heat Transfer* September, 2005, vol 127/ 957.

KAKAÇ, S., AUNG, W., SHAH, R.K. *Handbook of Single-phase Convective Heat Transfer*. 1987, Wiley, NewYork

PATEK, J. and KLOMFAR, J. Simple functions for fast calculations of selected thermodynamic properties of the ammonia-water system: *Int. J. Refrigeration* 18, No. 4, pp. 228–234, 1995.

TREYBAL, R.E., *Mass Transfer Operations*, McGraw-Hill, New York, 1968

TRICHÉ D., BONNOTA, S., PERIER-MUZETA, M., BOUDÉHENNA F. DEMASLESA H., CANEY, N. Modeling and experimental study of an ammonia-water falling film Absorber SHC 2015, *International Conference on Solar Heating and Cooling for Buildings and Industry Energy Procedia* 91 (2016) 857 – 867.

TRICHÉ D., BONNOTA, S., PERIER-MUZETA, M., BOUDÉHENNA F. DEMASLESA H., CANEY, N. PERIER-MUZET, M. Experimental and numerical study of a falling film absorber in an ammonia-water absorption chiller. *International Journal of Heat and Mass Transfer* 111 (2017) 374–385

YIH, S. M., *Modeling heat and mass transport in Falling Film Liquid Films*, *Handbook of heat and Mass Transfer: Mass Transfer and Reactor Design*, N. P: Cheremisinoff, eds., Gulf Publishing Company, 1986, Houston, pp 111-120.

ZIEGLER, B., Ch. Trepp, Equation of state of ammonia–water mixtures, *Int. J. Refrig.* 7, 1984, 101–106.

# APPENDIX B. PHYSICAL AND THERMAL PROPERTIES FOR NH<sub>3</sub> AND H<sub>2</sub>O MIXTURE

---

## 1. Introduction

This appendix has the goal to show the models used to calculate some transport and thermodynamics properties, such as: enthalpies and specific heat for the system NH<sub>3</sub> and H<sub>2</sub>O in liquid and vapor phase. Besides, all the parameters necessary are shown, as well the validation of each property. The thermal and physics properties shown here are: specific heat, viscosity, thermal conductive, diffusivity, density, enthalpies and specific partial enthalpies. Some of them (viscosity, thermal conductive and density) are calculated by TEA (Thermodynamics for Engineering Applications). TEA is a CAPE (Computer-Aided Process Engineering)-OPEN able to connect with other CAPE-OPEN softwares, such as Matlab. On the other hand, specific heat, diffusivity, enthalpies and mass partial enthalpies are calculated from literature correlations.

## 2. Specific Heat

Specific heat of ammonia and water in liquid phase,  $C_{p,L,i}$  (J/mol-K), are calculated by correlation from Perry (1999). For ammonia, it is given by:

$$C_{p,L,NH_3} = \frac{C_1^2}{t} + C_2 - 2C_1 C_3 t - C_1 C_4 t^2 - \frac{C_3^2 t^3}{3} - \frac{C_3 C_4 t^4}{2} - \frac{C_4^2 t^5}{5} \quad \text{B.1}$$

where  $C_1, C_2, C_3$  and  $C_4$  are parameters (Table B.1) and  $t = 1 - T_r$ .  $T_r$  is reduced temperature calculated by:

$$T_r = T/T_c \quad \text{B.2}$$

where  $T_c$  is critical temperature, for ammonia is 405.1 K. For water, the specific heat is given by:

$$C_{p,L,H_2O} = C_1 + C_2 T + C_3 T^2 + C_4 T^3 + C_5 T^4 \quad \text{B.3}$$

where  $C_1, C_2, C_3, C_4$  and  $C_5$  are parameters (Table B.1) and  $T$  (K) is temperature.

Parameter	NH <sub>3</sub>	H <sub>2</sub> O
$C_1$	61.289	276370
$C_2$	80925	-2090.1
$C_3$	799.4	8.125
$C_4$	-2651	-0.014116
$C_5$	-	$9.3701 \cdot 10^{-6}$

Figure B.1 shows the specific heat for ammonia (Figure B.1a) and water (Figure B.1b) in liquid phase. The average deviation between experimental and simulated data is 1.32% and 2.41% for ammonia and water, respectively. These results indicate that the specific heats for both species in liquid phase are calculated with a good agreement with experimental data (Perry, 1999).

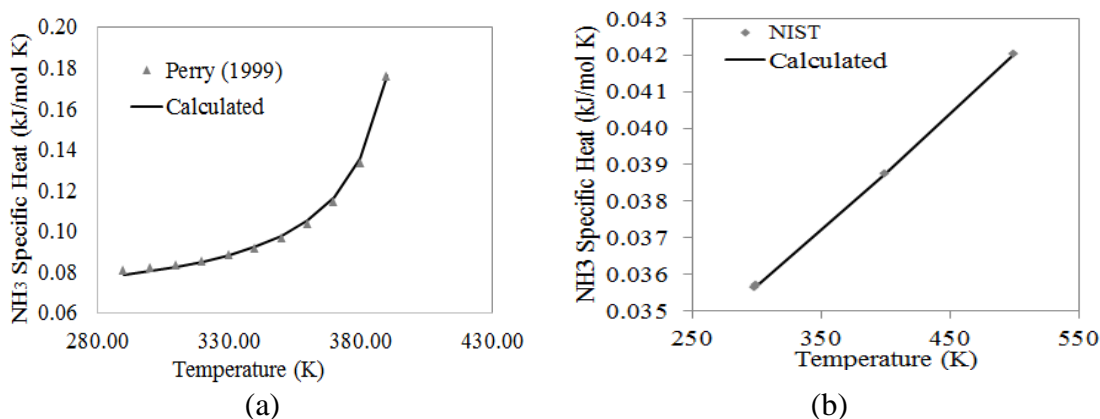


Figure B.1- Specific heat for (a) ammonia (b) and water in liquid phase

Specific heat of ammonia and water in vapor phase,  $Cp_{v,i}$  (J/mol-K), are calculated by correlation from Van Ness et al. (2007):

$$\frac{Cp_{v,i}}{R} = A + BT + CT^2 + DT^{-2} \quad \text{B.4}$$

where  $A, B, C$  and  $D$  are parameters (Table B.2),  $T$  (K) is temperature and  $R$  (J/mol-K) is gases constant.

Table B.2- Vapor Specific Heat Parameters (Van Ness et al., 2007)

Parameter	NH <sub>3</sub>	H <sub>2</sub> O
A	3.578	3.470
10 <sup>3</sup> B	3.020	1.450
10 <sup>6</sup> C	-	-
10 <sup>-5</sup> D	-0.186	0.121

Simulated results of the specific heat for ammonia and water in vapor phase are shown in Figure B.1 and Table B.2b, respectively. The validations of these simulations are done against experimental data from literature (Perry, 1999). These results indicate that the specific heats for both species in vapor phase are calculated with a good agreement with experimental data, with average deviation between experimental and simulated data is 0.11% and 0.08% for ammonia and water, respectively.

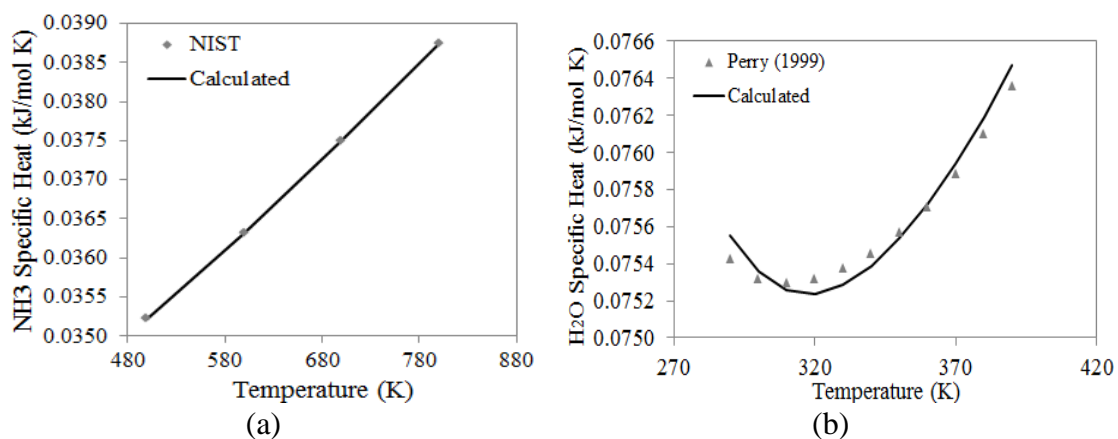


Figure B.2- Specific heat for ammonia (a) and water (b) in vapor phase

Specific heat of the liquid and vapor mixture are calculated by weighting equation of the specific heats for the pure components. The same procedure is done by Conde (2005), Prata (2012) and Triché (2017). The correlations for liquid and vapor mixture are respectively given by:

$$Cp_{L,mix} = x_{NH_3} Cp_{L,NH_3} + x_{H_2O} Cp_{L,H_2O} \quad B.5$$

$$Cp_{V,mix} = y_{NH_3} Cp_{V,NH_3} + y_{H_2O} Cp_{V,H_2O} \quad B.6$$

Simulated results of specific heat for the ammonia and water mixture are shown in Figure B.3 the temperature range is from 280 to 360 K whereas the composition range

is from 0.15 to 0.84 molar of ammonia. The average deviations between the experimental data and the simulated data is 1.70%, that is means the specific heat for the liquid mixture is in good agreement with experimental data (Fujita et al., 2008).

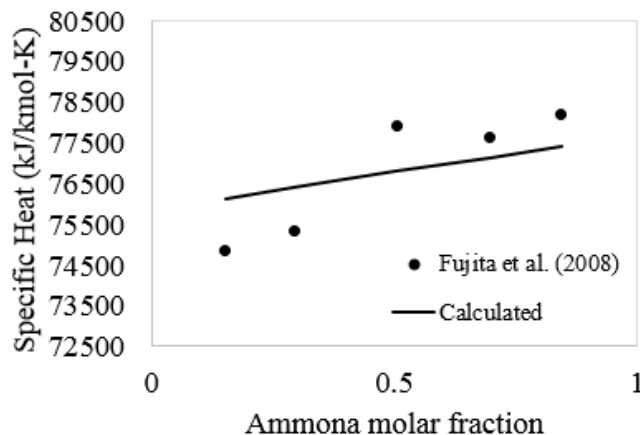


Figure B.3- Specific heat for ammonia and water mixture in liquid phase

### 3. Enthalpies of the mixture ammonia and water

The enthalpies for ammonia and water liquid and vapor mixture are shown in this section. For the liquid phase the enthalpy mixture is calculated by a correlation from Pretek and Klomfar (1995):

$$h_{L,mix} = h_0 \sum_i a_i \left( \frac{T}{T_0} - 1 \right)^{m_i} x_{NH_3}^{n_i} \quad \text{B.7}$$

where  $T$  is temperature,  $x_{NH_3}$  is ammonia composition,  $h_0 = 100$  kJ/Kg is enthalpy in reference state,  $T_0 = 273.16$  K is the reference temperature,  $a_i$ ,  $m_i$  and  $n_i$  are parameters available in Pretek and Klomfar (1995). The enthalpy for the vapor phase is computed by weighting expression (Equation B.6) from the pure components enthalpies because the vapor phase is considered an ideal mixture, as recommended for Triché (2016, 2017a and 2017b):

$$h_{V,mix} = x_{NH_3} h_{NH_3} + (1 - x_{NH_3}) h_{H_2O} \quad \text{B.8}$$

where  $h_{NH_3}$  is ammonia enthalpy and  $h_{H_2O}$  is the water enthalpy, calculated by Equations B.6 and B.7, respectively.

$$\frac{h_{V,i}}{R} = A(T - T_{ref}) + \frac{B(T - T_{ref})^2}{2} + \frac{C(T - T_{ref})^3}{3} - DT(T - T_{ref})^{-1} \quad \text{B.9}$$

where  $A, B, C$  and  $D$  are parameters (Table B.2),  $T$  (K) is temperature,  $R$  (J/mol-K) is gases constant and  $T_{ref}$  is reference temperature.

Figure B.4 shows the mixture enthalpies results for an ammonia composition from 0.02 to 0.99 for the liquid phase and from 0.93 to 0.99 for the vapor phase. The average deviations of these simulations against data from IGT are 3.49% and 3.99% for the liquid and vapor mixture, respectively. It means that the enthalpy mixture calculation is in good agreement with experimental data.

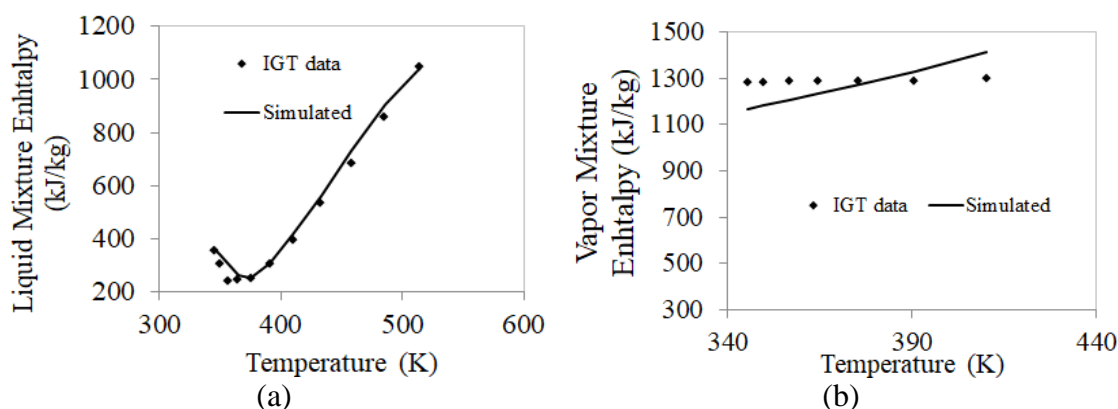


Figure B.4- Enthalpies for ammonia and water mixture in the (a) liquid and (b) vapor phases.

#### 4. Partial Specific Enthalpies for the liquid phase

This section shows the partial specific enthalpy for the components in the liquid phase. As shown in the section above, the vapor mixture is considered ideal (Triché 2016, 2017a and 2017b), so the partial specific enthalpy for vapor phase is given by the enthalpy of the ideal components.

The partial specific enthalpy for ammonia,  $\tilde{H}_{L,NH_3}$ , and for water,  $\tilde{H}_{L,H_2O}$ , in an ammonia and water binary mixture can be calculated using equations derived from Gibbs-Duhem equation as suggested by Ziegler et al. (1984):

$$\tilde{H}_{L,NH_3} = H_{m,L} + (1 - x_{NH_3}) \frac{\partial H_{m,L}}{\partial x} \quad \text{B.10}$$

$$\tilde{H}_{L,H_2O} = H_{m,L} + x_{NH_3} \frac{\partial H_{m,L}}{\partial x} \quad \text{B.11}$$

where  $x_{NH_3}$  is molar composition of ammonia in liquid phase,  $H_{m,L}$  is the enthalpy of liquid mixture expressed as follows:

$$H_{m,L} = x_{NH_3} H_{L,NH_3} + (1 - x_{NH_3}) H_{L,H_2O} + H_E \quad \text{B.12}$$

where  $H_{L,NH_3}$  and  $H_{L,H_2O}$  are the ammonia and water enthalpies for a pure component, computed by Equations B.13 and B.14, respectively,  $H_E$  is the excess enthalpy calculated by Equation B.15.

$$\begin{aligned} H_{L,NH_3} = & RT_{Ref} (-H_{r,0,NH_3}^L + B_{1,NH_3} (T_{r,0,NH_3} - T_r)) \\ & + \frac{B_{2,NH_3}}{2} (T_{r,0,NH_3}^2 - T_r^2) + \frac{B_{3,NH_3}}{3} (T_{r,0,NH_3}^3 + 2T_r^3) \\ & - B_{3,NH_3} T_r^3 (P_r - P_{r,0,NH_3}) (-A_{1,NH_3} + A_{4,NH_3} T_r^2) \\ & - \frac{A_{2,NH_3}}{2} (P_r^2 - P_{r,0,NH_3}^2) \end{aligned} \quad \text{B.13}$$

where  $R$  is gas constant,  $T_{Ref}$  is reference temperature,  $P_r$  is reduced pressure,  $T_r$  is reduced temperature,  $A_{1,NH_3}$ ,  $A_{2,NH_3}$ ,  $A_{4,NH_3}$ ,  $B_{1,NH_3}$ ,  $B_{2,NH_3}$ ,  $B_{3,NH_3}$ ,  $H_{r,0,NH_3}^L$ ,  $T_{r,0,NH_3}$  and  $P_{r,0,NH_3}$  are ammonia parameters as Table B. shows.

$$\begin{aligned} H_{L,H_2O} = & -RT_{Ref} (-H_{r,0,H_2O}^L + B_{1,H_2O} (T_{r,0,H_2O} - T_r)) \\ & + \frac{B_{2,H_2O}}{2} (T_{r,0,H_2O}^2 - T_r^2) + \frac{B_{3,H_2O}}{3} (T_{r,0,H_2O}^3 + 2T_r^3) \\ & - B_{3,H_2O} T_r^3 (P_r - P_{r,0,H_2O}) (-A_{1,H_2O} + A_{4,H_2O} T_r^2) \\ & - \frac{A_{2,H_2O}}{2} (P_r^2 - P_{r,0,H_2O}^2) \end{aligned} \quad \text{B.14}$$

where  $R$  is gas constant,  $T_{Ref}$  is reference temperature,  $P_r$  is reduced pressure (Equation B.17),  $T_r$  is reduced temperature (Equation B.16),  $A_{1,NH_3}$ ,  $A_{2,H_2O}$ ,  $A_{4,NH_3}$ ,  $B_{1,H_2O}$ ,  $B_{2,H_2O}$ ,  $B_{3,H_2O}$ ,  $H_{r,0,H_2O}^L$ ,  $T_{r,0,H_2O}$  and  $P_{r,0,H_2O}$  are water parameters as Table B. shows.

$$\begin{aligned}
 H_E = & -RT_{Ref}x_{NH_3}(1-x_{NH_3})\left(-E_1 - E_2P_r - \frac{2E_5}{T_r} - \frac{3E_6}{T_r^2}\right) \\
 & + (2x_{NH_3} - 1)\left(-E_7E_8P_r - \frac{2E_{11}}{T_r} - \frac{3E_{12}}{T_r^2}\right) \\
 & + (2x_{NH_3} - 1)^2\left(-E_{13} - E_{14}P_r - \frac{2E_{15}}{T_r} - \frac{3E_{16}}{T_r^2}\right)
 \end{aligned} \tag{B.15}$$

where  $R$  is gas constant,  $T_{Ref}$  is reference temperature,  $P_r$  is reduced pressure (Equation B.17),  $T_r$  is reduced temperature (Equation B.16),  $x_{NH_3}$  is ammonia composition,  $E_1, E_2, E_3, E_4, E_5, E_6, E_7$  and  $E_8$  are water parameters as Tble B.3

Table B.3-Excess Enthalpy Parameters (Ziegler et al., 1984)

Parameters	Ammonia	Water
$A_1$	$3.971423 \cdot 10^{-2}$	$2.748796 \cdot 10^{-2}$
$A_2$	$-1.790557 \cdot 10^{-5}$	$-1.016665 \cdot 10^{-5}$
$A_3$	$-1.308905 \cdot 10^{-2}$	$-4.452025 \cdot 10^{-3}$
$A_4$	$3.752836 \cdot 10^{-3}$	$8.389246 \cdot 10^{-4}$
$B_1$	$1.634519 \cdot 10^1$	$1.214557 \cdot 10^1$
$B_2$	$-6.508119$	$-1.898065$
$B_3$	$1.448937$	$2.911966 \cdot 10^{-1}$
$P_{r,0}$	2	3
$T_{r,0}$	3.2252	5.0705
$H_{r,0}^L$	4.878573	21.821141

$$T_r = \frac{T}{T_{Ref}} \quad (T_{Ref} = 100 \text{ K}) \tag{B.16}$$

$$P_r = \frac{P}{P_{Ref}} \quad (P_{Ref} = 10 \text{ K}) \tag{B.17}$$

Table B.4- Excess Enthalpy Parameters (Ziegler et al., 1984)

Ammonia and water mixture			
$E_1$	-46.26129	$E_9$	-1.475383
$E_2$	0.02060225	$E_{10}$	-0.005038107
$E_3$	7.292369	$E_{11}$	-96.40398
$E_4$	-0.01032613	$E_{12}$	122.6973
$E_5$	80.74824	$E_{13}$	-7.582637
$E_6$	-84.61214	$E_{14}$	0.0006012445
$E_7$	24.52882	$E_{15}$	54.87018
$E_8$	0.009598767	$E_{16}$	-76.67596



### 5. Viscosity

The viscosity for the system ammonia and water for the pure components in liquid and in vapor phase and for liquid mixture is calculated by TEA. In order to verify the quality of fit of the predictions made by TEA, this propriety is validated with experimental data from literature. Viscosity of the vapor phase mixture is not shown here because the ammonia concentration in vapor phase for the system is around 0.99. That means the results are very similar from the pure ammonia in vapor phase, hence are not shown for the sake of simplicity. Figure B.5 shows a comparison of experimental (Perry et al., 1998) and simulated viscosity of ammonia in liquid and in vapor phase, whereas Figure B.6 shows the viscosity of water and shows the viscosity of the liquid mixture with  $x_{NH_3} = 0.15$ .

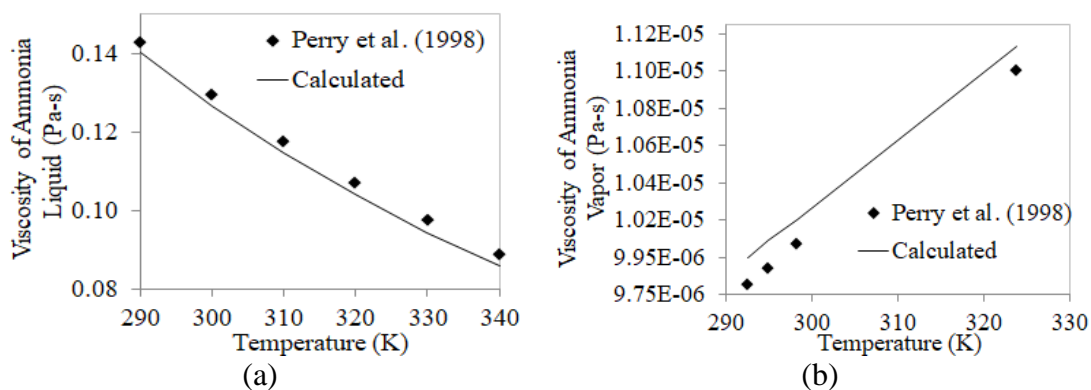


Figure B.5-Viscosity of ammonia pure in liquid phase (a) and in vapor phase (b)

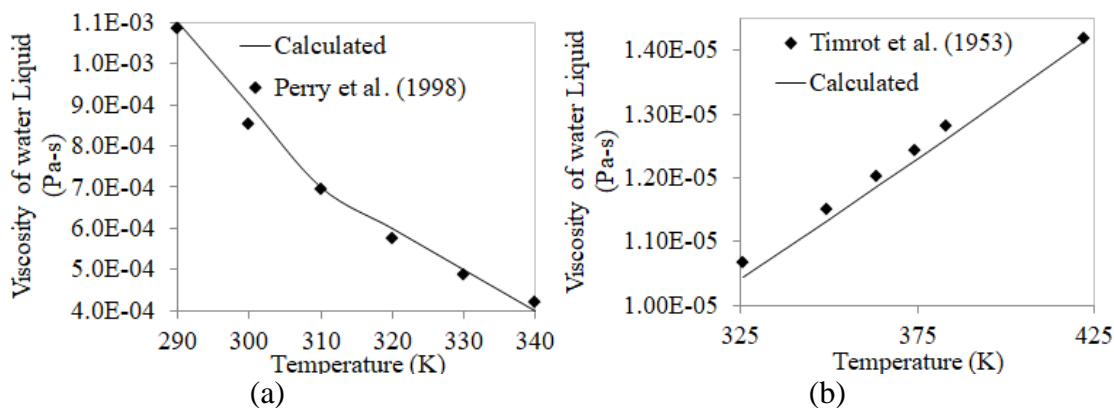


Figure B.6- Viscosity of water pure in liquid phase (a) and in vapor phase (b)

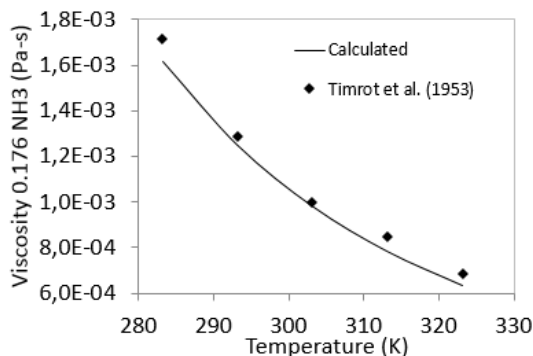


Figure B.7- Viscosity of ammonia and water liquid mixture

The results shown in Figures B5, B6 and B7 indicate that the simulated data of viscosity for pure components and for the liquid mixtures are in good agreement with experimental data. Table B.3 shows the average deviation between the experimental and simulated results.

Table B.3- Viscosity of ammonia and water liquid mixture

Viscosity (Pa-s)	Ammonia		Water	
	Liquid	Vapor	Liquid	Vapor
Experimental data:	Laeseck <i>et. al.</i> (199	Trautz (1931)	Agaev <i>et al.</i> (196	Timrot (1950)
Average Deviation (%):	2.55%	1.41%	3.06%	1.37%
Ammonia and water liquid mixture ( $x_{NH_3} = 0.15$ )				
Experimental data:	Timrot (1950)		Average Deviation (%)	5.51 %

## 6. Thermal Conductivity

The thermal conductivity for the system ammonia and water is calculated by TEA. Like in viscosity calculations, the results are for the pure components and for the liquid mixture. They are validated against experimental data from literature (Verlashkin et al., 1953). Thermal conductivity of the vapor phase mixture is not shown here because the vapor phase is almost pure ammonia. Figure B.8 shows a comparison of experimental and

simulated thermal conductivity of ammonia in liquid and in vapor phase. Figure B.9 shows the thermal conductivity for water and Figure B.10 shows the liquid mixture results for  $0 \leq x_{NH_3} \leq 0.27$ .

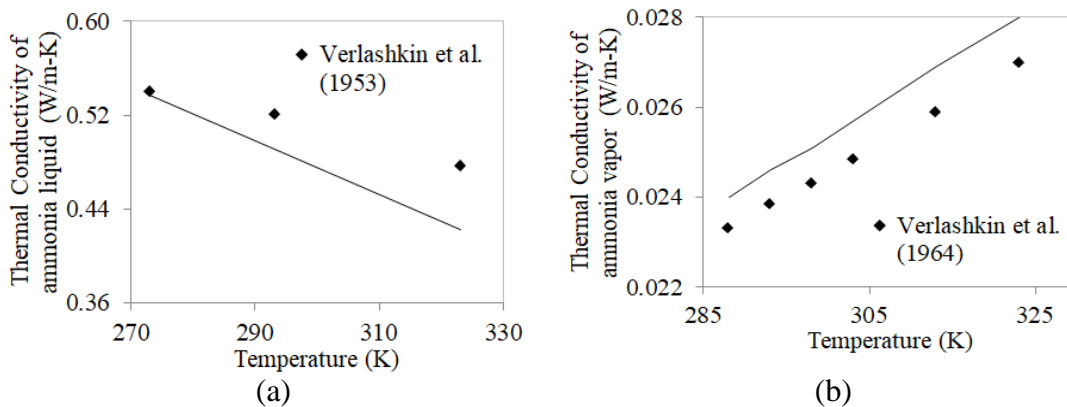


Figure B.8- Thermal conductivity of ammonia pure in liquid phase (a) and in vapor phase (b)

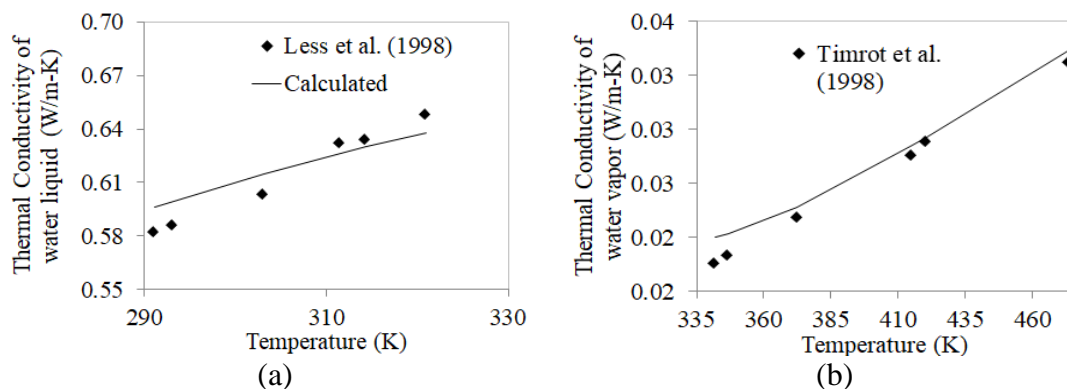


Figure B.9- Thermal conductivity of water pure in liquid phase (a) and in vapor phase (b)

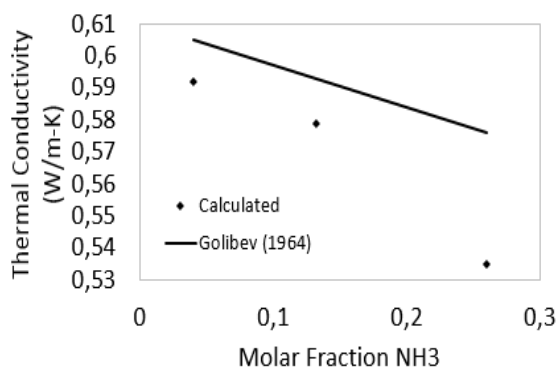


Figure B.10- Thermal conductivity of ammonia and water liquid mixture

Table B.4 shows the average deviation between the experimental and simulated results shown in Figure B.8, Figure B.9, Figure B.10. These results indicate that the

simulated data of thermal conductivity for pure components and for the liquid mixtures are in good agreement with experimental data

Table B.4-Thermal conductivity of ammonia and water liquid mixture

Thermal conductivity (W/m-K)	Ammonia		Water	
	Liquid	Vapor	Liquid	Vapor
Experimental data:	Varlashkin <i>et al.</i> (195), Golubev (1964), Less <i>et al.</i> (1898), Timrot (1950)			
Average Deviation (%):	5.74%	3.38%	1.74%	0.68%

Ammonia and water liquid mixture (0-0.27 of ammonia)			
Experimental data:	Golubev (1964)	Average Deviation (%)	2.43

**7. Density**

The density for the system ammonia and water for the pure components in liquid and in vapor phases and for liquid mixture is calculated by TEA. The validation of the predictions made by TEA is done with experimental data from literature (Cragoe et al., 1921). Density of the vapor phase mixture is not shown here because it is almost pure ammonia. Figure B.11 shows a comparison of experimental and simulated density of ammonia in liquid and in vapor phase. Figure B.12 shows the results for water and Figure B.13 shows the results for the liquid mixture.

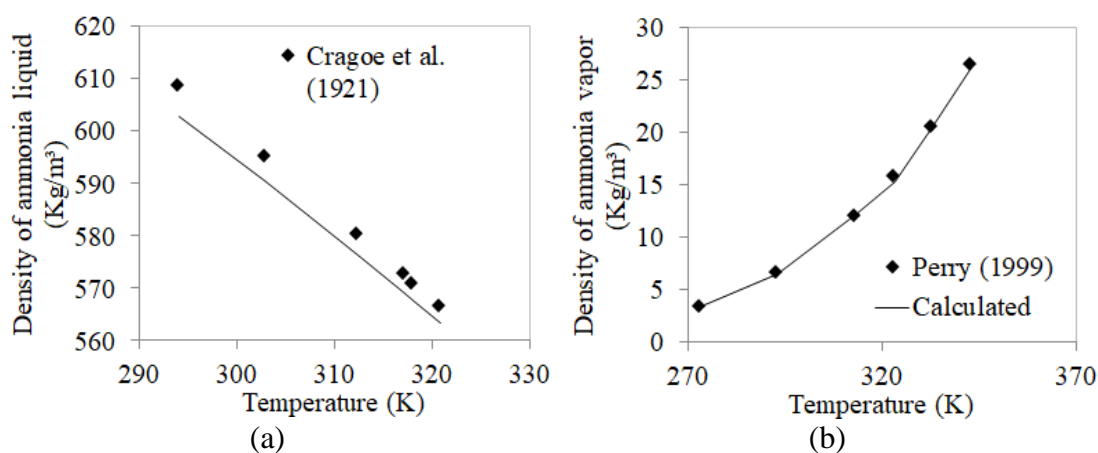


Figure B.11-Density of pure ammonia in liquid phase (a) and in vapor phase (b).

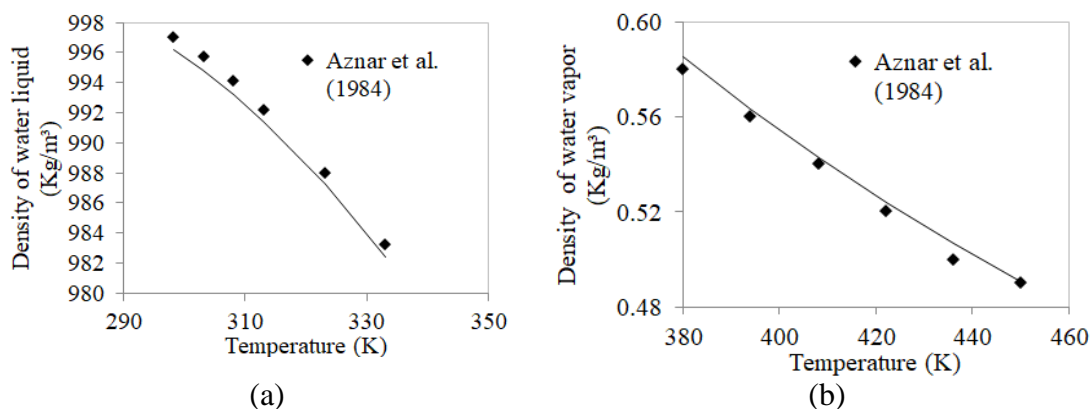


Figure B.12- Density of pure water in liquid phase (a) and in vapor phase (b).

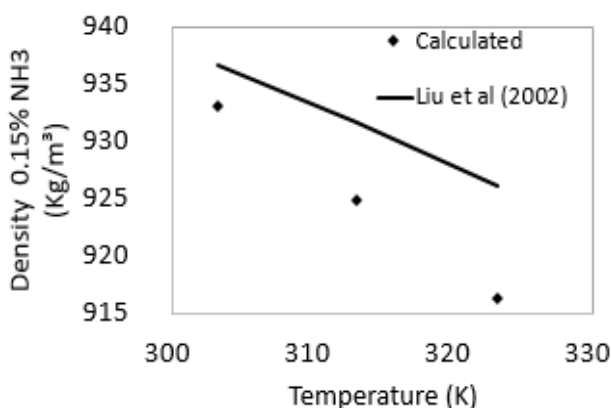


Figure B.13- Density of ammonia and water liquid mixture.

The results from Figure B.11, Figure B.12 and Figure B.13 show that the simulated data of density for pure components and for the liquid mixtures are in very good agreement with experimental data. The average deviations between the experimental and simulated results are shown in Table B.5.

Table B.5- Density of ammonia and water liquid mixture

Density (kg/m <sup>3</sup> )	Ammonia		Water	
	Liquid	Vapor	Liquid	Vapor
Experimental data:	Cragoe <i>et al.</i> (1921), Perry (1999)		Aznar <i>et al.</i> (1984), Perry (1999)	
Average Deviation (%):	0.70%	1.87%	0.08%	0.68%
Ammonia and water liquid mixture (0.176 of ammonia)				
Experimental data:	Liu <i>et al.</i> (2002)		Average Deviation (%)	
			0.74%	

## 8. Diffusivity

The binary diffusivity coefficient for ammonia and water liquid mixture can be calculated by an equation developed by Conde (2005):

$$D_{Liq} = 117.282 \cdot 10^{-18} T \frac{\sqrt{\Psi_m M_m}}{\mu_m V_{diff}^{0.6}} \quad \text{B.18}$$

where  $T$  (K) is mixture temperature,  $\mu_m$  (Pa-s) is dynamic viscosity,  $M_m$  (g/mol) is molecular weight of the mixture and  $V_{diff}$  (cm<sup>3</sup>/mol) is the molar volume,  $\Psi_m$  is association factor of the mixture, which can be calculated by (Wilk and Chang, 1955):

$$\Psi_m = x_{NH_3} \Psi_{NH_3} + (1 - x_{NH_3}) \Psi_{H_2O} \quad \text{B.19}$$

where  $\Psi_{NH_3}$  and  $\Psi_{H_2O}$  are the associations factors for the ammonia and water, respectively. According to Wilk and Chang (1955),  $\Psi_{NH_3} = 1.7$  and  $\Psi_{H_2O} = 2.6$ .

The binary diffusivity coefficient for the vapor phase can be computed by Chapman-Enskog equation from Bird et al. (2002):

$$D_{Vap} = 0.0018583 \sqrt{T^3 \left( \frac{1}{M_{NH_3}} + \frac{1}{M_{H_2O}} \right) \left( \frac{1}{P \sigma_{NH_3, H_2O} \Omega_D} 10^{-4} \right)} \quad \text{B.20}$$

where  $T$  (K) is temperature,  $M_{NH_3}$  and  $M_{H_2O}$  are the molecular weight for ammonia and water, respectively,  $P$  (atm) is pressure,  $\sigma_{NH_3, H_2O}$  (Å) is the molecular diameter calculated by:

$$\sigma_{NH_3, H_2O} = \frac{\sigma_{NH_3} + \sigma_{H_2O}}{2} \quad \text{B.21}$$

where  $\sigma_{NH_3}$  and  $\sigma_{H_2O}$  are the molecular diameter for the pure components,  $\sigma_{NH_3} = 0.2641$  and  $\sigma_{H_2O} = 0.29$  (Triché, 2017a). The collision integral,  $\Omega_D$ , can be computed by:

$$\Omega_D = \frac{1.06036}{(T^*)^{0.15610}} + \frac{0.19300}{\exp(0.47635T^*)} + \frac{1.03587}{\exp(1.52996T^*)} + \frac{1.76474}{\exp(3.89411T^*)} \quad \text{B.22}$$

where  $T^*$  is calculate by:

$$T^* = \frac{kT}{\varepsilon_{NH_3,H_2O}} \quad \text{B.23}$$

where  $T$  (K) is temperature,  $k$  ( $m^2kg/s^2K$ ) is Boltzmann constant and  $\varepsilon_{NH_3,H_2O}$  (K) is Lennard-Jones potential, computed by:

$$\varepsilon_{NH_3,H_2O} = (\varepsilon_{NH_3} \varepsilon_{H_2O})^{\frac{1}{2}} \quad \text{B.24}$$

where  $\varepsilon_{NH_3} = 558.3$  and  $\varepsilon_{H_2O} = 809.1$  are the Lennard-Jones potential for ammonia and water, respectively.

These properties are needed in the liquid phase and in the vapor phase for all calculations relating to the phenomenon of ammonia-water absorption.

## 9. References

AGAIEV, N. A.; USIBOVA, A. D. DOKL. AKAD. NAUK AZ. SSR, Viscosity of ordinary and heavy water at high pressures in the temperature range from 0 to 150 C 1968, 180(2), 334-337.

AZNAR M, A.; GIMENO R., J.; PEREZ G., D.; CARRASCO G., AFINIDAD, J. L., Density and excess volume of alkyl pyridine-water systems 1984, 41, 355.

BIRD, B., STEWART, W., LIGHTFOOT, E. Transport Phenomena, Revised second ed. JohnWiley & Sons, Inc., 2006Conde (2005).

CRAGOE, C. S.; HARPER, D. R. Specific Volume of Liquid Ammonia Sci. Pap. Bur. Stand. (U. S.), 1921, 17, 287-315.

GOLUBEV, I. F.; SOKOLOVA, V. P. TEPLOENERGETIKA, Thermal conductivity of ammonia at various temperatures and pressures. 1964, No. 11, 64-67.

LAESECKE, A.; LUEDDECKE, T. O. D.; HAFER, R. F.; MORRIS, D. J. Viscosity measurements to ammonia, R32, and R134a. Vapor buoyancy and radial acceleration in capillary viscometers. Int. J. Thermophys., 1999, 20, 401-434.

LEES, C. H. PHILOS. TRANS. R. On the Thermal Conductivities of Single and Mixed Solids and Liquids and their Variation with Temperature Soc. London, Ser. A, 1898, 191, 339-440 X.

LIU, J.; WANG, S.; HARTONO, A.; SVENDSEN, H. F. Solubility of N<sub>2</sub>O in and Density and Viscosity of Aqueous Solutions of Piperazine, Ammonia, and Their Mixtures from (283.15 to 323.15) K ; Chen, C. J. Chem. Eng. Data, 2012, 57(9), 2387-2393 .

PERRY, R. H.; GREEN, D. W. (Ed.) Perry's Chemical Engineers' Handbook. McGraw-Hill: New York, 1999. Prata (2012).

PATEK, J. and KLOMFAR, J. Simple functions for fast calculations of selected thermodynamic properties of the ammonia-water system: Int. J. Refrigeration 18, No. 4, pp. 228-234, 1995. VARLASHKIN, P. G.; THOMPSON, J. C. J. Thermal Conductivity of liquid Ammonia Chem. Eng. Data, 1963, 8, 526-526.

TIMROT, D. L. PAR VYSOKIH , Steam of high parameters in energetics: Properties of water steam, 1950, Parametrov Energetike, Gosenergoizdat: Moscow.

TIMROT, D. L.; SEREDNITSKAYA, M. A.; BESPALOV, M. S. TEPLOENERGETIKA, Experimental study of the viscosity of water vapor at temperatures from 50 to 500 C and at pressures from 0.06 to 1.5 bar 1973, No. 8, 78-80.

TRAUTZ, M.; HEBERLING, R. ANN. PHYSIK, 1931, 10, 155 Viscosity of ammonia & its mixture with hydrogen, nitrogen, ethylene.

TRICHÉ D., BONNOTA, S., PERIER-MUZETA, M., BOUDÉHENNA F. DEMASLESA H., CANEY, N. Modeling and experimental study of an ammonia-water falling film Absorber SHC 2015, International Conference on Solar Heating and Cooling for Buildings and Industry Energy Procedia 91 (2016) 857 – 867. Triché 2017a

TRICHÉ D., BONNOTA, S., PERIER-MUZETA, M., BOUDÉHENNA F. DEMASLESA H., CANEY, N. PERIER-MUZET, M. Experimental and numerical study of a falling film absorber in an ammonia-water absorption chiller. International Journal of Heat and Mass Transfer 111 (2017) 374–385.

SMITH, J. M., & VAN, N. H. C. Introduction to chemical engineering thermodynamics. (2007). New York: McGraw-Hill.

WILKE, C.R., CHANG, P., Correlation of diffusion coefficients in dilute solutions, AIChE Journal 1, 1955, 264-270.

ZIEGLER, B., Ch. Trepp, Equation of state of ammonia–water mixtures, Int. J. Refrig. 7, 1984, 101–106.



**UFBA**  
UNIVERSIDADE FEDERAL DA BAHIA  
ESCOLA POLITÉCNICA

PROGRAMA DE PÓS GRADUAÇÃO EM ENGENHARIA  
INDUSTRIAL - PEI

Rua Aristides Novis, 02, 6º andar, Federação, Salvador BA  
CEP: 40.210-630  
Telefone: (71) 3283-9800  
E-mail: [pei@ufba.br](mailto:pei@ufba.br)  
Home page: <http://www.pei.ufba.br>

